國 立 交 通 大 學

電信工程研究所

博 士 論 文

綠色無線接取網路之通訊協定設計與實作

Protocol Design and Implementation for Green Wireless Access Networks

研 究 生： 劉 文 俊 (Wen-Jiunn Liu)

指 導 教 授： 方 凱 田 (Kai-Ten Feng)

中 華 民 國 九 十 九 年 六 月

綠色無線接取網路之通訊協定設計與實作

Protocol Design and Implementation for Green Wireless Access Networks

研究生：劉文俊　　Student：Wen-Jiunn Liu

指導教授：方凱田　博士　　Advisor：Dr. Kai-Ten Feng

國立交通大學

電信工程研究所

博士論文

A Dissertation
Submitted to Institute of Communications Engineering
College of Electrical and Computer Engineering
National Chiao Tung University
in Partial Fulfillment of the Requirements
for the Degree of Doctor of Philosophy
in
Communications Engineering
Hsinchu, Taiwan

2010 年 6 月

綠色無線接取網路之通訊協定設計與實作

學生：劉文俊　　指導教授：方凱田 博士

國立交通大學
電信工程研究所博士班

摘要

近年來由於節能省電與環境友善議題發酵，綠色觀念 (Green Concept) 得到了很多方面的注意。如何設計一個綠色無線接取網路也已經在通訊領域變成一個相當熱門的主題。在網路系統設計方面，通訊堆疊最重要的部分通常為網路層 (Network Layer)、資料連結層 (Data Link Layer) 和實體層 (Physical Layer)，因為這三層最被通訊端點與通訊中介點所使用。然而實體層通常與所存取的媒介體相關，因為不同的媒介體會有不同的訊號產生與調變方式。因此在設計與媒介體獨立的演算法或通訊協定方面，網路層和資料連結層吸引了更多的注意。於是為了要建立一個綠色無線接取網路，本論文在網路層和資料連結層上提出了一系列的節能通訊協定設計與相關的實作方式。

在網路層通訊協定設計方面，基於貪婪選徑演算法 (Greedy Forwarding, GF)，本論文分別為二維平面與三維空間，提出貪婪抗無效問題選徑演算法 (Greedy Anti-void Routing, GAR) 和三維貪婪抗無效問題選徑演算法 (Three-Dimensional Greedy Anti-void Routing, 3D-GAR) 作為低通訊消耗且保證到達的單播演算法 (Unicast)。對於低通訊消耗多播演算法 (Multicast) 設計方面，本論文也提出了一個節能省電多播選徑演算法 (Energy Conserving Multicast Routing, ECMR)，用以減少多播樹 (Multicast Tree) 通訊中介點的個數。此演算法可以顯著的降低非必要的通訊花費。此外，本論文基於 Linux 嵌入式系統提出了元件導向選徑實作平台 (Component-based Routing Platform, CRP) 用以實現這些所提出的選徑演算法。以上所提出的網路層通訊協定可以直接使無線接取網路更省電綠化，因為通訊花費的節省可以直接降低能源的消耗。

在資料連結層通訊協定設計方面，依同樣能源消耗下，系統吞吐量的加強可以視為一種非直接的方式實現綠色無線接取網路，因為平均傳輸每單位資料所消耗的能源可以被降低。因此本論文提出了一種貪婪快速移動區塊確認演算法 (Greedy Fast-Shift Block Acknowledgement, GFS)，透過減少傳統區塊確認演算法中緩慢移動確認窗(Acknowledgement Window) 所帶來的負面效應，最後加強整

個系統的吞吐量。除了加強系統吞吐量這種非直接方式，另外還有一種直接的方式，即：透過節能省電排程演算法可以直接達成節能省電的目的。節能省電排程演算法可以透過適當的封包傳輸安排，減少最終的總能源消耗量。因此本論文對於此直接省電的分類，也提出了一種訊框聚集節能省電排程演算法 (Frame Aggregation-based Power-Saving Scheduling Algorithm, FAPS)，此演算法可以將數個未填滿的訊框合併成為一個填滿的訊框，進而達到節能省電的目的。另外值得注意的是本訊框聚集節能省電排程演算法仍然可以維持住每個封包的服務品質 (Quality-of-Service, QoS)。此外，訊框聚集節能省電排程演算法在輸入皆為階梯狀允許空間 (Stepwise Grant Space Set) 的條件之下，也可以產生最少的聆聽訊框 (Listen Frame)。相關的正確性證明皆整理並提供於本論文之內。最後多數的系統訊框皆可以處於在睡眠模式之下，睡眠模式可以消耗相對於正常模式還少的能源，因此可以達成節能省電的目的。透過本論文所提出在網路層與資料連結層上的軟體通訊協定設計與實作，綠色無線接取網路將可以被廣泛的建立與使用。

Protocol Design and Implementation for Green Wireless Access Networks

Student: Wen-Jiunn Liu Advisor: Dr. Kai-Ten Feng

Institute of Communications Engineering

National Chiao Tung University

ABSTRACT

In recent years, the green concept has received more attention due to the energy efficient and environmentally friendly issues. How to develop the green wireless access network also has become a hot topic in the communications society. In terms of the network system design, the most important parts of the communication stacks are in general the network layer, the data link layer, and the physical layer since these three layers are utilized mostly in the terminal hosts and the intermediate nodes. However, the physical layer is usually medium dependent for signaling different transmission media. As a result, the network layer and the data link layer will gain more attraction in designing the medium independent algorithms and protocols. Therefore, in order to achieve the green wireless access networks, the protocol design and implementation on the network layer and the data link layer are collectively proposed in this dissertation.

In the network layer protocol design, a greedy anti-void routing (GAR) protocol and the three-dimensional greedy anti-void routing (3D-GAR) protocol for both two-dimensional and three-dimensional environments are proposed as the low-overhead delivery-guaranteed unicast routing protocols based on the well-known greedy forwarding (GF) algorithm. In the low-overhead multicast routing protocol design, an energy conserving multicast routing (ECMR) protocol is also proposed to reduce the total number of relaying nodes for the construction of a multicast tree, which can significantly eliminate the unnecessary communication overheads. Moreover, based on the Linux embedded systems, the associated component-based routing platform (CRP) for implementing routing protocols is also introduced. These proposed network layer protocols can make the wireless access networks greener directly since the reduction of the communication overheads can effectively suppress the energy expenses.

On the other hand, in the data link layer protocol design, the system throughput enhancement under the same power consumption can be considered an indirect way to realize the green wireless access networks since the power expenses can be degraded for transmitting the same amount of information. As a result, the greedy fast-shift block acknowledgement (GFS) mechanism is proposed for enhancing the system throughput by reducing the inefficiency caused by the slow sliding of the conventional acknowledgement window. Thanks to the fast shifting property of the acknowledgement window in our proposed GFS scheme, significant throughput enhancement can therefore be observed. In addition to the indirect method of enhancing the system throughput, the direct method for achieving the green concept should be the power-saving scheduling algorithm, which can arrange the packets with the proper transmission schedules, suppressing the total energy consumption. The frame aggregation-based power-saving (FAPS) scheduling algorithm is therefore proposed for this type of direct methods by aggregating several under-utilized frames into fully-utilized ones. The quality-of-service (QoS) of each data packet can still be maintained in our proposed FAPS algorithm. In addition, the optimality on the minimum number of listen frames in the proposed FAPS algorithm is also provided under the stepwise grant space set and further verified via the correctness proof. Finally, more number of system frames can be in the sleep mode, which consumes less energy compared to the active mode. With our proposed software protocol design and implementation in the network layer and the data link layer, the green wireless access networks can therefore be achieved.

Acknowledgements

I would like to show my gratitude to my supervisor, Dr. Kai-Ten Feng, whose encouragement, guidance and support enabled me to complete this dissertation. Moreover, I owe my deepest gratitude to my family, who helped me when I had any request. I also would like to thank my colleagues in the mobile intelligent network technology (MINT) laboratory and the friends around the world, who enriched my school life and expanded my international views. Furthermore, I would like to acknowledge those associations and companies which had ever given me the financial support and scholarships during my degree program. Lastly, I offer my regards and blessings to all of those who supported me in any respect during the completion of the dissertation.

Contents

List of Tables

List of Figures

Chapter 1

Dissertation Overview

1.1 Introduction

A wireless access network is a type of communication networks that exchange information and interconnect with network stations via the wireless media, such as infrared, laser, ultrasound, and radio waves [1]. As a result of the wireless characteristics, the wireless access network has many advantages against its wired counterpart, e.g., support of device mobility, simple installation, and ease of deployment. In the developing countries, the telecommunications companies may abandon the traditional wired telephones and directly migrate to the wireless access systems, e.g., the global system for mobile communications (GSM) and the universal mobile telecommunications system (UMTS), since the operating cost and the construction fee of the network infrastructures can be greatly reduced. In addition to cutting the money expenses, the wireless network systems can also be considered environmentally friendly since the deployment of the wireless system can result in less damage to the natural environment compared to the placement of wire lines. It is much close to the green concept which is popular and urgent in these years due to the global warming and the climate changes. The definition of green [2] is shown as follows:

Definition 1 (Green). *Energy efficient. Environmentally friendly. The term is applied to systems and products that save energy directly or indirectly.*

The wireless access networks account for a large portion of total power consumption of the communication systems in these years. This situation is expected to be enlarged with the growth of the Internet traffics and the popularity of the information and communication technology (ICT). The total power consumption of the future wireless networks is considered unaffordable if the energy expense per unit data maintains the current level [3]. Therefore, making the wireless access networks greener, i.e., more energy efficient, can not only reduce the greenhouse gas emissions and protect our natural environment, but also help to maintain the future system operation of the telecommunications companies. With proper protocol design and implementation of the green wireless access network, the protection of the natural environment and the long-term profitability of the system operators can be ultimately achieved.

In terms of the size of wireless coverage, several categories for classifying the wireless networks can be described as follows: The largest one is the wireless regional area network (WRAN), which is targeted at bringing broadband access to the rural and remote areas. The IEEE standards association establishes a standard series of IEEE 802.22 for this type of networks. The wireless wide area network (WWAN) is the second largest category which can cover a whole nation, even up to multiple countries. The representative technologies will be the IEEE 802.20 standard suite and the 2G and 3G cellular systems. The next one is the wireless metropolitan area network (WMAN), which can help to support the network services from several blocks of buildings to the entire city. The IEEE 802.16 standard series belong to this category. The wireless local area network (WLAN) is considered the most popular one in our daily life since the IEEE 802.11 standard series or the Wi-Fi technologies have gained the remarkable success in both design and deployment. The transmission range of the WLAN devices will be in several hundred meters, and the WLAN will usually be installed in the office or at home in order to provide the networking devices, e.g., the laptop computers, with the high speed Internet access. Moreover, the category of the wireless personal area network (WPAN) can be constructed to replace the physical cable line between the computer and its peripherals, such as the earphones and the portable storage. The famous IEEE 802.15 standard suite and the commercial Bluetooth and ZigBee protocols fall into this category.

Based on the specific characteristics, there are also plenty of wireless networks specialized for different applications. The wireless mobile ad hoc network (MANET) is a general type distributed system consisting of wireless-capable nodes which can communicate with each other via the multi-hop forwarding manner. The representative application is the military communication systems since there do not exist fixed or functioning infrastructures in the battle fields, i.e., lack of centralized controllers to organize the radio links and schedule the packet transmissions. If these wireless-capable nodes are small sensors with limited available resources, such as the limited battery life time and the small transmission range, this type of networks can be categorized as the wireless sensor network (WSN), which usually handles the environmental sensing tasks, such as the forest and slope monitoring. In general, there will be a sink node to gather the information reported by all the other sensor nodes. Since a large portion of environmental sensing occurs in the ocean, the underwater wireless sensor network (UWSN) has therefore received its popularity in the field of oceanographic engineering, including data collection, water monitoring, pollution control, and ocean surveillance. The major characteristics are the three-dimensional (3D) network spaces and the usages of the acoustic wave to overcome the high frequency radio wave absorbtion in the water. The acoustic wave will elongate the propagation delay in the packet transmission, which can significantly reduce the performance on the system throughput.

The wireless vehicular ad hoc networks (VANET) is another type of MANETs whose interconnected members consist of the vehicles and the road side units, i.e., the fixed equipments on the road. These vehicles will have constrained or similar statistical mobility model. For example, in the highways, the vehicle drivers should drive along the road or follow the highway directions to get off from the interchanges. On the other hand, the road side units can communicate with each vehicle and provide information for the drivers, such as the traffic conditions and the car accidents. The next wireless network category is the wireless mesh network (WMN), which is a special type of wireless ad hoc networks. Compared with the equal view to the network members in the traditional ad hoc networks, the members in WMNs will often be labeled as in different types of the mesh clients, mesh routers and gateways. The mesh clients will forward or receive data from the mesh routers; while the mesh routers will

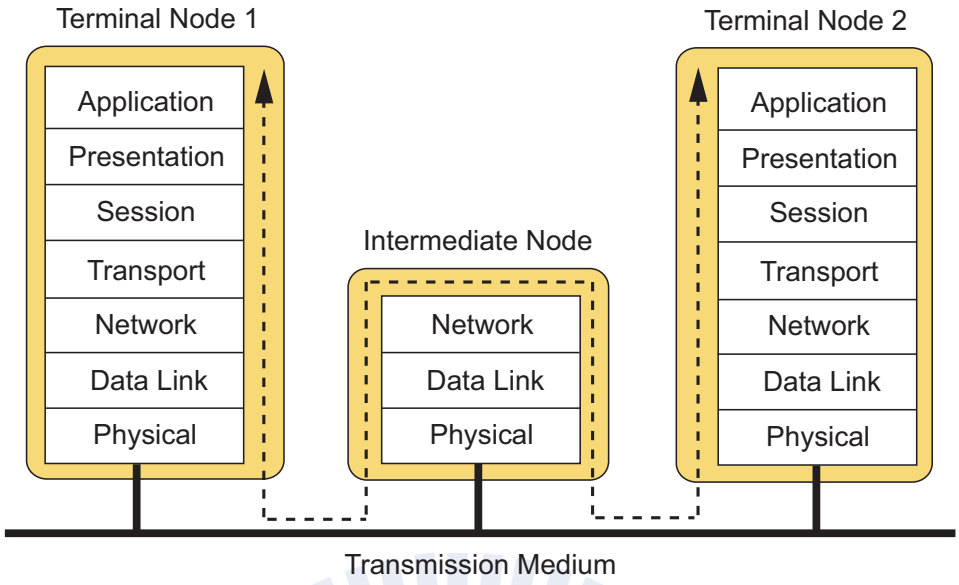

Figure 1.1: The OSI reference model and the data transmission paradigm.

also help to relay data from the gateways. When some network members are out of operation, the others can still help to maintain the network connectivity by using intermediate nodes, which is the merit of the mesh networks.

Due to the urgent needs of green wireless access networks mentioned in the beginning of this section, the researchers and the engineers are now trying to let the network systems more power efficient either in the direct or indirect ways, such as reducing the communication overhead or enhancing the system throughput under the same power consumption. Compared to the hardware evolutions, the more feasible and convenient way to make the wireless network greener is from the software point of view. The International Organization for Standardization (ISO) proposes the famous open system interconnection (OSI) reference model for dividing the entire system into seven parts, i.e., the seven layers. As shown in Fig. 1.1, the modular seven layers from the user application to the transmission medium are respectively the application layer, the presentation layer, the session layer, the transport layer, the network layer, the data link layer, and the physical layer. The application layer will interact with the users and generate the corresponding application data. The presentation layer handles the data representation, encryption, and decryption; while the host-to-host communication negotiation is conducted by the session layer. The traffic flow control and the connection reliability are

maintained by the transport layer. The network layer will try to find a feasible path to the destination with proper medium access control provided by the data link layer. Finally, the physical layer transmits the data signals over the transmission medium to the other network station.

As shown in Fig. 1.1, the information flow from the terminal node 1 to the terminal node 2 can be constructed via intermediate nodes. The data generated by the application of the terminal node 1 will be sent to the lower layers till the physical layer. The physical layer data signals will be received by the intermediate node from the transmission medium, and then the data signals will be decoded and forwarded to the upper layers. In the network layer, the routing decision will be made, and subsequently the intermediate node will conduct the packet forwarding down to the physical medium. If there is any other intermediate node, the same procedure will be repeated. Finally, the terminal node 2 will receive the data from the transmission medium. Moreover, as can be seen in Fig. 1.1, the most important parts of the network stacks are the network layer, the data link layer, and the physical layer since these three layers are utilized mostly in the terminal hosts and the intermediate nodes. However, the physical layer is usually medium dependent for signaling different transmission media. As a result, the network layer and the data link layer will receive more attention in designing the medium independent algorithms and protocols for the green wireless access networks.

Based on the aforementioned reasons, the protocol design and implementation for the green wireless access networks will mainly focus on the network layer and the data link layer. According to the green concept defined in Definition 1, the algorithms or software systems to save energy directly or indirectly can be considered green or environmental friendly. In the traditional protocol design of the network layer, there are more communication overhead observed in both the unicast and multicast routing algorithms, such as the control packet flooding and the periodic route maintenance. In this dissertation, a greedy anti-void routing (GAR) protocol and the three-dimensional greedy anti-void routing (3D-GAR) protocol for both two-dimensional (2D) and three-dimensional (3D) environments are proposed as the low-overhead delivery-guaranteed unicast routing protocols based on the well-known greedy forwarding (GF) algorithm [4]. In the low-overhead multicast routing protocol design, an

energy conserving multicast routing (ECMR) protocol is also proposed to reduce the total number of relaying nodes for the construction of a multicast tree, which can significantly eliminate the unnecessary communication overheads. Moreover, based on the Linux embedded systems, the associated component-based routing platform (CRP) for implementing routing protocols is also introduced. These proposed network layer protocols can make the wireless access networks greener directly since the reduction of the communication overheads can effectively suppress the energy expenses.

On the other hand, in the data link layer protocol design, the system throughput enhancement under the same power consumption can be considered an indirect way to realize the green wireless access networks since the power expenses can be degraded for transmitting the same amount of information. As a result, the greedy fast-shift block acknowledgement (GFS) mechanism is proposed for enhancing the system throughput by reducing the inefficiency caused by the slow sliding of the conventional acknowledgement window. Thanks to the fast shifting property of the acknowledgement window in our proposed GFS scheme, significant throughput enhancement can therefore be observed. In addition to the indirect method of enhancing the system throughput, the direct method for achieving the green concept should be the power-saving scheduling algorithm, which can arrange the packets with the proper transmission schedules, suppressing the total energy consumption. The frame aggregation-based power-saving (FAPS) scheduling algorithm is therefore proposed for this type of direct methods by aggregating several under-utilized frames into fully-utilized ones. The quality-of-service (QoS) of each data packet can still be maintained in our proposed FAPS algorithm. In addition, the optimality on the minimum number of listen frames in the proposed FAPS algorithm is also provided under the stepwise grant space set and further verified via the correctness proof. Finally, more number of system frames can be in the sleep mode, which consumes less energy compared to the active mode. With our proposed software protocol design and implementation in the network layer and the data link layer, the green wireless access networks can therefore be achieved.

The rest of this chapter is organized as follows: The core issues of this dissertation and the corresponding problems for achieving the green wireless access networks are illustrated

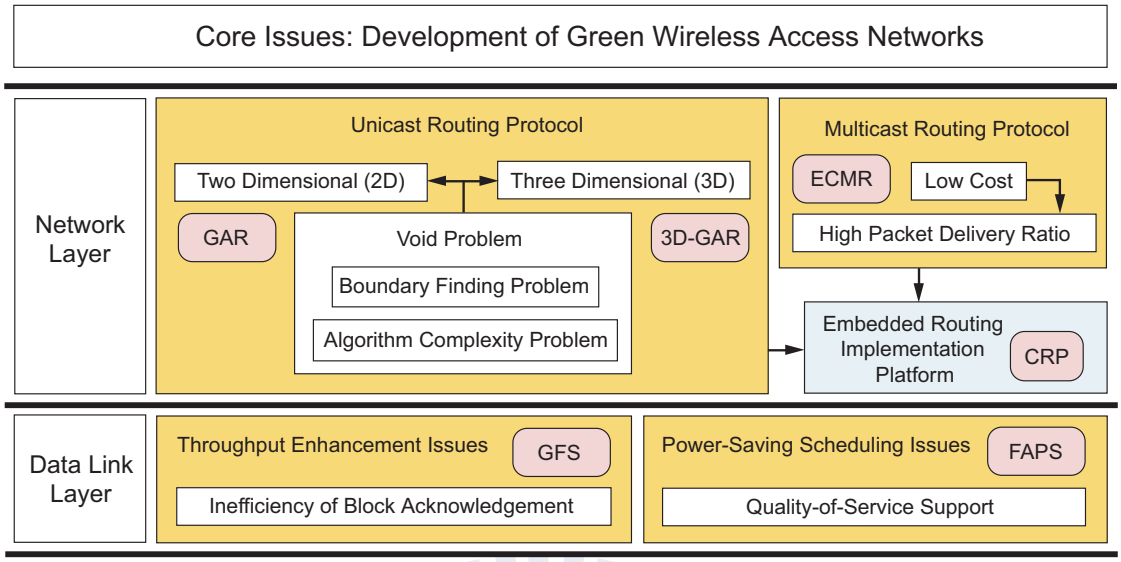

Figure 1.2: The core issues and the corresponding problems with solutions in this dissertation.

in Section 1.2. Section 1.3 further describes the contribution of this dissertation; while the organization of this dissertation is finally provided in Section 1.4.

1.2 Problem Statement

The core issues in this dissertation are on the software techniques for developing the green wireless access network in the aspects of the network layer and the data link layer protocols, which can be identified as follows:

Problem 1 (Core Issues). *How to develop the green wireless access network in terms of the protocol design and implementation within the network layer and the data link layer?*

In the network layer unicast routing protocol design, for fulfilling the green concept defined in Definition 1 and solving the core issues stated in Problem 1, the greedy forwarding (GF) technique [4] is therefore considered a superior scheme mainly due to its extremely low routing overhead. Based on the current one-hop neighbor information, the GF algorithm will always forward packets to the node which is the closest to the destination. However, the void problem [5], which makes the GF technique unable to find its next closer hop to the destination, will cause the GF algorithm failing to guarantee the delivery of data packets. The void problem not

only exists in the two-dimensional (2D) plane but also occurs in the three-dimensional (3D) space. Different recovery techniques should be considered to guarantee the packet delivery and retain the merits of low routing overhead. The formal definitions of the void problem under the 2D and 3D environments can be found in Chapter 2 and Chapter 3, respectively. In addition to the void problem, the implementation related issues, such as the boundary finding problem and the algorithm complexity problem, will be further stated in the corresponding chapters.

On the other hand, the multicast routing protocol should also be considered in the development of the green wireless access networks due to the popularity of the multiple host applications, such as the instant messaging and the online games. Therefore, how to provide low energy consumption and high packet delivery ratio becomes another issue in the green multicast protocol design. In the wired networks, the Steiner tree [6] technique is regarded as the optimal approach for constructing the multicast structure for specific senders and receivers. However, this technique can not be directly applied to the wireless environment due to the wireless broadcast nature. Different techniques should further be investigated. Moreover, the lack of a friendly embedded implementation platform is another issue for realizing the routing protocols. If there exists such an embedded platform for the performance evaluation and the field experiments on the routing protocols, the development of the green wireless access networks will further be boosted and accelerated.

Subsequently, in the data link layer protocol design, two techniques can be deemed as the fulfillment of the green concept defined in Definition 1. The first one is the indirect method which enhances the overall system throughput since the same information can be transmitted with less power consumption. The existing inefficiency problem has been found in the conventional block acknowledgement mechanism due to its slow movement of the acknowledgement window. The other one is the direct method of the power-saving scheduling algorithm for achieving the aforementioned green concept. The power-saving scheduling algorithm should arrange the packets with the proper transmission schedules, reducing the total number of high power consumption active frames. Moreover, the QoS for each data packet must be guaranteed, i.e., the packet arrangement can not violate the QoS requirements. The respec-

tive protocols for these two types of techniques should be proposed collectively for enhancing the performance of the green wireless access networks. Finally, the core issues and the corresponding problems for this dissertation are illustrated and summarized in Fig. 1.2, which completes the description of problem statement.

1.3 Contribution

The contribution of this dissertation can be described in Fig. 1.2 as follows. In the unicast routing for achieving the green wireless access network, a greedy anti-void routing (GAR) protocol is proposed to resolve the void problem due to the low-overhead green concept-based GF algorithm under the 2D environment. The proposed GAR protocol can guarantee the packet delivery with increased routing efficiency based on the unit disk graph (UDG) settings. According to the proposed GAR protocol, a rolling-ball UDG boundary traversal (RUT) scheme is proposed to resolve the boundary finding problem. The network boundary can therefore be obtained and utilized to escape from the void region where the void problem occurs, guaranteeing the packet delivery. In the GAR realization, the boundary map (BM) and the indirect map searching (IMS) algorithm for the BM construction are proposed as feasible computer procedures to reduce the impractically high algorithm complexity that is required by the traditional brute-force method.

Furthermore, the associated three additional mechanisms are also exploited to enhance the system performance, including the hop count reduction (HCR), the intersection navigation (IN), and the partial UDG construction (PUC) schemes. The HCR scheme is a short-cutting technique that acquires information by listening to one-hop neighbor's packet forwarding. With the occurrence of the void node, the IN mechanism determines its rolling direction based on the criterion of smallest hop counts (HCs) for the boundary traversal. Moreover, in order to meet the network requirement for the RUT scheme under non-UDG networks, the PUC mechanism is utilized to transform the non-UDG into the UDG setting for the nodes that are adopted for boundary traversal. On the other hand, in the 3D space of the green wireless access networks, a three-dimensional greedy anti-void routing (3D-GAR) protocol is

proposed to solve the void problem under the unit ball graph (UBG) settings. The associated three-dimensional rolling-ball UBG boundary traversal (3D-RUT) scheme is exploited within the 3D-GAR algorithm with the assurance for packet delivery. The proofs of correctness and the enhanced performance gain can be obtained and observed, which shows the achievement of the green wireless access networks in the aspects of the unicast routing protocols.

In the green concept-based low-overhead multicast routing protocol design, an energy conserving multicast routing (ECMR) protocol is proposed to reduce the total number of relaying nodes for the construction of a multicast tree, which can significantly reduce the unnecessary communication overheads. Based on the performance evaluation results, the low overhead and high delivery ratio can be observed. The multicast routing for the green wireless access network can therefore be constructed. Moreover, a component-based routing platform (CRP) for implementing routing protocols is also proposed based on the Linux embedded systems. The software interfaces for the Linux kernel in the proposed CRP system have been well developed, which can let the protocol designers conduct the field experiments more easily. The proposed ECMR protocol is also realized on the proposed CRP system for the performance evaluation and the validation of the proposed CRP implementation platform.

As shown in Fig. 1.2, for the data link layer of the green wireless access networks, two types of methods can be utilized to achieve the green concept, including the throughput enhancement and the power-saving scheduling algorithm. In the throughput enhancement aspect, a greedy fast-shift (GFS) block acknowledgement mechanism is proposed to provide the receiver-defined starting sequence number (SSN), which can both implicitly acknowledge the correctly received packets before the SSN and explicitly identify the correctness information for the packets after the SSN. In order to evaluate the protocol effectiveness, the analytical models for both the proposed GFS scheme and the conventional greedy scheme are also proposed based on the throughput-related performance metric of the window utilization. Compared to the conventional scheme, it is observed from the simulation results that the proposed GFS method can provide better performance and effectively reduce the inefficiency caused by the conventional block acknowledgement scheme owing to its fast-shift behavior on acknowledgement window.

In the power-saving scheduling algorithm aspect for constructing the green wireless access networks, a frame aggregation-based power-saving scheduling (FAPS) algorithm is proposed to achieve the green concept by aggregating multiple under-utilized frames into fully-utilized ones. The scenarios of multiple connections and their QoS constraints are also considered in the algorithm design. The proposed FAPS scheme can maintain the QoS requirements and maximize the number of sleep frames, which can lead to the significant energy saving required by the green concept since the sleep frame has less power consumption. The optimality on the minimum number of listen frames in the proposed FAPS algorithm is also provided under the stepwise grant space set and further verified via the correctness proof. Simulation results validate that the power efficiency metric of sleep frame ratio in the proposed FAPS algorithm can outperform the baseline protocols with tolerable delay. In the end, with the help of these green protocol designs in both the network layer and the data link layer, the core issues of this dissertation in Definition 1 can be alleviated for the green wireless access network.

1.4 Dissertation Organization

The rest of this dissertation is organized as follows: The greedy anti-void routing (GAR) protocol and the associated proofs of correctness are described in Chapter 2. The three-dimensional greedy anti-void routing (3D-GAR) protocol and the corresponding proofs of correctness are provided in Chapter 3. Chapter 4 proposes the component-based routing platform (CRP) and the energy conserving multicast routing (ECMR) protocol. Chapter 5 shows the greedy fast-shift (GFS) block acknowledgement and the corresponding analytical models. The frame aggregation-based power-saving (FAPS) scheduling algorithm is introduced in Chapter 6. Chapter 7 draws the conclusions of this dissertation.

Chapter 2

Greedy Anti-Void Routing Protocol

Chapter Overview

In the network layer unicast protocol design for achieving the green wireless access networks, a greedy anti-void routing (GAR) protocol is proposed in this chapter with the main theme of the wireless sensor network (WSN) since the WSN has stringent requirements on the energy saving issues. Exploiting the boundary finding technique for the unit disk graph (UDG), the proposed GAR protocol solves the void problem, i.e., the unreachability problem, incurred by the low-overhead green concept-based greedy forwarding (GF) algorithm associated with increased routing efficiency. The proposed rolling-ball UDG boundary traversal (RUT) is employed to completely guarantee the delivery of packets from the source to the destination node under the UDG settings. The boundary map (BM) and the indirect map searching (IMS) scheme are proposed as efficient algorithms for the realization of the RUT technique. Moreover, the hop count reduction (HCR) scheme is utilized as a short-cutting technique to reduce the routing hops by listening to the neighbor's traffic; while the intersection navigation (IN) mechanism is proposed to obtained the best rolling direction for boundary traversal with the adoption of shortest path criterion. In order to maintain the network requirement of the proposed RUT scheme under the non-UDG networks, the partial UDG construction (PUC) mechanism is proposed to transform the non-UDG into UDG settings for a portion of nodes that facilitate boundary traversal. These three schemes are incorporated within the GAR

protocol to further enhance the routing performance with reduced communication overhead. The proofs of correctness for the GAR scheme are also given in this chapter. Comparing with the existing localized routing algorithms, the simulation results show that the proposed GAR-based protocols can provide better routing efficiency. These proposed GAR-based protocols can therefore be adopted as the unicast protocols in the green wireless access networks.

2.1 Introduction

A wireless sensor network (WSN) consists of sensor nodes (SNs) with wireless communication capabilities for specific sensing tasks. Due to the limited available resources, efficient design of localized multi-hop routing protocols [7] becomes a crucial subject within the WSNs. How to guarantee delivery of packets is considered an important issue for the localized routing algorithms. The well-known greedy forwarding (GF) algorithm [4] is considered a superior scheme with its low routing overheads. However, the void problem [5], which makes the GF technique unable to find its next closer hop to the destination, will cause the GF algorithm failing to guarantee the delivery of data packets.

Several routing algorithms are proposed to either resolve or reduce the void problem, which can be classified into non-graph-based and graph-based schemes. In the non-graph-based algorithms [8–19], the intuitive schemes as proposed in [8] construct a two-hop neighbor table for implementing the GF algorithm. The network flooding mechanism is adopted within the GRA [9] and PSR [10] schemes while the void problem occurs. There also exist routing protocols that adopt the backtracking method at the occurrence of the network holes (such as GEDIR, [8], DFS [11], and SPEED [12]). The routing schemes as proposed by ARP [13] and LFR [14] memorize the routing path after the void problem takes place. Moreover, other routing protocols (such as PAGER [15], NEAR [16], DUA [17], INF [18], and YAGR [19]) propagate and update the information of the observed void node in order to reduce the probability of encountering the void problem. By exploiting these routing algorithms, however, the void problem can only be either (*i*) partially alleviated or (*ii*) resolved with considerable routing overheads and significant converging time.

On the other hand, there are research works on the design of graph-based routing algorithms [5, 20–27] to deal with the void problem. Several routing schemes as surveyed in [20] adopt the planar graph [28] derived from the unit disk graph (UDG) as their network topologies, such as GPSR [5], GFG [21], Compass Routing II [22], AFR [23], GOAFR [24] GOAFR+ [25], GOAFR++ [20], and GPVFR [26]. For conducting the above planar graph-based algorithms, the planarization technique is required to transform the underlying network graph into the planar graph. The Gabriel graph (GG) [29] and the relative neighborhood graph (RNG) [30] are the two commonly-used localized planarization techniques which abandon some communication links from the UDG for achieving the planar graph. Nevertheless, the usage of the GG and RNG graphs has significant pitfalls due to the removal of critical communication links, leading to longer routing paths to the destination. As shown in Fig. 2.1, the nodes (N_S, N_D) are considered the transmission pair; while N_V represents the node that the void problem occurs. The representative planar graph-based GPSR scheme can not forward the packets from N_V to N_A directly since both the GG and the RNG planarization rules abandon the communication link from N_V to N_A. Considering the GG planarization rule for example, the communication link from N_V to N_A is discarded since both N_J and N_K are located within the forbidden region, which is defined as the smallest disk passing through both N_V and N_A. Therefore, based on the right-hand rule, the resulting path by adopting the GPSR protocol can be obtained as $\{N_S, N_V, N_J, N_K, N_A, N_B, N_X, N_Y, N_Z, N_D\}$. The two unnecessary forwarding nodes N_J and N_K are observed as in Fig. 2.1.

Furthermore, the planar graph-based schemes, e.g., the GPSR and GOAFR++ algorithms, will in general lose their properties of guaranteed packet delivery due to the unexpected network partition within the non-UDG networks. The reason is also attributed to the situations that critical communication links are removed by adopting the GG and RNG planarization techniques. In order to resolve the network partition problem, a cross-link detection protocol (CLDP) is therefore suggested in [31] for planarization of the underlying non-UDG networks. However, for the purposes of both detecting the cross links and planarizing the underlying network, the CLDP planarization will introduce excessive control overhead since all communication links are required to be probed and frequently traversed. Moreover, the

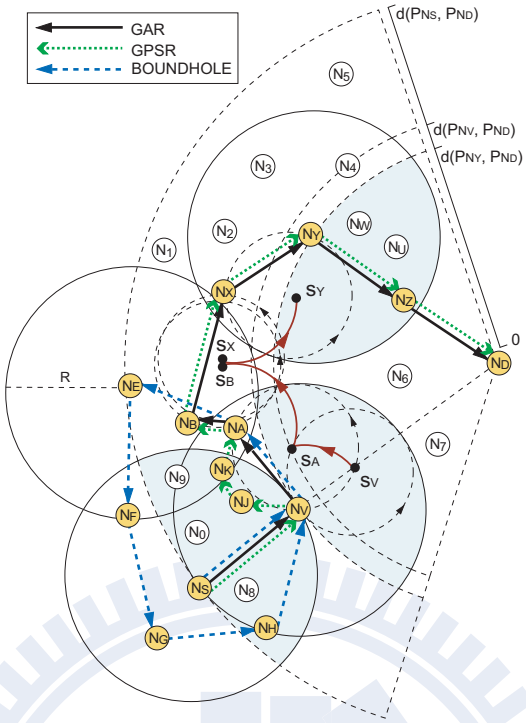

Figure 2.1: The example routing paths constructed by using the proposed GAR protocol and the conventional schemes under the existence of the void problem.

problems of multiple cross links and concurrent probing can further enlarge the total number of communication overhead within the CLDP technique.

Due to the drawbacks of link removal from the planar graph-based algorithms, the adoption of UDG without planarization for the modeling of underlying network is suggested. A representative UDG-based routing scheme, i.e., the BOUNDHOLE algorithm [27], forwards the packets around the network holes by identifying the locations of the holes. However, due to the occurrence of routing loop, the delivery of packets can not be guaranteed in the BOUNDHOLE scheme even if a route exists from the source to the destination node. For example, as shown in Fig. 2.1, it is assumed that the node N_X is located within the transmission range of N_B; while it is considered out of the transmission ranges of nodes N_A and N_E. Based on the minimal sweeping angle criterion within the BOUNDHOLE algorithm, N_A will choose N_E as its next hop node since the counter-clockwise sweeping from N_V to N_E (hinged at N_A) is smaller comparing with that from N_V to N_B. Therefore, the missing communication link from N_B to N_X can be observed, and the resulting path by adopting the BOUNDHOLE

scheme becomes $\{N_S, N_V, N_A, N_E, N_F, N_G, N_H, N_V\}$. It is observed that the undeliverable routing path from the source node N_S is constructed even with un-partitioned network topology. Moreover, two cases of edge intersections within the BOUNDHOLE algorithm [27] result in high routing overhead in order to identify the network holes.

In this chapter, a greedy anti-void routing (GAR) protocol is proposed to guarantee packet delivery with increased routing efficiency by completely resolving the void problem based on the UDG setting. The GAR protocol is designed to be a combination of both the conventional GF algorithm and the proposed rolling-ball UDG boundary traversal (RUT) scheme. The GF scheme is executed by the GAR algorithm without the occurrence of void problem; while the RUT scheme is served as the remedy for resolving the void problem, leading to the assurance for packet delivery. Moreover, the correctness of the proposed GAR protocol is validated via the given proofs. The implementation and computational complexities of the GAR protocol are also explained, including that for the proposed boundary map (BM) and the indirect map searching (IMS) algorithm for the BM construction.

Furthermore, the associated three additional enhanced mechanisms are also exploited, including the hop count reduction (HCR), the intersection navigation (IN), and the partial UDG construction (PUC) schemes. The HCR scheme is a short-cutting technique that acquires information by listening to one-hop neighbor's packet forwarding; while the other short-cutting method as proposed in [32] requires information from two-hop neighbors which can result in excessive control packet exchanges. With the occurrence of void node, the IN mechanism determines its rolling direction based on the criterion of smallest hop counts for boundary traversal. Similar to the CLDP method [31], the IN scheme acquires information over multiple hops in order to process its algorithm. However, it is required for the CLDP technique to traverse all the communication links in the networks; while the IN scheme only exploits a small portion of network links for conducting the boundary traversal. Moreover, in order to meet the network requirement for the RUT scheme under non-UDG network, the PUC mechanism is utilized to transform the non-UDG into the UDG setting for the nodes that are adopted for boundary traversal.

By adopting these three enhanced schemes, both the routing efficiency and the communi-

cation overhead of the original GAR algorithm can further be improved. The performance of the proposed GAR protocol and the version with the enhanced mechanisms (denoted as the GAR-E algorithm) is evaluated via simulations under both the UDG network for ideal case and the non-UDG setting for realistic scenario. The simulation results show that the GAR-based schemes can both guarantee the delivery of data packets and pertain better routing performance under the UDG network. On the other hand, comparing with the other existing schemes, feasible routing performance with reduced communication overhead can be provided by the GAR-based algorithms within the non-UDG network environment.

The remainder of this chapter is organized as follows. Section 2.2 describes the network model and the problem statement. The proposed GAR protocol is explained in Section 2.3; while Section 2.4 provides the practical realization of the GAR algorithm. Section 2.5 exploits the three enhanced mechanisms, including the hop count reduction (HCR), the intersection navigation (IN), and the partial UDG construction (PUC) mechanisms. The performance of the GAR-based protocols is evaluated and compared in Section 2.6. Section 2.7 summarizes this chapter.

2.2 Network Model and Problem Statement

Considering a set of SNs $\mathbf{N} = \{N_i \,|\, \forall\, i\}$ within a two-dimensional Euclidean plane, the locations of the set $\mathbf{N}$, which can be acquired by their own positioning systems, are represented by the set $\mathbf{P} = \{P_{N_i} \,|\, P_{N_i} = (x_{N_i}, y_{N_i}), \forall i\}$. It is assumed that all the SNs are homogeneous and equipped with omnidirectional antennas. The set of closed disks defining the transmission ranges of $\mathbf{N}$ is denoted as $\overline{\mathbf{D}} = \{\overline{D}(P_{N_i}, R) \,|\, \forall\, i\}$, where $\overline{D}(P_{N_i}, R) = \{x \,|\, \|x - P_{N_i}\| \leq R, \forall\, x \in \mathbb{R}^2\}$. It is noted that P_{N_i} is the center of the closed disk with R denoted as the radius of the transmission range for each N_i. Therefore, the network model for the WSNs can be represented by a UDG as $G(\mathbf{P}, \mathbf{E})$ with the edge set $\mathbf{E} = \{E_{ij} \,|\, E_{ij} = (P_{N_i}, P_{N_j}), P_{N_i} \in \overline{D}(P_{N_j}, R), \forall\, i \neq j\}$. The edge E_{ij} indicates the unidirectional link from P_{N_i} to P_{N_j} whenever the position P_{N_i} is within the closed disk region $\overline{D}(P_{N_j}, R)$. Moreover, the one-hop neighbor

table for each N_i is defined as

$$\mathbf{T}_{N_i} = \{[ID_{N_k}, P_{N_k}] \mid P_{N_k} \in \overline{D}(P_{N_i}, R), \forall\, k \neq i\}, \tag{2.1}$$

where ID_{N_k} represents the designated identification number for N_k. In the greedy forwarding (GF) algorithm, it is assumed that the source node N_S is aware of the location of the destination node N_D. If N_S wants to transmit packets to N_D, it will choose the next hop node from its $\mathbf{T}_{N_S}$ which (i) has the shortest Euclidean distance to N_D among all the SNs in $\mathbf{T}_{N_S}$ and (ii) is located closer to N_D compared to the distance between N_S and N_D (e.g., N_V as in Fig. 2.1). The same procedure will be performed by the intermediate nodes (such as N_V) until N_D is reached. However, the GF algorithm will be inclined to fail due to the occurrences of voids even though some routing paths exist from N_S to N_D. The void problem is defined as follows.

Problem 2 (Void Problem). *The greedy forwarding (GF) algorithm is exploited for packet delivery from N_S to N_D. The void problem occurs while there exists a void node (N_V) in the network such that no neighbor of N_V is closer to the destination as*

$$\{P_{N_k} \mid d(P_{N_k}, P_{N_D}) < d(P_{N_V}, P_{N_D}), \forall\, P_{N_k} \in \mathbf{T}_{N_V}\} = \emptyset, \tag{2.2}$$

where $d(x, y)$ represents the Euclidean distance between x and y. $\mathbf{T}_{N_V}$ is the one-hop neighbor table of N_V.

2.3 Proposed Greedy Anti-Void Routing (GAR) Protocol

The objective of the GAR protocol is to resolve the void problem such that the packet delivery from N_S to N_D can be guaranteed. Before diving into the detail formulation of the proposed GAR algorithm, an introductory example is described in order to facilitate the understanding of the GAR protocol. As shown in Fig. 2.1, the data packets initiated from the source node N_S to the destination node N_D will arrive in N_V based on the GF algorithm. The void problem occurs as N_V receives the packets, which leads to the adoption of the RUT scheme

as the forwarding strategy of the GAR protocol. A circle is formed by centering at $\boldsymbol{s}_V$ with its radius being equal to half of the transmission range $R/2$. The circle is hinged at N_V and starts to conduct counter-clockwise rolling until an SN has been encountered by the boundary of the circle, i.e., N_A as in Fig. 2.1. Consequently, the data packets in N_V will be forwarded to the encountered node N_A.

Subsequently, a new equal-sized circle will be formed, which is centered at $\boldsymbol{s}_A$ and hinged at node N_A. The counter-clockwise rolling procedure will be proceeded in order to select the next hop node, i.e., N_B in this case. Similarly, same process will be performed by other intermediate nodes (such as N_B and N_X) until the node N_Y is reached, which is considered to have a smaller distance to N_D than that of N_V to N_D. The conventional GF scheme will be resumed at N_Y for delivering data packets to the destination node N_D. As a consequence, the resulting path by adopting the GAR protocol becomes $\{N_S, N_V, N_A, N_B, N_X, N_Y, N_Z, N_D\}$. In the following subsections, the formal description of the RUT scheme will be described in Subsection 2.3.1; while the detail of the GAR algorithm is explained in Subsection 2.3.2. The proofs of correctness of the GAR protocol are given in Subsection 2.3.3.

2.3.1 Rolling-ball UDG Boundary Traversal (RUT) Scheme

The RUT scheme is adopted to solve the boundary finding problem, and the combination of the GF and the RUT scheme (i.e., the GAR protocol) can resolve the void problem, leading to the guaranteed packet delivery. The definition of boundary and the problem statement are described as follows.

Definition 2 (Boundary). *If there exists a set* $\mathbf{B} \subseteq \mathbf{N}$ *such that (i) the nodes in* $\mathbf{B}$ *form a simple unidirectional ring and (ii) the nodes located on and inside the ring are disconnected with those outside of the ring,* $\mathbf{B}$ *is denoted as the boundary set and the unidirectional ring is called a boundary.*

Problem 3 (Boundary Finding Problem). *Given a UDG* $G(\mathbf{P}, \mathbf{E})$ *and the one-hop neighbor tables* $\mathbf{T} = \{\mathbf{T}_{N_i} \,|\, \forall\, N_i \in \mathbf{N}\}$*, how can a boundary be obtained by exploiting the distributed computing techniques?*

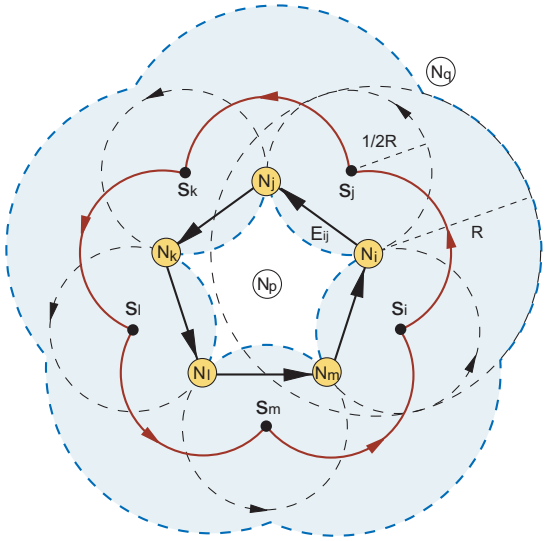

Figure 2.2: The rolling-ball UDG boundary traversal (RUT) scheme.

There are three phases within the RUT scheme, including the initialization, the boundary traversal, and the termination phases.

2.3.1.1 Initialization Phase

No algorithm can be executed without the algorithm-specific trigger event. The trigger event within the RUT scheme is called the starting point (SP). The RUT scheme can be initialized from any SP, which is defined as follows.

Definition 3 (Rolling Ball). *Given $N_i \in \mathbf{N}$, a rolling ball $RB_{N_i}(\boldsymbol{s}_i, R/2)$ is defined by (i) a rolling circle hinged at P_{N_i} with its center point at $\boldsymbol{s}_i \in \mathbb{R}^2$ and the radius equal to $R/2$; and (ii) there does not exist any $N_k \in \mathbf{N}$ located inside the rolling ball as $\{RB^{\sim}_{N_i}(\boldsymbol{s}_i, R/2) \cap \mathbf{N}\} = \emptyset$, where $RB^{\sim}_{N_i}(\boldsymbol{s}_i, R/2)$ denotes the open disk within the rolling ball.*

Definition 4 (Starting Point). *The starting point of N_i within the RUT scheme is defined as the center point $\boldsymbol{s}_i \in \mathbb{R}^2$ of $RB_{N_i}(\boldsymbol{s}_i, R/2)$.*

As shown in Fig. 2.2, each node N_i can verify if there exists an SP since the rolling ball $RB_{N_i}(\mathbf{s}_i, R/2)$ is bounded by the transmission range of N_i. According to Definition 4, the SPs should be located on the circle centered at P_{N_i} with a radius of $R/2$. As will be proven

in Lemmas 1 and 2, all the SPs will result in the red solid flower-shaped arcs as in Fig. 2.2. It is noticed that there should always exist an SP while the void problem occurs within the network, which will be explained in Subsection 2.3.2. At this initial phase, the location $\boldsymbol{s}_i$ can be selected as the SP for the RUT scheme.

2.3.1.2 Boundary Traversal Phase

Given $\boldsymbol{s}_i$ as the SP associated with its $RB_{N_i}(\mathbf{s}_i, R/2)$ hinged at N_i, either the counter-clockwise or clockwise rolling direction can be utilized. As shown in Fig. 2.2, $RB_{N_i}(\boldsymbol{s}_i, R/2)$ is rolled counter-clockwise until the next SN is reached (i.e., N_j in Fig. 2.2). The unidirectional edge $E_{ij} = (P_{N_i}, P_{N_j})$ can therefore be constructed. A new SP and the corresponding rolling ball hinged at N_j (i.e., $\boldsymbol{s}_j$ and $RB_{N_j}(\mathbf{s}_j, R/2)$) will be assigned, and consequently the same procedure can be conducted continuously.

2.3.1.3 Termination Phase

The termination condition for the RUT scheme happens while the first unidirectional edge is revisited. As shown in Fig. 2.2, the RUT scheme will be terminated if the edge E_{ij} is visited again after the edges E_{ij}, E_{jk}, E_{kl}, E_{lm}, and E_{mi} are traversed. The boundary set initiated from N_i can therefore be obtained as $\mathbf{B} = \{N_i, N_j, N_k, N_l, N_m\}$.

2.3.2 Detail Description of Proposed GAR Protocol

As shown in Fig. 2.1, the packets are intended to be delivered from N_S to N_D. N_S will select N_V as the next hop node by adopting the GF algorithm. However, the void problem prohibits N_V to continue utilizing the same GF algorithm for packet forwarding. The RUT scheme is therefore employed by assigning an SP (i.e., $\boldsymbol{s}_V$) associated with the rolling ball $RB_{N_V}(\boldsymbol{s}_V, R/2)$ hinged at N_V. As illustrated in Fig. 2.1, $\boldsymbol{s}_V$ can be chosen to locate on the connecting line between N_V and N_D with $R/2$ away from N_V. It is noticed that there always exists an SP for the void node (N_V) since there is not supposed to have any SN located within the blue-shaded region (as in Fig. 2.1), which is large enough to satisfy the requirements as in Definitions 3 and 4. The RUT scheme is utilized until N_Y is reached (after traversing

N_A, N_B, and N_X). Since $d(P_{N_Y}, P_{N_D}) < d(P_{N_V}, P_{N_D})$, the GF algorithm is resumed at N_Y and the next hop node will be selected as N_Z. The route from N_S to N_D can therefore be constructed for packet delivery. Moreover, if there does not exist a node N_Y such that $d(P_{N_Y}, P_{N_D}) < d(P_{N_V}, P_{N_D})$ within the boundary traversal phase, the RUT scheme will be terminated after revisiting the edge E_{VA}. The result indicates that there does not exist a routing path between N_S and N_D.

2.3.3 Proof of Correctness

In this subsection, the correctness of the RUT scheme is proven in order to solve Problem 3; while the GAR protocol is also proven for resolving the void problem (i.e., Problem 2) in order to guarantee packet delivery.

Fact 1. *A simple closed curve is formed by traversing a point on the border of a closed filled two-dimensional geometry with fixed orientation.*

Lemma 1. *All the SPs within the RUT scheme form the border of a shape that results from overlapping the closed disks $\overline{D}(P_{N_i}, R/2)$ for all $N_i \in \mathbf{N}$, and vice versa.*

Proof: Based on Definitions 3 and 4, the set of SPs can be obtained as $\mathbf{S} = \mathbf{R_1} \cap \mathbf{R_2} = \{\boldsymbol{s}_i \,|\, \|\boldsymbol{s}_i - P_{N_i}\| = R/2, \exists N_i \in \mathbf{N}, \boldsymbol{s}_i \in \mathbb{R}^2\} \cap \{\boldsymbol{s}_j \,|\, \|\boldsymbol{s}_j - P_{N_j}\| \geq R/2, \forall N_j \in \mathbf{N}, \boldsymbol{s}_j \in \mathbb{R}^2\}$ by adopting the (i) and (ii) rules within Definition 3. On the other hand, the border of the resulting shape from the overlapped closed disks $\overline{D}(P_{N_i}, R/2)$ for all $N_i \in \mathbf{N}$ can be denoted as $\mathbf{\Omega} = \mathbf{Q_1} - \mathbf{Q_2} = \bigcup_{N_i \in \mathbf{N}} C(P_{N_i}, R/2) - \bigcup_{N_i \in \mathbf{N}} D(P_{N_i}, R/2)$, where $C(P_{N_i}, R/2)$ and $D(P_{N_i}, R/2)$ represent the circle and the open disk centered at P_{N_i} with a radius of $R/2$ respectively. It is obvious to notice that $\mathbf{R_1} = \mathbf{Q_1}$ and $\mathbf{R_2} = \mathbf{Q_2'}$, which result in $\mathbf{S} = \mathbf{\Omega}$. It completes the proof. □

Lemma 2. *A simple closed curve is formed by the trajectory of the SPs.*

Proof: Based on Lemma 1, the trajectory of the SPs forms the border of the overlapped closed disks $\overline{D}(P_{N_i}, R/2)$ for all $N_i \in \mathbf{N}$. Moreover, the border of a closed filled two-dimensional

geometry is a simple closed curve according to Fact 1. Therefore, a simple closed curve is constructed by the trajectory of the SPs, e.g., the solid flower-shaped closed curve as in Fig. 2.2. It completes the proof. □

Theorem 1. *The boundary finding problem (Problem 3) is resolved by the RUT scheme.*

Proof: Based on Lemma 2, the RUT scheme can draw a simple closed curve by rotating the rolling balls $RB_{N_i}(\boldsymbol{s}_i, R/2)$ hinged at P_{N_i} for all $N_i \in \mathbf{N}$. The closed curve can be divided into arc segments $S(\boldsymbol{s}_i, \boldsymbol{s}_j)$, where $\boldsymbol{s}_i$ is the starting SP associated with N_i; and $\boldsymbol{s}_j$ is the anchor point while rotating the $RB_{N_i}(\boldsymbol{s}_i, R/2)$ hinged at P_{N_i}. The arc segments $S(\boldsymbol{s}_i, \boldsymbol{s}_j)$ can be mapped into the unidirectional edges $E_{ij} = (P_{N_i}, P_{N_j})$ for all $N_i, N_j \in \mathbf{U}$, where $\mathbf{U} \subseteq \mathbf{N}$. Due to the one-to-one mapping between $S(\boldsymbol{s}_i, \boldsymbol{s}_j)$ and E_{ij}, a simple unidirectional ring is constructed by E_{ij} for all $N_i, N_j \in \mathbf{U}$.

According to the RUT scheme, there does not exist any $N_i \in \mathbf{N}$ within the area traversed by the rolling balls, i.e., inside the light blue region as in Fig. 3. For all $N_p \in \mathbf{N}$ located inside the simple unidirectional ring, the smallest distance from N_p to N_q, which is located outside of the ring, is greater than the SN's transmission range R. Therefore, there does not exist any $N_p \in \mathbf{N}$ inside the simple unidirectional ring that can communicate with $N_q \in \mathbf{N}$ located outside of the ring. Based on Definition 2, the set $\mathbf{U}$ is identical to the boundary set, i.e., $\mathbf{U} = \mathbf{B}$. It completes the proof. □

Theorem 2. *The void problem (Problem 2) in unit disk graphs is solved by the GAR protocol with guaranteed packet delivery.*

Proof: With the existence of the void problem occurred at the void node N_V, the RUT scheme is utilized by initiating an SP ($\boldsymbol{s}_V$) with the rolling ball $RB_{N_V}(\boldsymbol{s}_V, R/2)$ hinged at N_V. The RUT scheme within the GAR protocol will conduct boundary (i.e., the set $\mathbf{B}$) traversal under the condition that $d(P_{N_i}, P_{N_D}) \geq d(P_{N_V}, P_{N_D})$ for all $N_i \in \mathbf{B}$. If the boundary within the underlying network is completely traveled based on Theorem 1, it indicates that the SNs inside the boundary (e.g., N_V) are not capable of communicating with those located outside of the boundary (e.g., N_D). The result shows that there does not exist a route from the void

node (N_V) to the destination node (N_D), i.e., the existence of network partition. On the other hand, if there exists a node N_Y such that $d(P_{N_Y}, P_{N_D}) < d(P_{N_V}, P_{N_D})$ (as shown in Fig. 2), the GF algorithm will be adopted within the GAR protocol to conduct data delivery toward the destination node N_D. Therefore, the GAR protocol solves the void problem with guaranteed packet delivery, which completes the proof. □

2.4 Realization of Proposed GAR Protocol

The implementation of the proposed GAR protocol is explained in this section. The format of the one-hop neighbor table $\mathbf{T}_{N_i}$ as defined in (2.1) is realized for the implementation purpose. $\mathbf{T}_{N_i}$ is considered a major information source in the localized routing protocols, which can be obtained via the neighbor information acquisition [33]. It is noticed that the one-hop neighbor table $\mathbf{T}_{N_i}$ is considered stable while N_i is making its next-hop decision, i.e., $\mathbf{T}_{N_i}$ remains unchanged while N_i is determining the next-hop SN for packet transmission. Subsections 2.4.1 and 2.4.2 describe the implementation aspect of the GAR algorithm which consists of the GF and the RUT schemes. The proofs of correctness are illustrated in Subsection 2.4.3.

2.4.1 Implementation of GF Scheme

As described in Section 2.2, the GF scheme is considered a straightforward algorithm that only requires the implementation of the one-hop neighbor table $\mathbf{T}_{N_i}$. Owing to the linear search of $\mathbf{T}_{N_i}$, it is obvious that the time complexity of the GF algorithm is $O(m)$, where m denotes the total number of neighbors in $\mathbf{T}_{N_i}$. Likewise, the space complexity of the GF scheme is also observed to be $O(m)$ since the size of $\mathbf{T}_{N_i}$ is dependent to the number of neighbors m.

2.4.2 Implementation of RUT Scheme

2.4.2.1 Algorithm Complexity Problem

As mentioned in Subsection 2.3.2, the GAR protocol changes its routing mode into the RUT scheme while the void problem occurs at N_V. The boundary traversal phase is conducted by

assigning an SP (i.e., $\boldsymbol{s}_V$ as shown in Fig. 2.1) associated with the rolling ball $RB_{N_V}(\boldsymbol{s}_V, R/2)$ hinged at N_V. While there is no doubt regarding the description of boundary traversal, there can be considerable efforts required in order to realize the continuous rolling ball mechanism. A brute-force method can be adopted as a potential solution by rotating the rolling ball incrementally and verifying if a new SN has been encountered at each computing step. However, an infinite number of computational runs are required by adopting the brute-force method, which is considered impractical for realistic computing machines. Therefore, a feasible and efficient mechanism for the boundary traversal should be obtained in order to overcome the computational limitation.

2.4.2.2 Concept of Boundary Map

In order to resolve the implementation issue of the boundary traversal as mentioned above, a new parameter called boundary map (denoted as $\mathbf{M}_{N_i}$ for each N_i) is introduced in this subsection. Moreover, the boundary map $\mathbf{M}_{N_i}$ is mainly derived from the one-hop neighbor table $\mathbf{T}_{N_i}$ via the indirect map searching (IMS) method as shown in Algorithm 1. Instead of diving into the IMS algorithm, the functionality of $\mathbf{M}_{N_i}$ is first explained.

The purpose of the boundary map $\mathbf{M}_{N_i}$ is to provide a set of direct mappings between the input SNs and their corresponding output SNs w.r.t. N_i. Based on Theorem 1, the two adjacent communication links formed by the input node, the node N_i, and the corresponding output node within the RUT scheme consist part of the network boundary. Therefore, the direct mappings between the input SNs and their corresponding output SNs w.r.t. N_i lead to the so-called boundary map. It is noted that the time complexity for querying the output SN of a specific input SN via the boundary map $\mathbf{M}_{N_i}$ can be observed as $O(1)$ owing to the nature of direct mapping. An example is shown in Fig. 2.3 to illustrate the functionality of $\mathbf{M}_{N_i}$. Based on Definition 3, the rolling balls hinged at N_i can be constructed by rotating the dashed circle counter-clockwise from N_1 to N_2. The SPs associated with the rolling balls (from Definition 4) result in the arc segment $S_{N_i}^{SP}(P_1^L, P_2^R)$ between the endpoints P_1^L and P_2^R, i.e., the dashed arc segment as in Fig. 2.3. Similarly, the arc segment $S_{N_i}^{SP}(P_2^L, P_3^R)$ can be constructed by rotating the rolling balls (hinged at N_i) counter-clockwise from N_2 to N_3.

Algorithm 1: *Indirect Map Searching (IMS) Algorithm*

Data: $R, P_{N_i}, \mathbf{T}_{N_i}$
Result: $\mathbf{M}_{N_i}, \mathbf{L}_{N_i}$
begin
  $\mathbf{M}_{N_i} \leftarrow null$
  $\mathbf{L}_{N_i} \leftarrow null$
  if $\mathbf{T}_{N_i} \neq \emptyset$ **then**
    foreach $(id_{N_j}, P_{N_j}) \in \mathbf{T}_{N_i}$ **do**
      compute $S^{\overline{SP}}_{N_i \circ N_j}(P_A, P_B)$ using R, P_{N_i}, and P_{N_j}
      $\Psi(P_A) \leftarrow [id_{N_j}, RIGHT, angle(P_A, P_{N_i}), FALSE, \Psi(P_B)]$
      $\Psi(P_B) \leftarrow [id_{N_j}, LEFT, angle(P_B, P_{N_i}), FALSE, \Psi(P_A)]$
      wrap and insert $\Psi(P_A)$ and $\Psi(P_B)$ into $\mathbf{L}_{N_i}$
    end
    $sort(\mathbf{L}_{N_i})$
    foreach $\ell_A \in \mathbf{L}_{N_i}$ ***and*** $\ell_A.flag() = RIGHT$ **do**
      $\ell_B \leftarrow \ell_A.counterpart()$
      foreach $\ell_C \in \mathbf{L}_{N_i}$ *located between* $[\ell_A, \ell_B]$ **do**
        set $Color$ for ℓ_C
      end
    end
    foreach $\ell_B \in \mathbf{L}_{N_i}$ ***and*** $\ell_B.flag() = LEFT$ **do**
      if $\ell_B.color() = FALSE$ **then**
        $\ell_C \leftarrow \ell_B.next()$
        while $\ell_C.flag() = LEFT$ **do**
          $\ell_C \leftarrow \ell_C.next()$
        end
        get the SNs N_B and N_C from ℓ_B and ℓ_C
        create the direct mapping from N_B to N_C
        insert the mapping $N_B \rightarrow N_C$ into $\mathbf{M}_{N_i}$
      end
    end
  end
end

Notation	Description
R	Maximum Communication Distance
P_{N_i}	Position of N_i
$\mathbf{T}_{N_i}$	One-hop Neighbor Table of N_i
$\mathbf{M}_{N_i}$	Boundary Map of N_i
$\mathbf{L}_{N_i}$	Circular Doubly-linked List of N_i
(id_{N_j}, P_{N_j})	ID and Position of a Neighbor N_j
$S^{\overline{SP}}_{N_i \circ N_j}(P_A, P_B)$	Neighbor-related Non-SP Arc Segment
$\Psi(P_A), \Psi(P_B)$	Endpoint Entries of $S^{\overline{SP}}_{N_i \circ N_j}(P_A, P_B)$
ℓ_A, ℓ_B, ℓ_C	List Items of $\mathbf{L}_{N_i}$

Table 2.1: Notations for IMS Algorithm

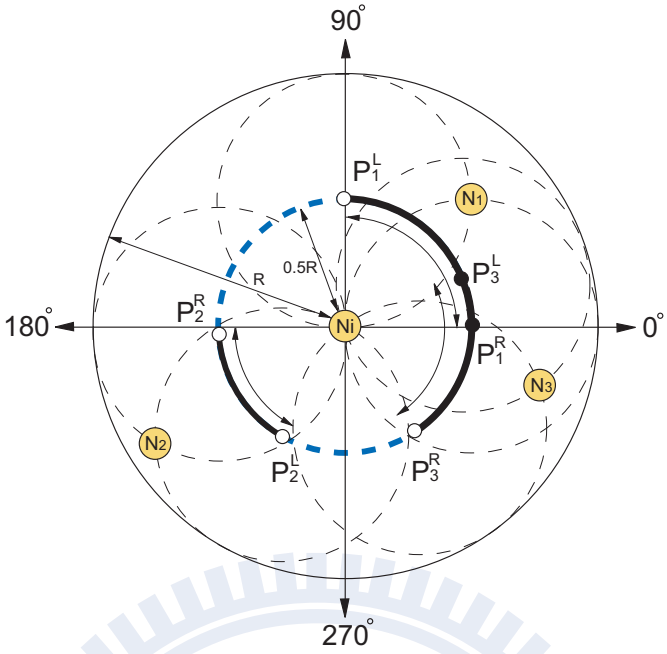

Figure 2.3: The converged SP and non-SP arc segments w.r.t. N_i and the boundary map.

Based on the description as above, the following definitions are introduced.

Definition 5 (SP and Non-SP Arc Segments). *Given $N_i \in \mathbf{N}$ and a pair of points (P_A, P_B) on the circle (centered at P_{N_i} with a radius of $R/2$), an SP arc segment $S^{SP}_{N_i}(P_A, P_B)$ of N_i is defined by the arc from P_A to P_B counter-clockwise where all points on this arc segment are SPs. Likewise, a non-SP arc segment $S^{\overline{SP}}_{N_i}(P_A, P_B)$ of N_i is defined by the endpoint-excluding arc from P_A to P_B counter-clockwise where all points on this arc segment are not SPs.*

Definition 6 (Converged SP and Non-SP Arc Segments). *Given an SP arc segment $S^{SP}_{N_i}(P_A,\ P_B)$, it is regarded as a converged SP arc segment if there does not exist any SP arc segment $S^{SP}_{N_i}(P_J, P_K)$ such that $S^{SP}_{N_i}(P_A, P_B) \subset S^{SP}_{N_i}(P_J, P_K)$. Similarly, a non-SP arc segment $S^{\overline{SP}}_{N_i}(P_A, P_B)$ is considered as a converged non-SP arc segment if there exists no other non-SP arc segment $S^{\overline{SP}}_{N_i}(P_J, P_K)$ such that $S^{\overline{SP}}_{N_i}(P_A, P_B) \subset S^{\overline{SP}}_{N_i}(P_J, P_K)$.*

It is noticed that the converged arc segments are defined to represent the combined arc segments, e.g., the converged non-SP arc segment $S^{\overline{SP}}_{N_i}(P_3^R, P_1^L)$ is formed by overlapping the

non-SP segments $S_{N_i}^{\overline{SP}}(P_3^R, P_3^L)$ and $S_{N_i}^{\overline{SP}}(P_1^R, P_1^L)$ as shown in Fig. 2.3. As will be proven in Theorem 3, all incoming packets to N_i that are acquired from its neighbor node N_1 (which induces the rightmost endpoint P_1^L of the converged SP arc segment $S_{N_i}^{SP}(P_1^L, P_2^R)$) will be forwarded to its neighbor node N_2 (which results in the leftmost endpoint P_2^R of the same converged SP arc segment) under the counter-clockwise rolling direction. Consequently, if all the converged SP arc segments of N_i can be obtained, the direct mappings between the input SNs and their corresponding output SNs w.r.t. N_i can also be constructed. As shown in Fig. 2.3, there exist two converged SP arc segments $S_{N_i}^{SP}(P_1^L, P_2^R)$ and $S_{N_i}^{SP}(P_2^L, P_3^R)$, where $S_{N_i}^{SP}(P_1^L, P_2^R)$ is constructed by the input SN N_1 and the corresponding output SN N_2 and $S_{N_i}^{SP}(P_2^L, P_3^R)$ is established by the input N_2 and the output N_3. As a result, the boundary map w.r.t. N_i can be obtained as $\mathbf{M}_{N_i} = \{(N_1 \rightarrow N_2), (N_2 \rightarrow N_3)\}$. Therefore, all packets from N_1 will be forwarded to N_2; while those from N_2 will be relayed to N_3 according to the boundary map.

2.4.2.3 Construction of Boundary Map

As mentioned above, the boundary map $\mathbf{M}_{N_i}$ can be constructed via the converged SP arc segments w.r.t. N_i. However, it is observed to be a difficult task for obtaining the converged SP arc segments directly in realization. An indirect map searching (IMS) algorithm is proposed in this subsection in order to acquire the boundary map for implementation. The definition of the neighbor-related non-SP arc segment and two associated properties are first introduced.

Definition 7 (Neighbor-related Non-SP Arc Segment). *Given a non-SP arc segment $S_{N_i}^{\overline{SP}}(P_A, P_B)$ of N_i, if there exists $N_j \in \mathbf{N}$ as a neighbor node of N_i such that an arc segment of $C(P_{N_i}, R/2)$ which lies inside the closed disk $\overline{D}(P_{N_j}, R/2)$ is identical to $S_{N_i}^{\overline{SP}}(P_A, P_B)$, this segment $S_{N_i}^{\overline{SP}}(P_A, P_B)$ is called a neighbor-related non-SP arc segment $S_{N_i \circ N_j}^{\overline{SP}}(P_A, P_B)$ distinguished by N_j.*

Two properties related to the SP and non-SP arc segments are described as follows.

Property 1. *The circle $C(P_{N_i}, R/2)$ centered at P_{N_i} with a radius of $R/2$ is entirely composed by all the converged SP and non-SP arc segments of N_i.*

Proof: Based on Definitions 3 and 4, it can be observed that each point on the circle $C(P_{N_i}, R/2)$ must either be an SP or a non-SP. A number of adjacent SPs on $C(P_{N_i}, R/2)$ will establish an SP arc segment w.r.t. N_i; while there must exist the largest number of adjacent SPs such that the underlying SP arc segment is a converged SP arc segments w.r.t. N_i. Therefore, all the adjacent SPs on $C(P_{N_i}, R/2)$ will result in converged SP arc segments w.r.t. N_i. Similarly, all the adjacent non-SPs on $C(P_{N_i}, R/2)$ must be aggregated into converged non-SP arc segments w.r.t. N_i. On the other hand, the circle $C(P_{N_i}, R/2)$ is entirely composed by the SPs and non-SPs corresponding to N_i. Consequently, all the converged SP and non-SP arc segments of N_i will construct the entire circle $C(P_{N_i}, R/2)$. It completes the proof. □

Property 2. *The union of all the neighbor-related non-SP arc segments w.r.t. N_i is equivalent to the union of all the converged non-SP arc segments w.r.t. N_i.*

Proof: This property will be proven by contradiction as follows. It is assumed that the union of all the neighbor-related non-SP arc segments corresponding to N_i is not equivalent to the union of all the converged non-SP arc segments w.r.t. N_i. Based on Definitions 5, 6, and Property 1, it is stated that all the converged non-SP arc segments w.r.t. N_i result in the union of all the non-SPs on $C(P_{N_i}, R/2)$. Therefore, there must exist a non-SP P_J located on $C(P_{N_i}, R/2)$ such that it does not relate to any neighbor-related non-SP arc segments w.r.t. N_i, i.e., there does not exist any $N_k \in \mathbf{T}_{N_i}$ that lies inside the rolling ball $RB_{N_i}(P_J, R/2)$. However, based on Definitions 3 and 4, there should exist at least a node N_k within the rolling ball $RB_{N_i}(P_J, R/2)$ since P_J is a non-SP on $C(P_{N_i}, R/2)$, which contradicts with the previous statement. It completes the proof. □

The concept of the proposed IMS algorithm is described as follows. Based on Property 1, the converged SP arc segments for each N_i can be obtained by acquiring its corresponding converged non-SP arc segments, i.e., the complement arc segments on the circle $C(N_i, R/2)$. Moreover, according to Property 2, the converged non-SP arc segments of N_i can be acquired via the neighbor-related non-SP arc segments. Consequently, the problem of finding the converged SP arc segments w.r.t. N_i is transformed into the problem of obtaining the

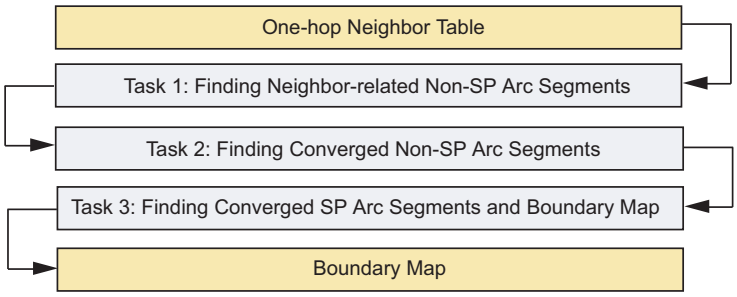

Figure 2.4: The process flow of the IMS algorithm.

converged non-SP arc segments w.r.t. N_i, which can be acquired via merging the corresponding neighbor-related non-SP arc segments. The boundary map $\mathbf{M}_{N_i}$ can therefore be indirectly established by adopting the IMS method. The process flow of the IMS algorithm is summarized as shown in Fig. 2.4.

In order to acquire and construct the boundary map $\mathbf{M}_{N_i}$ as shown in Algorithm 1, the IMS scheme is proposed. It is considered a localized algorithm where only three parameters are required within Algorithm 1, i.e., the maximum communication distance R, the position of N_i (P_{N_i}), and the one-hop neighbor table $\mathbf{T}_{N_i}$. Moreover, as will be proven in Theorem 4 in the next subsection, the time and space complexities of the IMS algorithm are observed to be $O(m^2)$ and $O(m)$ respectively.

Table 2.1 summarizes the notations in the IMS algorithm, and the pseudo code of the IMS method as shown in Algorithm 1 is explained as follows. Based on Fig. 2.4, the first task within the IMS algorithm is to identify each neighbor-related non-SP arc segment $S^{\overline{SP}}_{N_i \circ N_j}(P_A, P_B)$ w.r.t. N_i that is distinguished by its neighbor N_j. Intuitively, it is feasible to utilize the two endpoints P_A and P_B to represent $S^{\overline{SP}}_{N_i \circ N_j}(P_A, P_B)$, where each endpoint P_ζ (for $\zeta \in \{A, B\}$) can be characterized by an endpoint entry ($\Psi_{N_i}(P_\zeta)$) defined as

$$\Psi_{N_i}(P_\zeta) = [Id, Flag, Angle, Color, Counterpart]. \tag{2.3}$$

The parameter Id is utilized as the identification number of the corresponding neighbor SN for this entry. $Flag$ represents the endpoint type of this entry, which is denoted as either $RIGHT$ or $LEFT$ (e.g., the $Flag$ field of the right endpoint P_A is denoted as $RIGHT$; while that of

the left endpoint P_B is indicated as $LEFT$). The *Angle* field is adopted to represent the polar angle w.r.t. N_i by rotating counter-clockwise from the x-axis. The *Color* field is employed to indicate whether the endpoint P_ζ is a non-SP or not (i.e., $Color = TRUE$ denotes that P_ζ is a non-SP). The *Counterpart* field provides the linkage to the counterpart endpoint entry that possesses the opposite *Flag* value (e.g., the counterpart of $\Psi_{N_i}(P_A)$ is $\Psi_{N_i}(P_B)$ and vice versa). Therefore, the neighbor-related non-SP arc segment $S_{N_i \circ N_j}^{\overline{SP}}(P_A, P_B)$ can be denoted by a pair of the endpoint entries as $[\Psi_{N_i}(P_A), \Psi_{N_i}(P_B)]$.

In order to store and to maintain the relative locations among the entire set of endpoints $\mathbb{P}$ for all the neighbor-related non-SP arc segments w.r.t. N_i, a circular doubly-linked list [34] sorted by the polar angle is employed as

$$\mathbf{L}_{N_i} = \{\ell_{N_i}(P_\zeta) \,|\, \ell_{N_i}(P_\zeta) = [\Psi_{N_i}(P_\zeta), Next, Prev], \forall P_\zeta \in \mathbb{P}\}, \tag{2.4}$$

where the list item $\ell_{N_i}(P_\zeta)$ in $\mathbf{L}_{N_i}$ is composed by an endpoint entry $\Psi_{N_i}(P_\zeta)$ associated with two fields, $Next$ and $Prev$. The fields $Next$ and $Prev$ provide the addresses of the next and the previous entries of $\ell_{N_i}(P_\zeta)$ within $\mathbf{L}_{N_i}$. Considering the example as shown in Fig. 2.3, there exist three neighbor-related non-SP arc segments w.r.t. N_i as $S_{N_i \circ N_1}^{\overline{SP}}(P_1^R, P_1^L)$, $S_{N_i \circ N_2}^{\overline{SP}}(P_2^R, P_2^L)$, and $S_{N_i \circ N_3}^{\overline{SP}}(P_3^R, P_3^L)$, which result in three pairs of endpoint entries as $[\Psi_{N_i}(P_1^R), \Psi_{N_i}(P_1^L)]$, $[\Psi_{N_i}(P_2^R), \Psi_{N_i}(P_2^L)]$, and $[\Psi_{N_i}(P_3^R), \Psi_{N_i}(P_3^L)]$, respectively. Consequently, the linked list $\mathbf{L}_{N_i}$ will contain these endpoint entries as $\mathbf{L}_{N_i} = [\ell_{N_i}(P_1^R), \ell_{N_i}(P_3^L), \ell_{N_i}(P_1^L), \ell_{N_i}(P_2^R), \ell_{N_i}(P_2^L), \ell_{N_i}(P_3^R)]$. It is noticed that the endpoint entries are connected by their $Next$ and $Prev$ fields; while these entries are sorted by the corresponding *Angle* field in the ascending order. By taking the entry $\ell_{N_i}(P_3^L)$ as an example (as in Fig. 2.3), the parameter $Next$ refers to the address of $\ell_{N_i}(P_1^L)$ while the $Prev$ field is denoted as the address of $\ell_{N_i}(P_1^R)$. Since $\mathbf{L}_{N_i}$ is a circular doubly-linked list, the parameter $Prev$ for $\ell_{N_i}(P_1^R)$ points to the address of $\ell_{N_i}(P_3^R)$ while the $Next$ field of $\ell_{N_i}(P_3^R)$ refers to $\ell_{N_i}(P_1^R)$. In the case that two endpoint entries share the same *Angle* value, the *Flag* field will be utilized to provide the order of the entries, i.e., by taking the entry with $Flag = LEFT$ first and $Flag = RIGHT$ as the next entry in $\mathbf{L}_{N_i}$. It is noticed that the order of the endpoint entries within $\mathbf{L}_{N_i}$ is crucial for the construction

of $\mathbf{M}_{N_i}$. The construction and sorting mechanisms of $\mathbf{L}_{N_i}$ as described above are summarized at Line 1-11 in Algorithm 1, which completes the first task in Fig. 2.4.

The next task within the IMS algorithm as in Fig. 2.4 is to merge all the neighbor-related non-SP arc segments into the converged non-SP arc segments w.r.t. N_i. Given a neighbor-related non-SP arc segment $S^{\overline{SP}}_{N_i \circ N_j}(P_A, P_B)$ represented by $[\Psi_{N_i}(P_A), \Psi_{N_i}(P_B)]$, the combining process is to assign the *Color* field of each endpoint entry $\Psi_{N_i}(P_C)$ which is located within $[\Psi_{N_i}(P_A), \Psi_{N_i}(P_B)]$ to become colored, i.e., with the $TRUE$ value. This indicates that the endpoint P_C is merged into the neighbor-related non-SP arc segment $S^{\overline{SP}}_{N_i \circ N_j}(P_A, P_B)$. Based on Property 2, all the remaining uncolored endpoint entries consequently become the endpoints of the converged non-SP arc segments w.r.t. N_i. As shown in Fig. 2.3, $\Psi_{N_i}(P_1^R)$ and $\Psi_{N_i}(P_3^L)$ are the colored endpoint entries; while the uncolored ones are $\Psi_{N_i}(P_1^L)$, $\Psi_{N_i}(P_2^R)$, $\Psi_{N_i}(P_2^L)$, and $\Psi_{N_i}(P_3^R)$. It is noticed that the uncolored endpoint entries will establish the converged non-SP arc segments w.r.t. N_i, which are denoted as $[\Psi_{N_i}(P_3^R), \Psi_{N_i}(P_1^L)]$ and $[\Psi_{N_i}(P_2^R), \Psi_{N_i}(P_2^L)]$. The combining process for the neighbor-related non-SP arc segments is summarized at Line 12-17 in Algorithm 1, completing the second task in Fig. 2.4.

Within the last task listed in Fig. 2.4, based on Property 1, all the converged SP arc segments w.r.t. N_i can be obtained by excluding all the converged non-SP arc segments w.r.t. N_i on the circle $C(P_{N_i}, R/2)$. For each two sequential converged non-SP arc segments $S^{\overline{SP}}_{N_i}(P_A, P_B)$ and $S^{\overline{SP}}_{N_i}(P_C, P_D)$ (denoted as $[\Psi_{N_i}(P_A), \Psi_{N_i}(P_B)]$ and $[\Psi_{N_i}(P_C), \Psi_{N_i}(P_D)]$), the resulting converged SP arc segment $S^{SP}_{N_i}(P_B, P_C)$ can be obtained as $[\Psi_{N_i}(P_B), \Psi_{N_i}(P_C)]$ in view of endpoint entries. Consequently, the converged SP arc segment $S^{SP}_{N_i}(P_B, P_C)$ w.r.t. N_i can be acquired by taking each uncolored endpoint entry $\Psi_{N_i}(P_B)$ with $Flag = LEFT$ associated with the next endpoint entry $\Psi_{N_i}(P_C)$ with $Flag = RIGHT$. As shown in Fig. 2.3, the converged SP arc segments w.r.t. N_i are obtained as $S^{SP}_{N_i}(P_1^L, P_2^R)$ and $S^{SP}_{N_i}(P_2^L, P_3^R)$, which are denoted as $[\Psi_{N_i}(P_1^L), \Psi_{N_i}(P_2^R)]$ and $[\Psi_{N_i}(P_2^L), \Psi_{N_i}(P_3^R)]$. For each converged SP arc segment $S^{SP}_{N_i}(P_B, P_C)$ denoted as $[\Psi_{N_i}(P_B), \Psi_{N_i}(P_C)]$, the direct mapping (i.e., $N_B \rightarrow N_C$) between input/output SNs (as mentioned in Subsection 2.4.2.2) can therefore be obtained by mapping N_B specified in $\Psi_{N_i}(P_B)$ to N_C denoted in $\Psi_{N_i}(P_C)$. The acquisition of the converged SP arc segments and the construction of the boundary map $\mathbf{M}_{N_i}$ are summarized

at Line 18-30 in Algorithm 1.

2.4.3 Proof of Correctness

Theorem 3. *Given a converged SP arc segment $S_{N_i}^{SP}(P_S, P_T)$ w.r.t. N_i where (i) the rightmost endpoint P_S is an SP for both N_i and its neighbor N_S and (ii) the leftmost endpoint P_T is an SP for both N_i and its neighbor N_T respectively. All incoming packets to N_i that are acquired from its neighbor node N_S will be forwarded to N_T.*

Proof: Based on Definitions 5 and 6, a converged SP arc segment $S_{N_i}^{SP}(P_S, P_T)$ is an arc segment composed by some of the SPs w.r.t. N_i. According to Lemma 2, a simple closed curve is constructed by the trajectory of the SPs. In order to form the closed curve, there must exist other converged SP arc segments contributed by other SNs which are connected to the endpoints P_S and P_T. In other words, the endpoints P_S and P_T must also be owned by one of N_i's neighbor respectively. On the contrary, the other points on this converged SP arc segment $S_{N_i}^{SP}(P_S, P_T)$ should only be contributed by N_i based on Definitions 3 and 4. Moreover, it is intuitive to observe (from Definition 4) that the distances between the SNs related to the same endpoint SP (i.e., either P_S or P_T) must be located in their transmission ranges. By adopting the RUT scheme (as stated in Theorems 1 and 2) starting from N_S, the rolling ball will be traversed counter-clockwise via N_i to N_T. This corresponds to the situation that all the packets coming from N_S to N_i will be forwarded to N_T. It completes the proof. □

Theorem 4. *The IMS method as shown in Algorithm 1 has the time complexity of $O(m^2)$ and the space complexity of $O(m)$ respectively, where m is the number of entries in the neighbor table $\mathbf{T}_{N_i}$.*

Proof: Based on Fig. 2.4, the IMS method as in Algorithm 1 consists of three tasks: (a) finding neighbor-related non-SP arc segments (Line 1-11), (b) creating converged non-SP arc segments (Line 12-17), and (c) generating converged SP arc segments and the boundary map (Line 18-30).

It is noticed that all the basic functions and operations possess the time complexity of $O(1)$ except the *sort*() function as in Line 11. The *sort*() function can adopt the merge sort algorithm [35] in order to deal with ordering task with the time complexity of $O(m \log m)$. Moreover, the insertion of the endpoint entry into $\mathbf{L}_{N_i}$ can also be observed as $O(1)$ owing to the nature of the linked list structure [34]. The complexity for computing the neighbor-related non-SP arc segment $S_{N_i \circ N_j}^{\overline{SP}}(P_A, P_B)$ can be obtained as $O(1)$ since P_A and P_B (i.e., the intersecting points of $C(P_{N_i}, R/2)$ and $C(P_{N_j}, R/2)$) can be computed directly from R, P_{N_i}, and P_{N_j}.

In part (a) between Line 1-10, the time complexity is observed as $O(m)$ since the **foreach** loop is executed at most m times, where all the instructions have the same time complexity of $O(1)$. Since the sorting function (i.e., *sort*() in Line 11) has the time complexity of $O(m \log m)$, the total time complexity of part (a) becomes $O(m \log m)$. In both part (b) and (c), there exist two loops in each segment where each loop can be executed at most m times. The time complexity for either part (b) or (c) can be obtained as $O(m^2)$. Consequently, the total time complexity of Algorithm 1 can be acquired by combining the time complexities of the three parts, which results in $O(m^2)$. On the other hand, the space complexity can obviously be observed as $O(m)$ based on the size of the linked list $\mathbf{L}_{N_i}$. It completes the proof. □

2.5 Enhanced Mechanisms for Proposed GAR Protocol

In order to enhance the routing efficiency of the proposed GAR protocol, three mechanisms are proposed in this section, i.e., the hop count reduction (HCR), the intersection navigation (IN), and the partial UDG construction (PUC) schemes. These three mechanisms are described as follows.

2.5.1 Hop Count Reduction (HCR) Mechanism

Based on the rolling ball traversal within the RUT scheme, the selected next-hop nodes may not be optimal by considering the minimal hop count criterion. Excessive routing delay associated with power consumption can occur if additional hop nodes are traversed by adopting

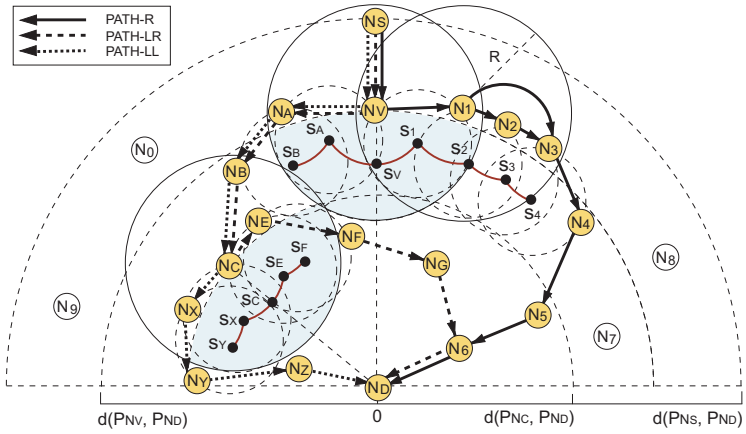

Figure 2.5: The hop count reduction (HCR) and the intersection navigation (IN) schemes.

the RUT scheme. As shown in Fig. 2.5, the void node N_V starts the RUT scheme by selecting N_1 as its next hop node with the counter-clockwise rolling direction; while N_2 and N_3 are continuously chosen as the next hop nodes. Considering the case that N_3 is located within the same transmission range of N_1, it is apparently to observe that the packets can directly be transmitted from N_1 to N_3. Excessive communication waste can be preserved without conducting the rerouting process to N_2. Moreover, the boundary set **B** forms a simple unidirectional ring based on Theorem 1, which indicates that a node's next-hop SN can be uniquely determined if its previous hop SN is already specified. For instance (as in Fig. 2.5), if N_V is the previous node of N_1, N_1's next hop node N_2 is uniquely determined, i.e., the transmission sequences of every three nodes (e.g., $\{N_V \rightarrow N_1 \rightarrow N_2\}$ or $\{N_1 \rightarrow N_2 \rightarrow N_3\}$) can be uniquely defined.

According to the concept as stated above, the hop count reduction (HCR) mechanism is to acquire the information of the next few hops of neighbors under the RUT scheme by listening to the same forwarded packet. It is also worthwhile to notice that the listening process does not incur additional transmission of control packets. As shown in Fig. 2.5, N_1 chooses N_2 as its next-hop node for packet forwarding; while N_2 selects N_3 as the next hop node in the same manner. Under the broadcast nature, N_1 will listen to the same packets in the forwarding process from N_2 to N_3. By adopting the HCR mechanism, N_1 will therefore select N_3 as its next hop node instead of choosing N_2 while adopting the original RUT scheme. Consequently,

N_1 will initiate its packet forwarding process to N_3 directly by informing the RUT scheme that the rerouting via N_2 can be skipped.

2.5.2 Intersection Navigation (IN) Mechanism

The intersection navigation (IN) mechanism is utilized to determine the rolling direction in the RUT scheme while the void problem occurs. It is noticed that the selection of rolling direction (i.e., either counter-clockwise or clockwise) does not influence the correctness of the proposed RUT scheme to solve Problem 3 as in Theorem 1. However, the routing efficiency may be severely degraded if a comparably longer routing path is selected at the occurrence of a void node. The primary benefit of the IN scheme is to choose a feasible rolling direction while a void node is encountered. Consequently, smaller rerouting hop counts (HC) and packet transmission delay can be achieved.

Based on the transmission pair (N_S, N_D) as shown in Fig. 2.5, N_V and N_C become the void nodes within the network topology. There exist three potential paths from N_S to N_D by adopting the RUT scheme, i.e., PATH-R, PATH-LR, and PATH-LL. The suffixes R, LR, and LL represent the sequences of the adopted rolling direction at each encountered void node, where the symbol R is denoted as counter-clockwise rolling direction and L represents clockwise direction. It is noted that the suffix with two symbols indicates that two void nodes are encountered within the path. The entire node traversal for each path is as follows: PATH-R = $\{N_S, N_V, N_1, N_3, N_4, N_5, N_6, N_D\}$, PATH-LR = $\{N_S, N_V, N_A, N_B, N_C, N_E, N_F, N_G, N_6, N_D\}$, PATH-LL = $\{N_S, N_V, N_A, N_B, N_C, N_X, N_Y, N_Z, N_D\}$. Different HCs are observed with each path as HC(PATH-R) = 7, HC(PATH-LR) = 9, and HC(PATH-LL) = 8.

The main objective of the IN scheme is to monitor the number of HC such that the path with the shortest HC can be selected, i.e., PATH-R in this case. A navigation map control packet (NAV_MAP) defined in the IN scheme is utilized to indicate the rolling direction while the void node is encountered. For example, two NAV_MAP packets are initiated after N_V is encountered, where NAV_MAP = {R} is delivered via the counter-clockwise direction to N_D and NAV_MAP = {L} is carried with the clockwise direction. It is noticed that the HC associated with each navigation path is also recorded within the NAV_MAP packets. As the

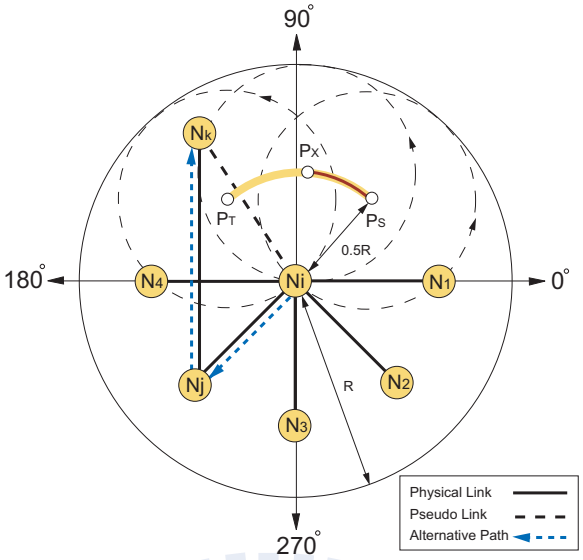

Figure 2.6: The partial UDG construction (PUC) mechanism.

second void node N_C is observed, the control message NAV_MAP = {L} is transformed into two different navigation packets (i.e., NAV_MAP = {LR} and NAV_MAP = {LL}), which traverse the two different rolling directions toward N_D. As a result, the destination node N_D will receive several NAV_MAP packets at different time instants associated with the on-going transmission of the data packets. The NAV_MAP packet with the shortest HC value (i.e., NAV_MAP = {R} in this case) will be selected as the targeting path. Therefore, the control packet with NAV_MAP = {R} will be traversed from N_D back to the N_S in order to notify the source node N_S with the shortest path for packet transmission. After acquiring the NAV_MAP information, N_S will conduct its remaining packet delivery based on the corresponding rolling direction. Considerable routing efficiency can be preserved as a shorter routing path is selected by adopting the IN mechanism.

2.5.3 Partial UDG Construction (PUC) Mechanism

The partial UDG construction (PUC) mechanism is targeted to recover the UDG linkage of the boundary node N_i within a non-UDG network. The boundary nodes within the proposed GAR protocol are defined as the SNs that are utilized to handle the packet delivery after encountering the void problem. As shown in Fig. 2.6, node N_i is considered a boundary node

since the converged SP arc segment $S_{N_i}^{SP}(P_S, P_T)$ exists after N_i conducts the proposed IMS algorithm by the input of the current one-hop neighbors $\{N_1, N_2, N_3, N_4, N_j\}$. It is noted that the boundary nodes consist of a portion of the network SNs. Therefore, conducting the PUC mechanism only by the boundary nodes can conserve more network resources than most of the existing flooding-based schemes that require information from all the network nodes.

The physical links of an exemplified topology are identified by the black solid lines as shown in Fig. 2.6. It is considered that the boundary node N_i does not possess full UDG linkages since a node N_k within N_i's transmission range can not directly communicate with N_i. The proposed PUC mechanism will be initiated at the boundary node N_i under the non-UDG networks as follows. Initially, N_i broadcasts the PUC_REQ control packet containing its neighbor list for requesting the recovery of UDG linkages. After the neighbor N_j receives the PUC_REQ packet, N_j's neighbor table will be examined to verify if there exists any neighbor node N_k that is not in the neighbor list of the PUC_REQ packet but is actually located within the transmission range of N_i. In the case that such node N_k is observed, N_j will initiate a feedback message, i.e., the PUC_REP control packet, in order to inform N_i that a pseudo link from N_i to N_k should be constructed via the alternative paths of the two physical links from N_i to N_j and from N_j to N_k. Therefore, the UDG linkage of N_i can be recovered which results in the current one-hop neighbors of N_i as $\{N_1, N_2, N_3, N_4, N_j, N_k\}$; while the converged SP arc segment $S_{N_i}^{SP}(P_S, P_T)$ will be changed into $S_{N_i}^{SP}(P_S, P_X)$.

2.6 Performance Evaluation

The performance of the proposed GAR algorithm is evaluated and compared with other existing localized schemes via simulations, including the reference GF algorithm, the planar graph-based GPSR and GOAFR++ schemes, and the UDG-based BOUNDHOLE algorithm. It is noted that the GPSR and GOAFR++ schemes which adopt the GG planarization technique to planarize the network graph are represented as the GPSR(GG) and GOAFR++(GG) algorithms; while the variants of these two schemes with the CLDP planarization algorithm are denoted as the GPSR(CLDP) and GOAFR++(CLDP) protocols. Both the grid and ran-

dom topologies are considered in two different types of network simulations as follows: (a) the pure UDG network as the ideal case; and (b) the non-UDG network for realistic network environment. Furthermore, the GAR protocol with the enhanced mechanisms (i.e., the HCR, the IN, and the PUC schemes) is also implemented, which is denoted as the GAR-E algorithm. The simulations are conducted in the network simulator (NS-2, [36]) with wireless extension, using the IEEE 802.11 DCF as the MAC protocol. The parameters utilized in the simulations are listed as shown in Table 2.2, and the following five performance metrics are utilized in the simulations for performance comparison:

1. Packet Arrival Rate: The ratio of the number of received data packets to the number of total data packets sent by the source.

2. Average End-to-End Delay: The average time elapsed for delivering a data packet within a successful transmission.

3. Path Efficiency: The ratio of the number of total hop counts within the entire routing path over the number of hop counts for the shortest path.

4. Communication Overhead: The average number of transmitted control bytes per second, including both the data packet header and the control packets.

5. Energy Consumption: The energy consumption for the entire network, including transmission energy consumption for both the data and control packets under the bit rate of 11 Mbps and the transmitting power of 15 dBm for each SN.

2.6.1 Grid Topology

The simulation scenario is described as follows. As shown in Fig. 2.7, the grid topology with the existence of a void block of size $500 \times 800\ m^2$ is considered in the simulation. It is noted that there are SNs located around the peripheral of the void block; while none of the SNs is situated inside the block. The source and destination nodes N_S and N_D are located at the center of the left and right boundaries as shown in Fig. 2.7. The data packets are transmitted

Parameter Type	Parameter Value
Network Size	1000 x 800 m^2
Simulation Time	150 sec
Transmission Range	250 m
Traffic Type	Constant Bit Rate (CBR)
Data Rate	12 Kbps
Size of Data Packet	512 Bytes
Average Node Degree	10, 12.5, 15, 17.5, 20
Void Height	150, 225, 300, 375, 450 m

Table 2.2: Simulation Parameters

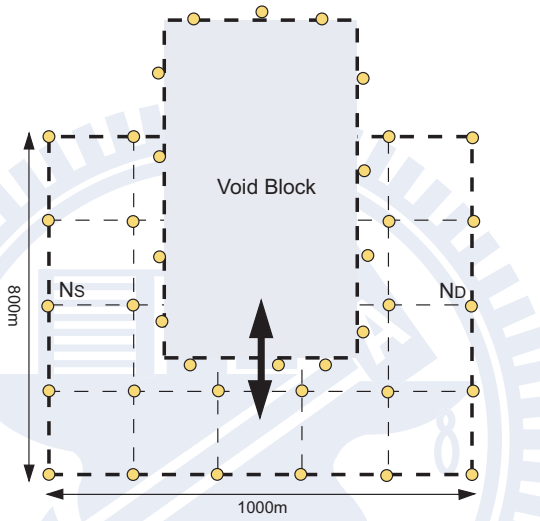

Figure 2.7: The simulation scenario of the grid topology.

from N_S to N_D with the void block that is randomly moved with vertical direction in order to simulate the existence of a void problem within the network. It is noted that network partition between N_S and N_D is not considered to exist in the simulation. One hundred simulation runs are conducted for each randomly moved void block case. The simulations of the performance metrics versus the node degree, i.e., the average number of nodes within a transmission range, are conducted and compared with other baseline protocols under the UDG and the non-UDG networks. The non-UDG network is obtained by randomly removing some of the communication links within the original UDG network for violating the properties of the UDG setting.

2.6.1.1 Simulation Results for UDG Network

Figs. 2.8(a) to 2.8(e) show the performance comparison between these six algorithms under different node degrees within the UDG network. It is noted that the node degree is defined as the average number of nodes within the transmission range of an SN. As can be seen from Fig. 2.8(a), the packet arrival rates obtained from these six algorithms are independent to the node degree within the network. This is attributed to the design nature of these schemes and the fact that the GF algorithm will fail owing to the location of the void block instead of the node degree. In both of the proposed GAR and GAR-E protocols, 100% of packet arrival rate is guaranteed under different node degrees. Moreover, the planar graph-based GPSR(GG) and GOAFR++(GG) schemes also possess the guaranteed packet delivery ratio. These results are consistent with the protocol design that is proven to ensure 100% of packet arrival rate as long as the network is not partitioned between N_S and N_D. It can also be observed in Fig. 2.8(a) that the BOUNDHOLE algorithm can achieve around 88% of packet arrival rate due to the occurrence of routing loop; while the GF scheme can only attain around 45% since the void problem is not considered within its protocol design.

Fig. 2.8(b) shows the average end-to-end delay for successful packet delivery by adopting these algorithms. The conventional GF protocol possesses the smallest end-to-end delay due to its negligence of the void problem, which leads to less than 50% of packet arrival rate as shown in Fig. 2.8(a). On the other hand, the GOAFR++(GG) scheme results in the largest delay due to its bounding techniques [20, 25] that in general cause the back-and-forth forwarding attempts around the large void block. It is also observed that the end-to-end delay acquired from the UDG-based BOUNDHOLD algorithm is larger than that of the GPSR(GG) scheme. The major reason can be attributed to the potential rerouting and looping caused by the BOUNDHOLD algorithm (as shown in Fig. 2.1), which supersedes the planarization drawbacks of the GPSR(GG) scheme. Furthermore, the planar graph-based GPSR(GG) and GOAFR++(GG) schemes require additional 15 to 35 ms of delay in comparison with the proposed UDG-based GAR and GAR-E protocols owing to the required unnecessary forwarding nodes as illustrated in Fig. 2.1. Due to the adoption of the enhanced

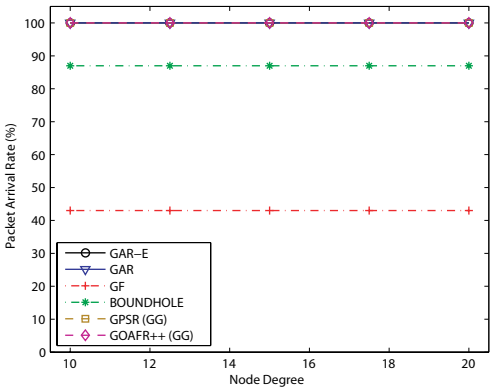

(a) Packet Arrival Rate vs. Node Degree

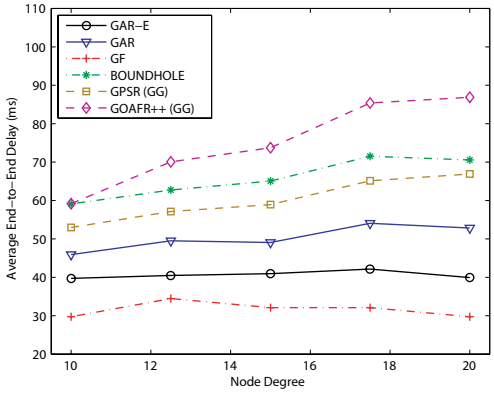

(b) Average End-to-End Delay vs. Node Degree

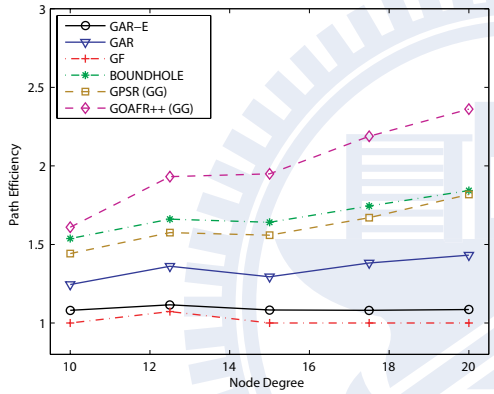

(c) Path Efficiency vs. Node Degree

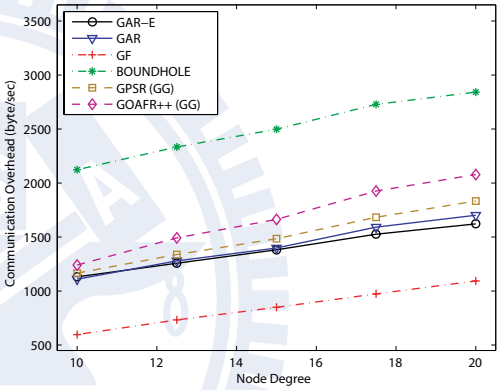

(d) Communication Overhead vs. Node Degree

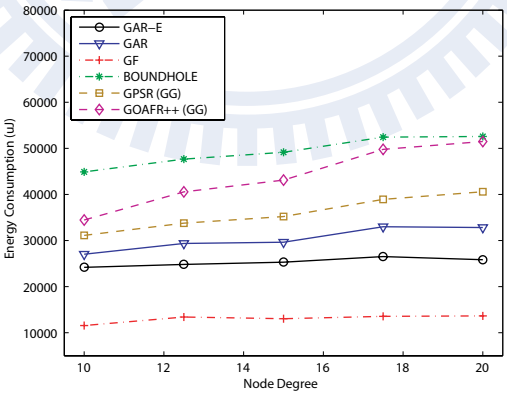

(e) Energy Consumption vs. Node Degree

Figure 2.8: Performance comparison for UDG networks with grid topology.

HCR and IN mechanisms, the GAR-E algorithm can provide comparably 8 to 15 ms less delay than that from the original GAR protocol. It is also noteworthy to observe the M-shape curves resulted within these six schemes. The primary reason is attributed to the different numbers of hop counts between the source/destination pair generated by the GF algorithm. It is noted that the GAR, GAR-E, GPSR(GG), GOAFR++(GG), and BOUNDHOLE schemes implement the GF algorithm without the occurrence of the void problem. The hop counts under the cases of the five different node degrees are computed as 5, 7, 6, 6, and 5. It can be apparently translated into the M-shape curves of end-to-end delay as shown in Fig. 2.8(b).

As shown in Fig. 2.8(c), the path efficiency acquired from these six schemes follows the similar trend as that from the average end-to-end delay. Due to the greedy nature and the negligence of the void problem, the path efficiency of the conventional GF scheme can achieve almost one in the simulations, i.e., the total number of hop counts is almost equal to that of the shortest path. The proposed GAR algorithm possesses the path efficiency of around 1.3 to 1.5. Furthermore, the GAR-E protocol further enhances the path efficiency to around the value of 1.1, which greatly outperforms the GPSR(GG), GOAFR++(GG), and BOUNDHOLE schemes.

Fig. 2.8(d) shows the communication overheads resulting from these six schemes, which are observed to increase as the increment of the node degree. The reason is attributed to the excessive control packets that are required for obtaining the neighbor's locations while the node degree is augmented. It is noted that the GF algorithm possesses the smallest communication overheads owing to its ignorance of the void problem. The BOUNDHOLE algorithm results in the largest communication overhead among all the schemes due to its usage of excessive header bytes for preventing the routing loops. It can be found that except the GF scheme, both the proposed GAR and GAR-E algorithms outperform the other three schemes with smaller amount of communication overhead under different node degrees. It is noticed that even though the GAR-E scheme requires additional NAV_MAP control packets for achieving the IN mechanism, the total required communication overhead is smaller than that from the GAR method due to its comparably smaller rerouting number of hop counts. The comparison for energy consumption between these algorithms is presented in Fig. 2.8(e).

Similar performance trends can be observed between the energy consumption and the communication overhead as shown in Fig. 2.8(d). Except for the reference GF protocol, the proposed GAR and GAR-E algorithms can effectively reduce the energy consumption in comparison with the other three schemes. The merits of the proposed GAR and GAR-E algorithms are observed and validated via the simulation results.

2.6.1.2 Simulation Results for Non-UDG Network

Figs. 2.9(a) to 2.9(e) illustrate the performance comparison between these eight algorithms with different node degrees under the non-UDG network. As can be seen from Fig. 2.9(a), the packet delivery can not be guaranteed in some of the schemes due to the GG planarization of the GPSR(GG) and GOAFR++(GG) protocols, the routing loops of the BOUNDHOLE scheme, and the negligence of the void problem from the GF algorithm. The proposed GAR protocol loses the property of guaranteed packet delivery since it is primarily designed for the UDG networks. However, it can still retain high packet delivery ratio of around 92%, which outperforms the BOUNDHOLE, GPSR(GG), GOAFR++(GG), and GF algorithms. On the other hand, the proposed GAR-E algorithm can achieve 100% packet delivery ratio with the adoption of the PUC mechanism. Even though both the GPSR(CLDP) and GOAFR++(CLDP) schemes can preserve 100% delivery ratio, significant amount of communication overhead associated with the CLDP mechanism is considered intolerable, which will be illustrated in Fig. 2.9(d). The comparisons for the end-to-end delay and the path efficiency between these schemes are shown in Figs. 2.9(b) and 2.9(c). It can be observed that the performance obtained form both the GPSR(GG) and GOAFR(GG) protocols outperform their CLDP counterparts, which is primarily due to the reason that the longer routing paths resulting from the CLDP mechanism will incur comparably larger end-to-end delay. The performance trend for the other algorithms follows that obtained from the UDG network setting as in Figs. 2.8(b) and 2.8(c). Excluding the GF scheme, the proposed GAR-E can still provide the most feasible performance comparing with the other algorithms under the non-UDG network.

Fig. 2.9(d) shows the comparison of communication overhead versus different node degrees

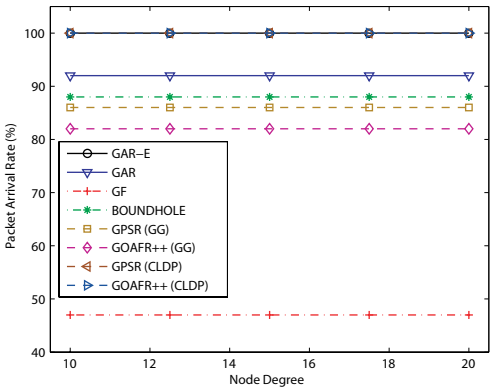

(a) Packet Arrival Rate vs. Node Degree

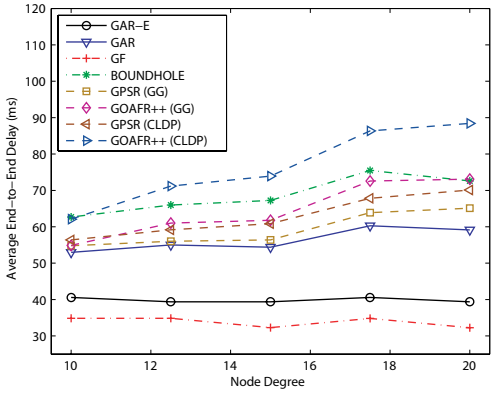

(b) Average End-to-End Delay vs. Node Degree

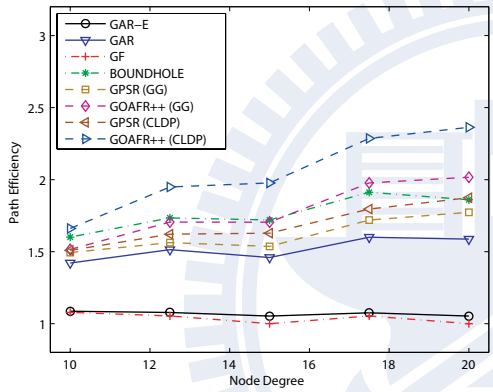

(c) Path Efficiency vs. Node Degree

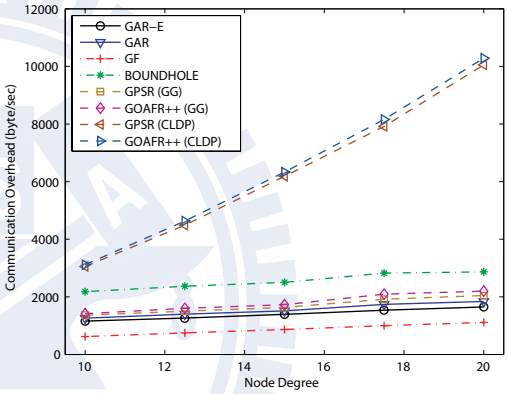

(d) Communication Overhead vs. Node Degree

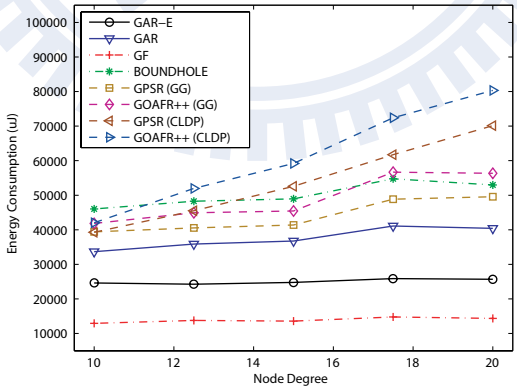

(e) Energy Consumption vs. Node Degree

Figure 2.9: Performance comparison for non-UDG networks with grid topology.

between these eight schemes. It is especially noticed that extremely high communication overheads are observed within the GPSR(CLDP) and GOAFR++(CLDP) schemes in comparison with the other six protocols. According to the CLDP algorithm, all communication links will be probed and traversed via additional control packets in order to fulfill the required tasks for planarization. Due to the excessive probing and traversing for all the communication links by the CLDP planarization algorithm, the significant increase rates of the GPSR(CLDP) and GOAFR++(CLDP) schemes are also observed in Fig. 2.9(d) w.r.t. the augmentation of the node degree. On the other hand, it is still found that the proposed GAR-based algorithms can provide relatively low communication overheads compared to the other schemes.

The comparison of energy consumption among these eight algorithms is shown in Fig. 2.9(e). Due to the high communication overhead required by adopting the CLDP planarization algorithm, both the GPSR(CLDP) and GOAFR++(CLDP) protocols consume comparably more energy than the proposed GAR-based algorithms, e.g., around three times more energy is consumed by the GOAFR++(CLDP) scheme comparing with the GAR-E algorithm under the node degree of 20. It is also noted that the BOUNDHOLE scheme requires more energy in comparison with the proposed GAR and GAR-E schemes due to its excessive header bytes for anti-looping. Owing to the required longer routing paths by adopting the GAR scheme as shown in Fig. 2.9(c), the proposed GAR-E algorithm can further conserve more energy than the GAR scheme. The effectiveness of the proposed GAR-E algorithm can therefore be perceived.

2.6.2 Random Topology

The simulation scenario for random topology is explained as follows. The SNs are randomly deployed with the node degree of 17.5 in the network, where three pairs of source and destination nodes are respectively located around the left and the right boundaries of the network area. There are three equal-height void blocks of width 300 meters that are randomly placed in the network in order to simulate the occurrence of void problems. In other words, there exist SNs around the peripheral of the void blocks; while none of the nodes is situated inside the void blocks. Performance comparisons under different void height, i.e., the height of each

void block, are conducted for these protocols under both the UDG and non-UDG networks.

2.6.2.1 Simulation Results for UDG Network

Figs. 2.10(a) to 2.10(e) present the performance comparison between these six algorithms with different void heights under the UDG network. As shown in Fig. 2.10(a), both the GAR-based algorithms and the planar graph-based GPSR(GG) and GOAFR++(GG) protocols can achieve 100% delivery rate owing to their design nature with guaranteed packet delivery. The BOUNDHOLE and GF algorithms result in lowered delivery ratio due to the occurrence of routing loop and the ignorance of the void problem respectively. Furthermore, with the augmentation of void height, decreased packet delivery rate can be observed from both the BOUNDHOLE and GF schemes since the probability of encountering the void problem is enlarged.

The performance of the average end-to-end delay versus the void height is shown in Fig. 2.10(b). The smallest end-to-end delay can be found in the GF algorithm owing to the negligence of the void problem; while the GOAFR++(GG) scheme results in the largest delay value due to its back-and-forth forwarding attempts around the large void block. With the adoption of both the HCR and IN mechanisms, the most feasible end-to-end delay performance can be observed from the proposed GAR-E protocol in comparison with the other schemes. It is also noted that the end-to-end delays from all the algorithms will be increased with the augmentation of the void height, which can be attributed to the enlarged number of forwarding hops for boundary traversal. Owing to the closely related characteristics with the end-to-end delay performance, the path efficiency obtained from these schemes follows similar trends as can be observed in Fig. 2.10(c).

Figs. 2.10(d) and 2.10(e) illustrate the performance comparisons for communication overhead and energy consumption versus the void height. Except for the BOUNDHOLE scheme, the performance trends from all the other protocols can be observed to be similar with that from the path efficiency in Fig. 2.10(c) due to the elongated routing path. Excessive communication overhead associated with more energy consumption will be produced from the BOUNDHOLE scheme comparing with the other algorithm. It is noted that the decreasing

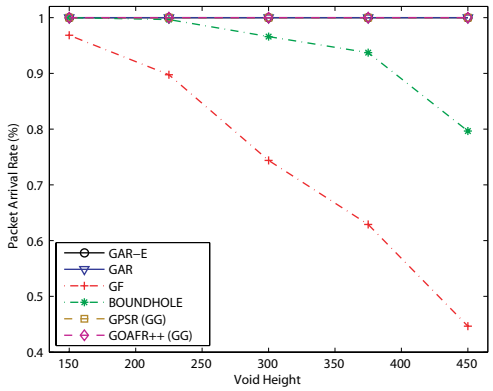

(a) Packet Arrival Rate vs. Void Height

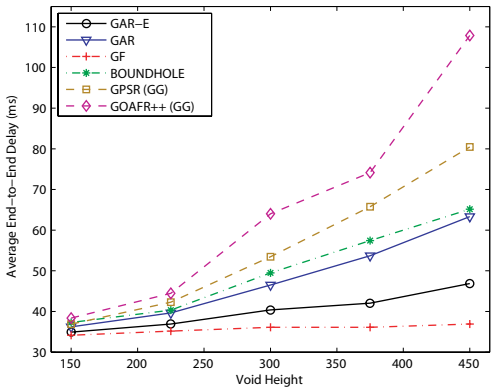

(b) Average End-to-End Delay vs. Void Height

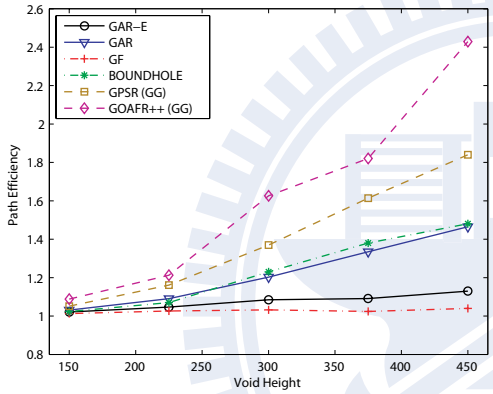

(c) Path Efficiency vs. Void Height

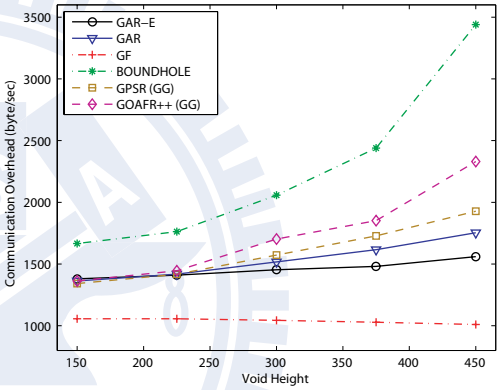

(d) Communication Overhead vs. Void Height

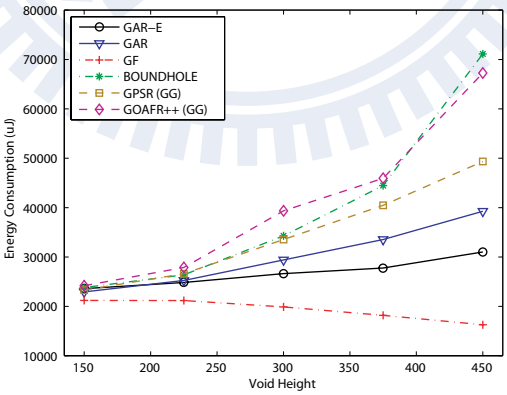

(e) Energy Consumption vs. Void Height

Figure 2.10: Performance comparison for UDG networks with random topology.

trend within the GF method is primarily due to its relative low packet delivery ratio, which results in less communication overhead and energy consumption. Except for the reference GF scheme, it can be expected that the GAR-E algorithm possesses the lowest communication overhead and the energy consumption, which support the merits of the protocol design.

2.6.2.2 Simulation Results for Non-UDG Network

Fig. 2.11(a) shows the performance comparison for packet arrival rate versus the void height under the non-UDG network. With the adoption of the PUC mechanism, 100% of packet arrival rate can be achieved by exploiting the proposed GAR-E protocol. Moreover, both the GPSR(CLDP) and GOAFR++(CLDP) schemes can also attain the same delivery rate. Nevertheless, these CLDP-enabled schemes will introduce extremely high communication overhead as illustrated in Fig. 2.11(d). With the augmentation of the void height, it is intuitive to observe that the packet arrival rate obtained from the remaining algorithms will be decreased owing to the increasing severity of the void problem.

The performance comparisons for the average end-to-end delay and the path efficiency are shown in Figs. 2.11(b) and 2.11(c). Owing to the guaranteed packet delivery rate, the GPSR(CLDP) and GOAFR++(CLDP) schemes will result in larger delay and worse path efficiency compared to their counterparts, i.e., the GPSR(GG) and GOAFR++(GG) protocols. It is observed that the proposed GAR-E scheme can still provide better routing efficiency comparing with other algorithms under the non-UDG networks. Figs. 2.11(d) and 2.11(e) present the performance comparisons for the communication overhead and the energy consumption versus the void height. Owing to the excessive control overheads required by the CLDP planarization, relatively high communication overhead and energy consumption are obtained by adopting the CLDP-enabled schemes. As can be expected, lowered communication overhead and energy consumption are acquired by the GAR-based algorithms in comparison with the other methods. The merits of the proposed GAR-E scheme can therefore be observed under the non-UDG networks.

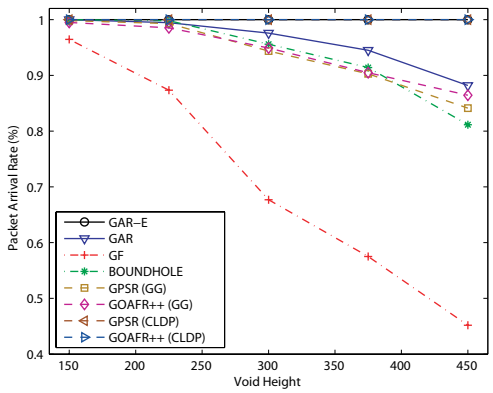

(a) Packet Arrival Rate vs. Void Height

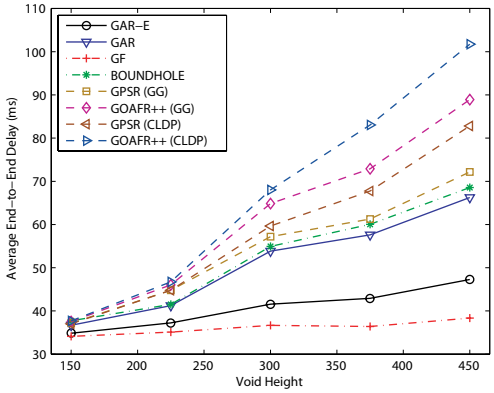

(b) Average End-to-End Delay vs. Void Height

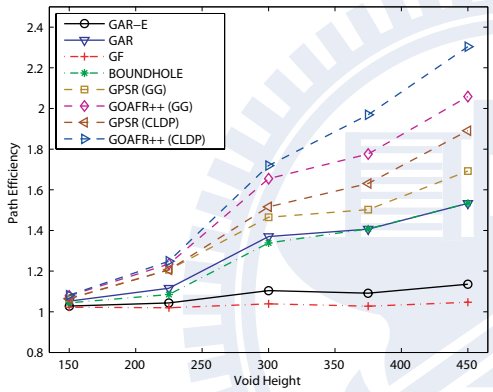

(c) Path Efficiency vs. Void Height

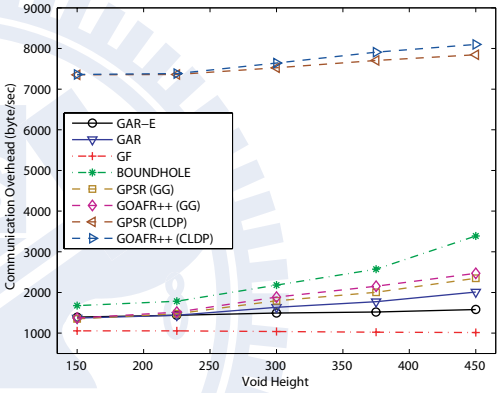

(d) Communication Overhead vs. Void Height

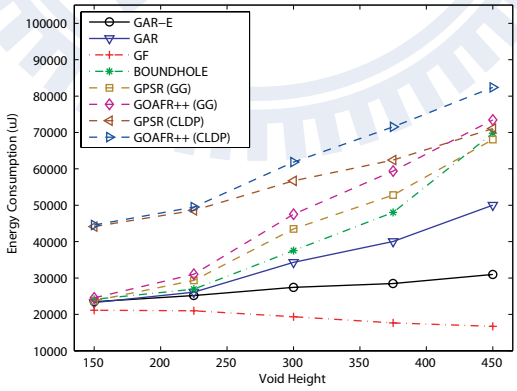

(e) Energy Consumption vs. Void Height

Figure 2.11: Performance comparison for non-UDG networks with random topology.

2.7 Summary

In this chapter, a UDG-based greedy anti-void routing (GAR) protocol is proposed to resolve the void problem incurred by the conventional green concept-based greedy forwarding algorithm. The rolling-ball UDG boundary traversal (RUT) scheme is adopted within the GAR protocol to solve the boundary finding problem, which results in guaranteed delivery of data packets under the UDG networks. The boundary map (BM) is also proposed to conquer the computational problem of the rolling mechanism in the RUT scheme, forming the direct mappings between the input/output nodes. The proposed indirect map searching (IMS) algorithm constructs the boundary map with the time and space complexities of $O(m^2)$ and $O(m)$, where m represents the number of neighbors. The correctness of the RUT scheme, the GAR algorithm, and the time/space complexity of the IMS method is properly proven. The hop count reduction (HCR) and the intersection navigation (IN) mechanisms are proposed as the delay-reducing schemes for the GAR algorithm; while the partial UDG construction (PUC) mechanism is utilized to generate the required topology for the RUT scheme under the non-UDG networks. All these enhanced mechanisms associated with the GAR protocol are proposed as the enhanced GAR (GAR-E) algorithm that inherits the merit of guaranteed delivery. The performance of both the GAR and GAR-E protocols is evaluated via simulations and is compared with existing localized routing algorithms. The simulation study shows that the proposed GAR and GAR-E algorithms can guarantee the delivery of data packets under the UDG network; while the GAR-E scheme further improves the routing performance with reduced communication overhead under different network scenarios. These proposed GAR-based schemes can therefore be adopted as the unicast protocols in the green wireless access networks.

Chapter 3

Three-Dimensional Greedy Anti-Void Routing Protocol

Chapter Overview

In the network layer unicast protocol design for achieving the green wireless access networks, a greedy anti-void routing (GAR) protocol is proposed in the previous chapter. However, the proposed GAR scheme is mainly designed for the two dimensional network. In the three dimensional space, the unreachability problem (i.e., the so-called void problem) resulting from the low-overhead green concept-based greedy forwarding (GF) algorithm has not been fully resolved. In this chapter, a three-dimensional greedy anti-void routing (3D-GAR) protocol is proposed to solve the 3D void problem by exploiting the boundary finding technique for the unit ball graph (UBG) with the main theme of the wireless sensor network (WSN) since the WSN has stringent requirements on the energy saving issues. The proposed 3D rolling-ball UBG boundary traversal (3D-RUT) scheme is employed to guarantee the delivery of packets from the source to the destination node. The correctness proofs, protocol implementation, and performance evaluation for the proposed 3D-GAR protocol are also given and properly explained. Based on the evaluation results, the proposed 3D-GAR protocol can guarantee the packet delivery and maintain comparably low routing overheads, which matches the unicast protocol design goal for achieving the green wireless access networks.

3.1 Introduction

In recent years, three-dimensional (3D) routing has gained attention in the wireless sensor networks (WSNs). For example, the applications for underwater sensor networks have become more popular in the field of oceanographic engineering, including data collection, water monitoring, pollution control, and ocean surveillance. Previous work on the routing protocols for the 3D WSNs can be found in [37]. Due to the limited available resources, efficient design of localized routing protocols becomes a crucial subject within the 3D WSNs. How to guarantee delivery of packets is considered an important issue for the localized routing algorithms. The well-known greedy forwarding (GF) protocol [4] is proposed as a superior scheme with its low routing overheads and the adaptability to the 3D-routing environment. However, the unreachability problem (i.e., the so-called void problem [5]) occurring within the GF algorithm will fail to guarantee the delivery of data packets. In order to alleviate the void problem, the 3D-ABLAR protocol [38] employs the heuristic next-hop selection techniques that forward packets to additional two neighbor nodes located in separated regions so as to gain more chance to escape from the void. The projection from two-dimensional (2D) face routing to 3D space is also proposed in [39] as another technique to deal with the void problem. However, the void problem resulting from the GF algorithm has not been fully resolved under the 3D environment. In this chapter, a 3D greedy anti-void routing (3D-GAR) protocol is proposed to solve the void problem under the unit ball graph (UBG) settings. The associated three-dimensional rolling-ball UBG boundary traversal (3D-RUT) scheme is exploited within the 3D-GAR algorithm with the assurance for packet delivery. Moreover, the proofs of correctness, protocol implementation, and performance evaluation for the proposed algorithms are also given and properly described.

The remainder of this chapter is organized as follows. Section 3.2 describes the network model and the problem statement. The proposed 3D-GAR protocol and the corresponding proofs of correctness are explained in Section 3.3. Section 3.4 provides the protocol implementation; while the performance evaluation is conducted and compared with other existing schemes in Section 3.5. Section 3.6 summarizes this chapter.

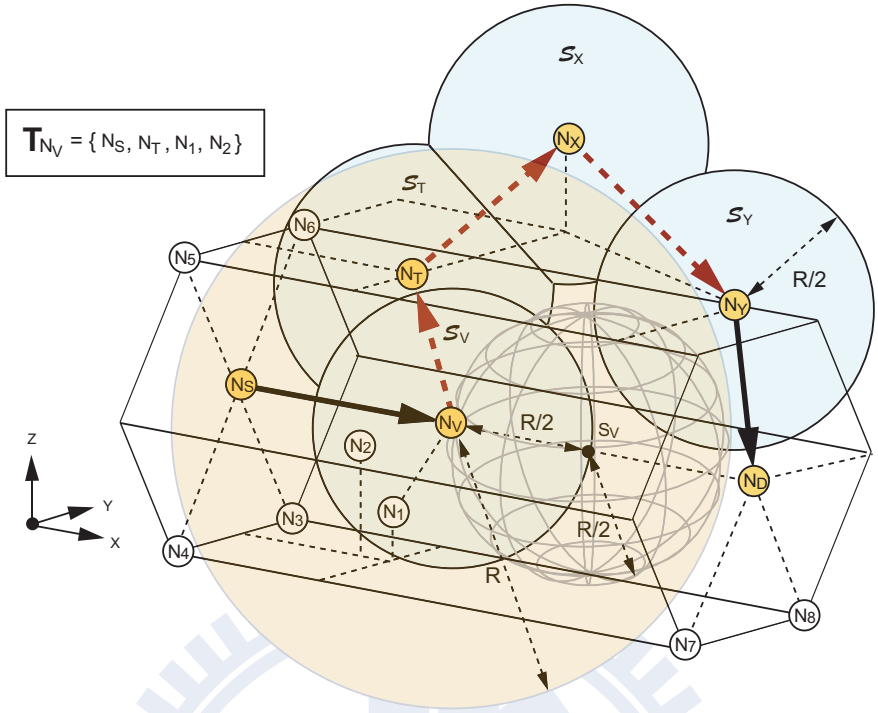

Figure 3.1: The example routing path constructed by using the 3D-GAR algorithm.

3.2 Network Model and Problem Statement

Considering a set of SNs $\mathbf{N} = \{N_i \,|\, \forall\, i\}$ within a 3D Euclidean space $\mathbb{R}^3$, the locations of the set $\mathbf{N}$ are represented by the set $\mathbf{P} = \{P_{N_i} \,|\, P_{N_i} = (x_{N_i}, y_{N_i}, z_{N_i}), \forall i\}$, which can be acquired by their own positioning systems. The set of closed balls defining the transmission ranges of $\mathbf{N}$ is denoted as $\overline{\mathbf{\Theta}} = \{\overline{\Theta}(P_{N_i}, R) \,|\, \forall\, i\}$, where $\overline{\Theta}(P_{N_i}, R) = \{\boldsymbol{x} \,|\, \|\boldsymbol{x} - P_{N_i}\| \leq R, \forall\, \boldsymbol{x} \in \mathbb{R}^3\}$. It is noted that P_{N_i} is the center of the closed ball with R denoted as the radius of the transmission range for each N_i. Furthermore, a unit ball graph (UBG) is defined as the intersection graph of a group of unit spheres in $\mathbb{R}^3$. Therefore, the network model for the 3D WSNs can be represented by a 3D UBG as $G(\mathbf{P}, \mathbf{E})$ with the edge set $\mathbf{E} = \{E_{ij} \,|\, E_{ij} = (P_{N_i}, P_{N_j}), P_{N_i} \in \overline{\Theta}(P_{N_j}, R), \forall\, i \neq j\}$. The edge E_{ij} indicates the unidirectional link from P_{N_i} to P_{N_j} whenever the position P_{N_i} is within the closed ball region $\overline{\Theta}(P_{N_j}, R)$. Moreover, the one-hop neighbor table for each N_i is defined as $\mathbf{T}_{N_i} = \{[ID_{N_k}, P_{N_k}] \,|\, P_{N_k} \in \overline{\Theta}(P_{N_i}, R), \forall\, k \neq i\}$, where ID_{N_k} represents the designated identification number for N_k. In the greedy forwarding (GF) algorithm, it is assumed that the source node N_S is aware of the

location of the destination node N_D. If N_S wants to transmit packets to N_D, it will choose the next hop from its $\mathbf{T}_{N_S}$ which (a) has the shortest Euclidean distance to N_D among all the SNs in $\mathbf{T}_{N_S}$ and (b) is located closer to N_D compared to the distance between N_S and N_D. The same procedure will be performed by the intermediate nodes (e.g., N_V as in Fig. 3.1) until N_D is reached. However, the GF algorithm will be inclined to fail due to the occurrences of voids even though some routing paths exist from N_S to N_D. The void problem is defined as follows:

Problem 4 (Void Problem). *The greedy forwarding (GF) algorithm is exploited for packet delivery from N_S to N_D. The void problem occurs while there exists a void node (N_V) in the network such that*

$$\{P_{N_k} \,|\, d(P_{N_k}, P_{N_D}) < d(P_{N_V}, P_{N_D}), \forall\, P_{N_k} \in \mathbf{T}_{N_V}\} = \emptyset, \tag{3.1}$$

where $d(x, y)$ represents the Euclidean distance between x and y. $\mathbf{T}_{N_V}$ is the one-hop neighbor table of N_V.

3.3 Proposed Three-Dimensional Greedy Anti-void Routing (3D-GAR) Protocol

The 3D-GAR protocol is a hybrid scheme consisting of both the GF algorithm and the 3D rolling-ball UBG boundary traversal (3D-RUT) scheme. The 3D-RUT algorithm is utilized to determine the boundary node set within the networks under the occurrence of void nodes. As the GF algorithm fails due to the void nodes, the 3D-RUT scheme can be utilized to escape from the void nodes by traversing the boundary node set and finally restart the GF forwarding process again. The packet delivery from N_S to N_D can therefore be guaranteed.

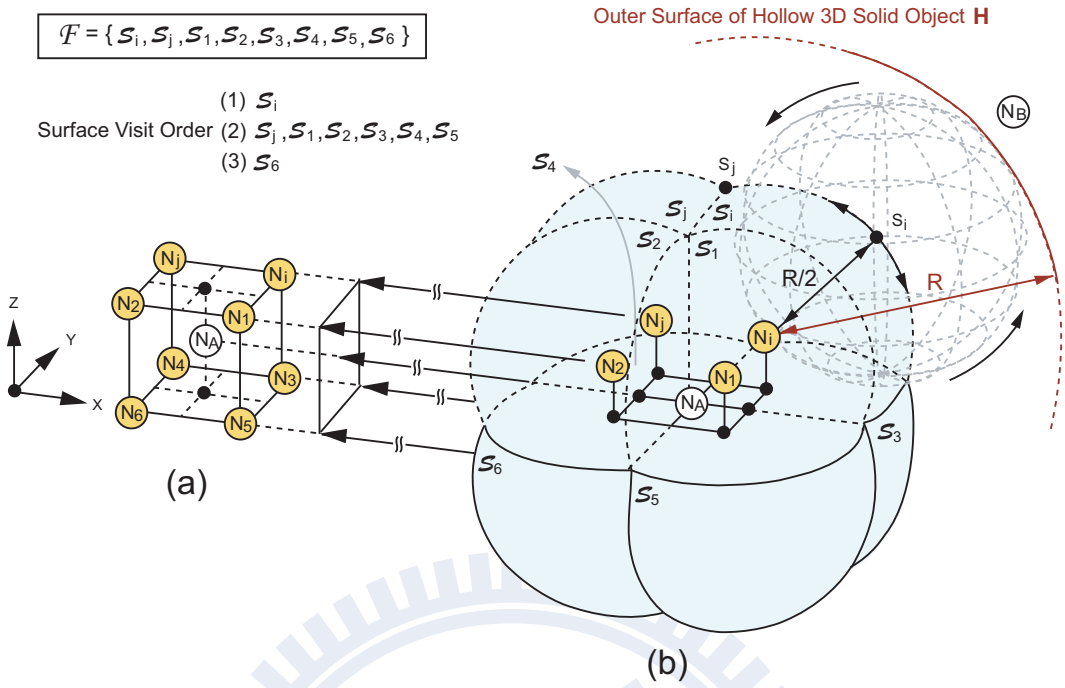

Figure 3.2: The three-dimensional rolling-ball UBG boundary traversal (3D-RUT) scheme.

3.3.1 Proposed Three-Dimensional Rolling-ball UBG Boundary Traversal (3D-RUT) Scheme

The 3D-RUT scheme is adopted to solve the boundary finding problem and acquire the so-called boundary node set (which will be defined later in this subsection) within the networks. The definition of boundary and the problem statement are described as follows.

Definition 8 (Boundary). *A boundary is defined as a closed surface that partitions the set of SNs* $\mathbf{N}$ *into two disconnected groups.*

Problem 5 (Boundary Finding Problem). *Given a UBG* $G(\mathbf{P}, \mathbf{E})$ *and the one-hop neighbor tables* $\mathbf{T} = \{\mathbf{T}_{N_i} \,|\, \forall\, N_i \in \mathbf{N}\}$*, how can a boundary be obtained by exploiting the distributed computing techniques?*

The concept of adopting the 3D-RUT scheme to resolve the boundary finding problem is briefly described as follows. Fig. 3.2(a) is the 3D scenograph of the internal part of Fig. 3.2(b), representing a cube with a node N_A at the center and $\{N_i, N_j, N_1, N_2, N_3, N_4, N_5, N_6\}$

at the eight corners. Considering the cube formed by the nine nodes as the vertices in Fig. 3.2(a), a 3D ball hinged at one of the vertex node with a radius of $R/2$ can be formed and freely rotated. It is noticed that the rolling ball is defined without any network node inside the ball. As in Fig. 3.2(b), it can be observed that the center points of the rotated balls can draw the closed blue surface, which is viewed as the boundary since this closed surface partitions the network into two disconnected parts, i.e., the nine nodes on the cube vertices as one network segment and node N_B as the other part. This type of rotated balls and their corresponding center points are formally defined as the rolling balls and the starting points (SPs) as follows:

Definition 9 (Rolling Ball). *Given $N_i \in \mathbf{N}$, a rolling ball $RB_{N_i}(\boldsymbol{s}_i, R/2)$ is defined as follows: (a) a closed ball hinged at P_{N_i} with its center point at $\boldsymbol{s}_i \in \mathbb{R}^3$ and the radius equal to $R/2$; and (b) there exists no node $N_k \in \mathbf{N}$ located inside the rolling ball.*

Definition 10 (Starting Point). *The starting point (SP) of N_i within the 3D-RUT scheme is defined as the center point $\boldsymbol{s}_i \in \mathbb{R}^3$ of $RB_{N_i}(\boldsymbol{s}_i, R/2)$.*

The detailed mechanism of the proposed 3D-RUT scheme is explained as follows. By means of computational geometry, each node N_i can verify if it has an SP or not by utilizing its one-hop neighbor table $\mathbf{T}_{N_i}$ since the rolling ball of N_i is always bounded by N_i's transmission range. Given $\boldsymbol{s}_i$ as an SP associated with its rolling ball $RB_{N_i}(\boldsymbol{s}_i, R/2)$ hinged at N_i, the rolling ball can freely rotate in all directions (i.e., 360°) within the 3D space as shown in Fig. 3.2. Based on the rotation of the rolling ball $RB_{N_i}(\boldsymbol{s}_i, R/2)$, an SP surface will be generated with the accumulation of the corresponding SPs. However, according to Definition 10 that there should not exist any SN located inside the rolling ball, the resulting SP surface will become a constrained SP surface $\mathcal{S}_i$ since the rolling ball can be stuck by some of the SNs in the network. These SNs are denoted as the surface-adjacent nodes of N_i, i.e., N_j, N_1, N_2, N_3, N_4, and N_5 as shown in Fig. 3.2. It is noticed that these surface-adjacent nodes can be served as the next hopping nodes of N_i.

Subsequently, N_i will inform these surface-adjacent nodes to continue the 3D-RUT scheme by sending control packets that contain the information of their corresponding SPs in order

to construct other constrained SP surfaces. For example, as shown in Fig. 3.2, the surface-adjacent node N_j can continue the 3D-RUT scheme by adopting the rolling ball $RB_{N_j}(\boldsymbol{s}_j, R/2)$ along with the newly assigned SP $\boldsymbol{s}_j$, which is located on the border of the constrained SP surface $\mathcal{S}_i$. Based on the same rotating procedure that is implemented by the rolling ball $RB_{N_j}(\boldsymbol{s}_j, R/2)$ hinged at N_j, the constrained SP surface $\mathcal{S}_j$ can therefore be constructed. Repeatedly, N_j's surface-adjacent nodes will be notified to continue the 3D-RUT scheme. As a result, all the constrained SP surfaces are established and identified as $\mathcal{S}_i$, $\mathcal{S}_j$, $\mathcal{S}_1$, $\mathcal{S}_2$, $\mathcal{S}_3$, $\mathcal{S}_4$, $\mathcal{S}_5$, and $\mathcal{S}_6$, which can be aggregated into a closed surface $\mathcal{F}$, i.e., the light-blue surface as in Fig. 3.2. For reader's clearness, the surface visit order starting from $\mathcal{S}_i$ is also summarized as in Fig. 3.2. This closed surface $\mathcal{F}$ is regarded as a boundary that is denoted in Definition 8; while the corresponding SNs that define the closed surface are represented as the elements in the boundary node set as follows:

Definition 11 (Boundary Node Set). *The boundary node set* $\mathbf{B} \subseteq \mathbf{N}$ *is defined as the SNs that construct the boundary based on the* 3*D-RUT scheme.*

Consequently, according to those eight constrained SP surfaces shown in Fig. 3.2, the boundary node set for this example can be obtained as $\mathbf{B} = \{N_i, N_j, N_1, N_2, N_3, N_4, N_5, N_6\}$. For preventing infinite recursion of the algorithm, each SN in $\mathbf{B}$ will only implement the 3D-RUT scheme once for the same boundary. Moreover, the reverse path of each SN in $\mathbf{B}$ to the original SN N_i can be obtained by referring to the previously visited constrained SP surfaces. For example, the surface traversing order can be obtained from $\mathcal{S}_i$, via $\mathcal{S}_j$, to $\mathcal{S}_6$ as in Fig. 3.2. Therefore, N_6 can construct the reverse path $N_6 \rightarrow N_j \rightarrow N_i$ in order to communicate with the original node N_i.

3.3.2 Detailed Descriptions of Proposed 3D-GAR Protocol

As shown in Fig. 3.1, the packets are intended to be delivered from the source node N_S to the destination node N_D. Moreover, N_S, N_T, N_1, and N_2 are within the light-yellow transmission range $\overline{\Theta}(P_{N_V}, R)$ of N_V, constructing the one-hop neighbor table $\mathbf{T}_{N_V}$. N_S will select N_V as the next hop by adopting the GF algorithm. However, the void problem prohibits N_V to

continue utilizing the same GF algorithm for packet forwarding since there exists no SN in $\mathbf{T}_{N_V}$ whose distance to N_D is smaller than that of N_V to N_D. The 3D-RUT scheme is therefore employed by assigning an SP (i.e., $\boldsymbol{s}_V$) associated with the rolling ball $RB_{N_V}(\boldsymbol{s}_V, R/2)$ hinged at N_V. It is noticed that there should always exist an SP for each void node (N_V), which can be proved in Property 3 as follows:

Property 3. *There always exists an SP $\boldsymbol{s}_V$ for a void node N_V with regard to the destination node N_D.*

Proof: It is assumed that γ is denoted as the Euclidean distance between N_V and N_D. Based on the definition of a void node, there will not be any SN located inside the intersection area Υ of the two closed balls $\overline{\Theta}(P_{N_V}, R)$ and $\overline{\Theta}(P_{N_D}, \gamma)$. Considering a point $\boldsymbol{s}_V$ located on the connecting line between N_V and N_D with $R/2$ away from N_V, the closed ball $\overline{\Theta}(\boldsymbol{s}_V, R/2)$ will be situated inside the node-free intersection region Υ. According to Definitions 9 and 10, $\boldsymbol{s}_V$ will be an SP for N_V. It completes the proof. □

Based on Property 3, $\boldsymbol{s}_V$ can be chosen to locate on the connecting line between N_V and N_D with $R/2$ away from N_V as illustrated in Fig. 3.1. The corresponding constrained SP surfaces can be established by adopting the proposed 3D-RUT scheme. In order to clearly visualize the 3D diagram, only the constrained SP surfaces $\mathcal{S}_V$, $\mathcal{S}_T$, $\mathcal{S}_X$, and $\mathcal{S}_Y$ are depicted in Fig. 3.1 as the light-blue surfaces. Since N_T is one of the surface-adjacent nodes of N_V, N_T will be chosen by N_V as the next hopping node for continuing the 3D-RUT scheme. Due to the nature of the void node N_V, the distance from N_T to N_D should be not smaller than that from N_V to N_D, i.e., $d(P_{N_T}, P_{N_D}) \geq d(P_{N_V}, P_{N_D})$. Similar procedure will recursively be conducted by nodes N_T, N_X, and others. In the case that there exists a surface-adjacent node N_Y such that $d(P_{N_Y}, P_{N_D}) < d(P_{N_V}, P_{N_D})$, N_Y will inform N_V regarding the escape route from the void node based on the reverse path identified by the 3D-RUT scheme, e.g., $N_V \rightarrow N_T \rightarrow N_X \rightarrow N_Y$ as illustrated in Fig. 3.1. Consequently, the GF algorithm will be resumed at N_Y, and the route from N_S to N_D can therefore be constructed for packet delivery, e.g., $\{N_S, N_V, N_T, N_X, N_Y, N_D\}$ as in Fig. 3.1. Moreover, if there does not exist a node N_Y such that $d(P_{N_Y}, P_{N_D}) < d(P_{N_V}, P_{N_D})$, the 3D-RUT scheme will be terminated

after completing the traversal of the boundary node set, e.g., the yellow nodes as depicted in Fig. 3.2. The result indicates that there is no routing path between N_S and N_D.

3.3.3 Proof of Correctness

Lemma 3. *A closed surface is established by all the SPs resulting from the 3D-RUT scheme.*

Proof: The relationship that "all the SPs within the 3D-RUT scheme form the surface of the resulting 3D solid object by overlapping the closed balls $\overline{\Theta}(P_{N_i}, R/2)$ for all $N_i \in \mathbf{N}$" is proven first. Based on Definitions 9 and 10, the set of SPs can be obtained as $\mathbf{S} = \mathbf{R_1} \cap \mathbf{R_2} = \{\boldsymbol{s}_i \,|\, \|\boldsymbol{s}_i - P_{N_i}\| = R/2, \exists N_i \in \mathbf{N}, \boldsymbol{s}_i \in \mathbb{R}^3\} \cap \{\boldsymbol{s}_j \,|\, \|\boldsymbol{s}_j - P_{N_j}\| \geq R/2, \forall N_j \in \mathbf{N}, \boldsymbol{s}_j \in \mathbb{R}^3\}$ by adopting the (a) and (b) rules within Definition 9. On the other hand, the surface of the resulting 3D solid object from the overlapped closed balls $\overline{\Theta}(P_{N_i}, R/2)$ for all $N_i \in \mathbf{N}$ can be denoted as $\mathbf{\Omega} = \mathbf{Q_1} - \mathbf{Q_2} = \bigcup_{N_i \in \mathbf{N}} K(P_{N_i}, R/2) - \bigcup_{N_i \in \mathbf{N}} \Theta(P_{N_i}, R/2)$, where $K(P_{N_i}, R/2)$ and $\Theta(P_{N_i}, R/2)$ represent the surface of a closed ball and the open ball centered at P_{N_i} with a radius of $R/2$ respectively. It is obvious to notice that $\mathbf{R_1} = \mathbf{Q_1}$ and $\mathbf{R_2} = \mathbf{Q_2'}$, which result in $\mathbf{S} = \mathbf{\Omega}$ and manifest the relationship in the beginning of this paragraph. Continuing the proof of this lemma, the surface of a 3D solid object will apparently result in a closed surface. Therefore, a closed surface is constructed by the combination of the SPs resulting from the 3D-RUT scheme, e.g., the light-blue surface as in Fig. 3.2. It completes the proof of this lemma. □

Theorem 5. *The boundary finding problem (Problem 5) is resolved by the 3D-RUT scheme.*

Proof: Based on Lemma 3, a closed surface (denoted as $\mathcal{F}$) is constructed from the 3D-RUT scheme by rotating the rolling balls $RB_{N_i}(\boldsymbol{s}_i, R/2)$ hinged at P_{N_i} for all $N_i \in \mathbf{N}$. For example, as shown in Fig. 3.2, $\mathcal{F} = \{\mathcal{S}_i, \mathcal{S}_j, \mathcal{S}_1, \mathcal{S}_2, \mathcal{S}_3, \mathcal{S}_4, \mathcal{S}_5, \mathcal{S}_6\}$ is represented as the light-blue surface, and all SNs at which the corresponding rolling balls have been hinged are denoted by the set $\mathbf{U} = \{N_i, N_j, N_1, N_2, N_3, N_4, N_5, N_6\}$. Moreover, a hollow 3D solid object $\mathbf{H}$ is defined by the space that are traversed by those rolling balls, where the thickness of the object $\mathbf{H}$ will be equal to R since it is equivalent to the diameter of the rolling balls. The partial outer

surface of **H** is illustrated as in Fig. 3.2(b). It is noticed that the closed surface $\mathcal{F}$ will become a layer of **H** situated at distance $R/2$ inward from the outer surface of **H**.

Based on Definition 9, there is no SN located inside the rolling ball which consequently results in the case that there will be no SN within the 3D solid object **H**. It can be observed that two disconnected regions can be derived as the inner and the outer spaces that are separated by **H** since, for all $N_A \in \mathbf{N}$ in the inner space, the smallest distance from N_A to N_B located in the outer space is greater than the SN's transmission range R. Consequently, the closed surface $\mathcal{F}$ situated within **H** can be considered as a boundary defined in Definition 8 that partitions **N** into two disconnected groups. As the example in Fig. 3.2(b), the set of nodes **U** and node N_A are located in the inner space; while node N_B is situated in the outer space. The set **U** can therefore be obtained as the boundary node set **B** based on Definition 11. It completes the proof. □

Theorem 6. *The void problem (Problem 4) is solved by the 3D-GAR protocol with guaranteed packet delivery.*

Proof: With the existence of the void problem occurring at any void node N_V, the 3D-RUT scheme is utilized by initiating an SP ($\boldsymbol{s}_V$) with the rolling ball $RB_{N_V}(\boldsymbol{s}_V, R/2)$ hinged at N_V. The 3D-RUT scheme within the 3D-GAR protocol will conduct boundary traversal via the associated boundary node set **B** under the condition that $d(P_{N_i}, P_{N_D}) \geq d(P_{N_V}, P_{N_D})$ for all $N_i \in \mathbf{B}$. If the boundary within the underlying network is completely traveled based on Theorem 5, it indicates that the SNs inside the boundary (e.g., N_V) are not capable of communicating with those located outside of the boundary (e.g., N_D). The result shows that there does not exist a route from the void node (N_V) to the destination node (N_D), i.e., the existence of network partition. On the other hand, if there exists a node N_Y such that $d(P_{N_Y}, P_{N_D}) < d(P_{N_V}, P_{N_D})$ (e.g., in Fig. 4), the GF algorithm will be adopted within the 3D-GAR protocol to conduct data delivery toward the destination node N_D. Therefore, the 3D-GAR protocol solves the void problem with guaranteed packet delivery, which completes the proof. □

3.4 Protocol Implementation

After describing the design concept of the proposed 3D-GAR scheme, the implementation issues of the proposed protocol consisting of both the GF and the 3D-RUT algorithms are explained in this section. The GF scheme is considered a sequential table-lookup algorithm that only requires the implementation of the one-hop neighbor table. Therefore, both the time and space complexities are $O(m)$, where m represents the number of neighbors specified in the one-hop neighbor table. If the void problem occurs, the 3D-RUT scheme is utilized to forward packets to the nodes in the boundary node set **B** as defined in Definition 11. Since a node N_i's neighbors in the boundary node set can construct rolling balls with N_i, the original mechanism of forwarding packets to the nodes in **B** can therefore be transformed into a simple forwarding rule. In other words, node N_i which currently conducts the 3D-RUT scheme simply forwards packets to those neighbors that can form a rolling ball with N_i, where these neighbors can be obtained by the following method. For each pair of nodes (N_j, N_k) in the one-hop neighbor table of N_i, if a node-free-inside circumscribed ball hinged at N_i with a radius of $R/2$ can be established with both nodes N_j and N_k on the surface of the ball, the definition of the rolling ball (i.e., Definition 9) will be satisfied since the two conditions are satisfied as follows: (a) node N_i is located on the surface of the ball; and (b) there does not exist any neighbor node situated inside the ball. As a result, both N_j and N_k are considered as the next hopping nodes of N_i for packet forwarding. It is noted that the time complexity of this process is $O(m^3)$ since three nested loops to go through the one-hop neighbor table are required to conduct this procedure; while the space complexity is still $O(m)$ since only the construction of the neighbor table is required. Finally, by considering both the GF and the 3D-RUT schemes, the time and space complexities of the 3D-GAR protocol can be acquired as $O(m^3)$ and $O(m)$ respectively, where m is the number of neighbors specified in the one-hop neighbor table.

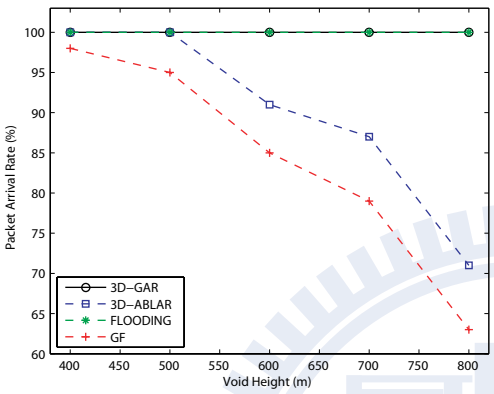

(a) Packet Arrival Rate (%)

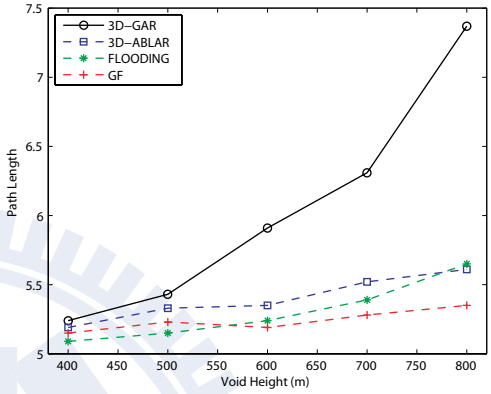

(b) Path Length for Successful Transmission

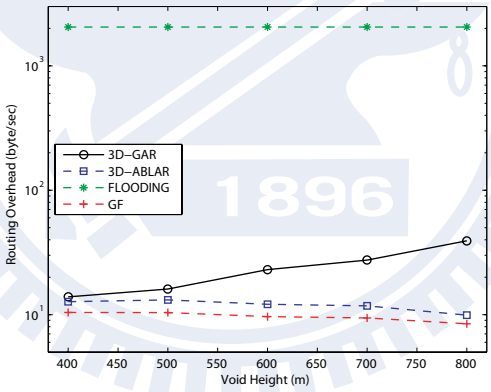

(c) Routing Overhead (byte/sec)

Figure 3.3: Performance evaluation for the proposed 3D-GAR protocol.

3.5 Performance Evaluation

The performance of the proposed 3D-GAR algorithm is evaluated and compared with other three protocols via simulations, including the 3D-ABLAR, the network flooding, and the reference GF algorithms. The simulation settings are explained as follows. A number of 1000 SNs are randomly deployed in the Euclidean 3D box ranging from (0, 0, 0) to (1000, 800, 1200) in the unit of meters. The transmission range of a node is 250 m. A pair of source and destination nodes are respectively located at (0, 400, 600) and (1000, 400, 600). The source node is with the data transmitting rate of 16 Kbps and data packet size of 512 bytes. There also exists a void block with length 400 m, width 800 m, and variable heights. This void block is randomly placed in the network in order to simulate the occurrence of void problems. In other words, there are SNs around the peripheral of the void block; while none of the nodes is situated inside the void block. Three performance metrics are utilized in the simulations for performance comparison as follows: (a) packet arrival rate: the ratio of the number of received data packets to the number of total data packets sent by the source; (b) path length: the average path length of successful routing in the unit of hop count; and (c) routing overhead: the average number of transmitted bytes per second for a network node.

Fig. 3.3(a) shows the packet arrival rate performance versus the void height. Due to the property of guaranteed delivery, both the 3D-GAR and network flooding algorithms will result in the delivery rate of 100%. The 3D-ABLAR and the GF protocols incur less delivery rate with regard to the increase of void height since the void problem occurs frequently when the void height becomes large. The 3D-ABLAR protocol has higher delivery rate than the GF algorithm owing to the reason that the GF scheme drops packet directly as the void problem occurs. Fig. 3.3(b) illustrates the performance of average path length for successful routing versus the void height. The network flooding algorithm results in the lowest value under small void heights since it can always find the shortest path between the source and the destination. However, as the void height becomes large, both the 3D-ABLAR and GF schemes will incur relatively smaller value of path length. The major reason is due to the 100% of packet delivery rate from the network flooding algorithm, which requires additional packet rerouting as the

void problem becomes severe. The same reason can be applied to the curve obtained from the 3D-GAR protocol, which possesses a slightly longer routing path than the other protocols, e.g., around 1.8 additional hops under the void height of 800 m. Nevertheless, even with the slightly larger path length, the 3D-GAR protocol can result in guaranteed delivery rate as shown in Fig. 3.3(a), which outperforms both the 3D-ABLAR and GF schemes with lowered packet delivery rate.

Fig. 3.3(c) shows the performance of routing overhead versus the void height. It can be observed that both the 3D-ABLAR and GF schemes result in comparatively low overhead since most of the packets are dropped due to the void problem. In order to guarantee delivery and to find the shortest path, the network flooding algorithm generates a large number of packets in comparison with other protocols, which contributes to a significant amount of routing overhead as shown in Fig. 3.3(c). Comparing with the network flooding algorithm, the 3D-GAR protocol can achieve guaranteed packet delivery with a comparably smaller number of packets since the 3D-GAR scheme limits the packet rerouting only to nodes that are in the boundary node set. The merits of the proposed 3D-GAR protocol can therefore be observed, which achieves guaranteed packet delivery with reasonable routing overhead.

3.6 Summary

In this chapter, a three-dimensional greedy anti-void routing (3D-GAR) protocol is proposed to completely resolve the void problem incurred by the conventional greedy forwarding algorithm under the 3D environment. The 3D rolling-ball UBG boundary traversal (3D-RUT) scheme is adopted within the 3D-GAR protocol to solve the boundary finding problem, which results in the guarantee of packet delivery. In the end, the correctness proofs, protocol implementation, and performance evaluation of the proposed algorithms are properly provided. According to the guaranteed packet delivery and the relatively low routing overhead properties, the proposed 3D-GAR protocol can be utilized to implement the green wireless access networks as a unicast routing protocol in the three dimensional space.

Chapter 4

Component-based Routing Platform and Energy Conserving Multicast Routing Protocol

Chapter Overview

In the network layer multicast protocol design for achieving the green wireless access networks, how to provide low energy consumption and maintain high packet delivery ratio is considered the major issue. Similar to the previous chapters, the main theme for this chapter is chosen as in the wireless sensor network (WSN) due to its stringent requirements on the power consumption. With regard to the multicast protocol design, reducing the number of data transmissions is considered a feasible method for decreasing the energy consumption of the network nodes. In the wired networks, the Steiner-tree is regarded as the optimal approach for constructing the multicast structure for specific senders and receivers. However, the results can not be directly applied to the wireless environment. Furthermore, in the aspect of protocol realization, the conventional implementations of routing algorithms are designed to be protocol specific, which results in the lack of flexibility for developers to implement other protocols. In this chapter, an energy conserving multicast routing (ECMR) protocol is proposed to

reduce the total number of relaying nodes for the construction of a multicast tree. It is designed to be a heuristic scheme since achieving a minimal cost multicast tree is considered an NP-hard problem in the wireless broadcast environment. Moreover, a component-based routing platform (CRP) with encapsulated software components (ESCs) is proposed to provide a generic routing implementation platform. Based on the design of the proposed ESCs, routing algorithms can be implemented in a more efficient manner. The ECMR algorithm can be implemented on the proposed CRP practical embedded platforms for performance evaluation. It validates that the CRP can be adopted as an effective design platform for the implementation of routing algorithms. Compared with the existing multicast routing protocol in the field experiments, the experimental results show that the proposed ECMR scheme can provide better energy conservation while the packet delivery ratio is still preserved. Thanks to the design of low energy consumption with high delivery ratio, the proposed ECMR protocol can be utilized in the establishment of the green wireless access networks as a feasible multicast routing protocol.

4.1 Introduction

Wireless sensor networks (WSNs) are composed by numerous sensor nodes (SNs) with information processing, sensing, and wireless communication capabilities. Various tasks can be cooperatively performed by the SNs, including monitoring, locationing, and data distribution [40]. Due to the distributed nature and hardware cost associated with the SNs, the available resources are considered limited for most of the current applications. Severe power constraint is considered one of the most challengeable design issues due to the difficulty in battery recharging for a large amount of SNs, especially in a remote or dangerous region.

The battery lifetime within an SN can be extended by technological advancement under different fields, e.g., hardware, software, or network design. Appropriate hardware design can fulfill the performance requirements that are agreeable to the least power consumption [41]. Dynamic power management within the software layers, e.g., application software or operating system, can also achieve energy conservation by adaptively adjusting the power modes of an

SN [42]. Moreover, energy conservation algorithms can be applied at the network level with the cooperation between the SNs. By adopting appropriate design of routing algorithms [43, 44] for packet delivery, the lifetime of the entire WSN can therefore be prolonged.

With the emergent applications for multicast data dissemination and aggregation, the design of multicast routing algorithms are considered one of the important topics within the WSNs. Different types of multicast routing protocols have been proposed for the mobile ad hoc network (MANET). Basically, these protocols can be categorized into the tree-based (such as MAODV [45], AMRIS [46], AMRoute [47], and GS [48]) and the mesh-based (such as ODMRP [49], CAMP [50], and MCEDAR [51]) algorithms. The fundamental topology of the tree-based network originates from a root, which stretches out its branches and the corresponding subbranches. The benefit of using the tree-based structure is its low energy consumption and the simplicity for maintaining the structure in static networks. In the mesh-based structure, there are at least two routes between each receiver and the transmitter. Compared with the tree-based networks, this architecture can provide more robust connectivity under the channel fading effect. However, the inherent complexity within the mesh-based structure makes it consume more system resources. Most of the existing multicast routing protocols designed for the MANET can not be directly adopted within the WSN for its stringent energy requirements. Moreover, these routing algorithms are considered infeasible for practical implementation either due to the protocol complexity or the excessive rerouting expenses.

Moreover, in terms of evaluating the routing algorithms, most of the existing research work conducts computer simulations for performance comparison. However, computer simulations are in general considered impractical due to the assumption of ideal network configurations. Therefore, field experiments with implementation testbeds become necessary for the evaluation of protocol performance. There are existing works that implement the ad hoc routing algorithms with field experiments, including Kernel-AODV [52], AODV-UCSB [53], and AODV-UU [54] schemes. However, these implementations are specifically designed to facilitate the design of their own routing protocols. It will be beneficial to provide a generic platform associated with development toolkits for evaluating different routing algorithms.

In this chapter, an energy conserving multicast routing (ECMR) protocol is proposed

for reducing the number of data transmissions within the WSNs. Since obtaining the minimal cost multicast tree under the wireless broadcast environment has been proven to be an NP-hard problem [55], a heuristic algorithm is exploited by the ECMR scheme for energy conservation purpose. By adopting the proposed algorithm, the conventional multicast structure (e.g., the ODMRP protocol [49]) can be converted into a light-weight topology. The total energy consumption can therefore be decreased; while the packet delivery ratio is still maintained. Furthermore, a component-based routing platform (CRP) is also proposed as a generic implementation testbed based on the Linux embedded system for the protocol realization. Field experiments are conducted in order to evaluate the performance of the proposed ECMR algorithm and validate the proposed CRP implementation platform. As can be seen from the experiment results, the proposed ECMR protocol is capable of providing better energy conservation comparing with the existing ODMRP algorithm.

The remainder of this chapter is organized as follows. The proposed ECMR protocol is presented in Section 4.2. Section 4.3 describes the proposed CRP implementation platform, including the software and hardware systems. Based on the proposed CRP testbed, the field experiments of the proposed ECMR protocol are conducted and compared with the baseline protocol in Section 4.4. Section 4.5 summaries this chapter.

4.2 Proposed Energy Conserving Multicast Routing (ECMR) Protocol

In this section, the proposed ECMR protocol is explained. The construction of the heuristic structure and the packet forwarding process are described in Subsection 4.2.1. Subsection 4.2.2 exploits the pseudo code of the heuristic structure construction. Examples for illustrating the benefits of the proposed ECMR protocol are shown in Subsection 4.2.3.

4.2.1 Heuristic Structure Construction and Data Packet Forwarding

In order to provide bandwidth efficiency, the proposed ECMR protocol establishes the multicast routes via the source-initiated and on-demand manners. The structure constructed

by the ECMR algorithm can be represented as $\mathcal{T} = \{S, \mathbf{I}, \mathbf{R}\}$, where S denotes the source node, $\mathbf{I} = \{I_i \,|\, \forall\, i \in \mathbb{N}\}$ and $\mathbf{R} = \{R_i \,|\, \forall\, i \in \mathbb{N}\}$ represent the sets of intermediate nodes and receiving nodes. There are two important parameters introduced within the ECMR protocol, which are denoted as the N_WGHT field within each node and the P_WGHT field for each constructed path. Both the N_WGHT and the P_WGHT parameters are utilized to indicate the significance of its corresponding node and route within the constructed structure $\mathcal{T}$.

The route request/reply process utilized in most of the on-demand unicast routing protocols is modified and employed within the proposed ECMR algorithm. The source node S advertises the join request (JREQ) packets for both initiating and updating the multicast routes within the structure $\mathcal{T}$. It is noted that the structure updates are conducted periodically with the time interval set by the JREQ flood timeout (FLDT) parameter. Initially, S will flood the JREQ packets (which include the ID of S) to its neighbor nodes while it has packets to be transmitted to the receiver set $\mathbf{R}$. After the intermediate node I_i receives the first JREQ packet, it will wait for the collection time of the intermediate node (CT_I) in order to obtain the other JREQ packets, which can be routed from other paths to I_i. After the collection time has expired, I_i will select the JREQ packet with its corresponding path that has the largest weight, i.e., the path $P_i = \max_{\forall k}\{P_k.\text{P\_WGHT}\}$. It is noted that the value recorded within the P_i.P_WGHT parameter is accumulated by the N_WGHT values of the nodes that consist of the corresponding path P_i. The intermediate node I_i will record the ID of its upstream node for backward tracking and continue to rebroadcast the JREQ packet.

As a JREQ packet has arrived in one of the receivers R_i, it will conduct the similar process to wait for other JREQ packets for the collection time of the receiving node (CT_R). R_i will select the path with the highest weight and initiate the transmission of a join reply (JREP) packet back to the source node S. While an intermediate node I_i receives the JREP packet, it will determine if it is on the reverse path towards S by verifying the next node ID in the JREP packet with its own ID. If the two IDs are identical, I_i will increment its node weighting (i.e., I_i.N_WGHT++) and continue to rebroadcast the JREP packet. On the other hand, the weighting will be decremented if I_i does not receive any JREP within the time interval specified in the N_WGHT count down timeout (CDT). This process will

be terminated until all the JREP packets have arrived in the source node S. Again, the routes within the structure $\mathcal{T}$ will be refreshed and updated with the periodic JREQ packet transmission by the source node S.

Within the proposed ECMR protocol, there is no additional control packet required for each node to depart from the existing structure $\mathcal{T}$. The source node S can terminate its periodic broadcast of the JREQ packets; while the receiving node R_i simply ceases the transmission of the JREP packet. Without receiving the JREP packet from R_i, the intermediate node I_i will also count down its weighting parameter (I_i.N_WGHT), which makes it become less important within the structure $\mathcal{T}$.

The forwarding process for the data packets can be initiated after the construction of the heuristic structure. As the structure $\mathcal{T}$ has been established, the source node S will directly broadcast the data packets to its neighboring SNs. After overhearing the data packets, the neighboring SNs will rebroadcast these packets if they possess nonzero N_WGHT parameters. As a result, the data packets will arrive in all the receivers within the set $\mathbf{R}$, which completes the process of multicast packet forwarding.

4.2.2 Pseudo Code Implementation of Heuristic Structure Construction

The pseudo codes of the ECMR algorithm for constructing the multicast routing structure $\mathcal{T}$ are shown in Algorithms 2, 3, and 4. The proposed heuristic algorithm can be separated into three parts, including the procedures of the source node, the procedures of the intermediate node, and the procedures of the receiving node.

In the procedures of the source node of Algorithm 2, the source node creates a JREQ packet (i.e., P_{new}) for every time period of FLDT, and also utilizes the variable *round* to record the round index of the newly generated P_{new}. According to the round index, the node overhearing the JREQ packet can determine the freshness of this JREQ packet, i.e., the larger round index represents the higher degree of freshness. Finally, the source node broadcasts the newly generated P_{new} to its neighboring SNs.

In the procedures of the intermediate node of Algorithm 3, the variable $demoteMechanism$ acts as the option of $SLOW$ or $FAST$ demotion of N_WGHT. If the value is $SLOW$, the

Algorithm 2: *Heuristic Structure Construction: Procedure of the Source Node*

```
begin
    round ← 0
    while true do
        round ← round + 1
        P_new ← new JREQ_Packet(ID_source, round)
        broadcast(P_new)
        waitTimeout(FLDT)
    end
end
```

N_WGHT parameter will decrease one after the CDT timer expires. On the other hand, if the value is set to be $FAST$, the N_WGHT parameter will become zero directly. It will be shown in Subsection 4.2.3 that the variable $demoteMechanism$ can affect the converging time of the structure $\mathcal{T}$. As shown in Algorithm 3, the procedures of the intermediate node mainly consist of four code sections which deal with the receiving JREQ packets, the receiving JREP packets, the expiration of the CT_I timer, and the termination of the CDT timer. In the first code section, the intermediate node collects the JREQ packets for the time period of CT_I, and determines the best collected JREQ packet according to the P_WGHT parameter and the round index. Consequently, the third code section rebroadcasts the best collected JREQ packet (i.e., P_{best}) while the CT_I timer expires. In the second code section, the incoming JREP packet whose *next_node_id* is equal to the intermediate node ID will be rebroadcasted with a new *next_node_id* of the corresponding upstream node ID that is recorded during the JREQ dissemination phase. It is noticed that this code section actually models the unicasting process by broadcasting. Finally, the fourth code section handles the decrement of the N_WGHT parameter as the CDT timer expires.

In the procedures of the receiving node of Algorithm 4, the receiving node collects JREQ packets within the time period of CT_R, and selects the JREQ packet with maximum P_WGHT. If there are two or more JREQ packets with the same maximum P_WGHT value, the random selection of these JREQ packets is adopted. This selected JREQ packet will be properly updated and transformed into the JREP packet (i.e., P_{out}). In the end, P_{out} will be broadcasted to the neighboring SNs, which completes the JREQ/JREP negotiation and concludes the construction of the structure $\mathcal{T}$.

Algorithm 3: *Heuristic Structure Construction: Procedure of the Intermediate Node*

```
begin
    demoteMechanism ← {SLOW or FAST}
    N_WGHT ← 0
    P_best ← null
    while true do
        P_in ← getIncomingPacket()
        if P_in.type = JREQ then
            if P_in.round = P_best.round then
                if P_in.P_WGHT > P_best.P_WGHT then P_best ← P_in
            end
            if P_in.round > P_best.round then
                P_best ← P_in
                startTimer(timerCT_I)
            end
        end
        if P_in.type = JREP then
            if ID_self = P_in.next_node_id then
                N_WGHT ← N_WGHT + 1
                P_out ← P_in
                P_out.next_node_id ← getUpStreamID(P_out)
                broadcast(P_out)
                stopTimer(timerCDT)
            end
        end
        if isExpired(timerCT_I) then
            P_best.P_WGHT ← P_best.P_WGHT + N_WGHT
            broadcast(P_best)
            startTimer(timerCDT)
        end
        if isExpired(timerCDT) then
            if N_WGHT ≠ 0 then
                if demoteMechanism = SLOW then
                    N_WGHT ← N_WGHT − 1
                else
                    N_WGHT ← 0
                end
            end
        end
    end
end
```

Algorithm 4: *Heuristic Structure Construction: Procedure of the Receiving Node*

```
begin
    while true do
        JREQset ← collectJREQwithin(CT_R)
        choice ← JREQset.pktWithMaxP_WGHT()
        if choice.itemCount() ≠ 1 then
            P_out ← randomPickOneIn(choice)
        else
            P_out ← choice.pop()
        end
        P_out.type ← JREP
        P_out.next_node_id ← getUpStreamID(P_out)
        broadcast(P_out)
    end
end
```

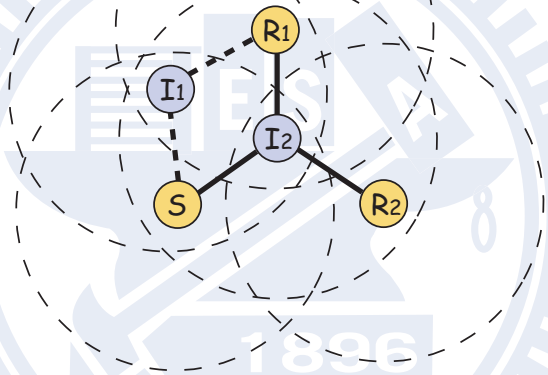

Figure 4.1: The example network of the ECMR protocol.

4.2.3 Examples for ECMR Protocol

Fig. 4.1 shows an example with one source node S that intends to transmit data packets to two receivers, R_1 and R_2. It is observed that S can initiate its JREQ packet to R_1 via both I_1 and I_2; while I_2 is the only intermediate node to R_2. As R_1 receives multiple JREQ packets from I_1 and I_2 respectively, it randomly selects its next hop back to S, e.g., via I_1. The JREP packet will be delivered from R_1 to I_1 associating with the next node ID equivalent to I_1. As I_1 receives the JREP packet, it will increase its weighting parameter (i.e., I_1.N_WGHT $= 0 + 1 = 1$) by recognizing itself being located on the reverse path towards S. Similarly,

I_2 receives the JREP packet from R_2 and also increases its N_WGHT by one (I_2.N_WGHT =1). For refreshing the delivering route, the second round of the JREQ/JREP process will be conducted by the source node S. Assuming that both R_1 and R_2 select I_2 as the intermediate node for sending the JREP packets to S, the weighting parameter of I_2 becomes I_2.N_WGHT = 1 + 2 = 3. Since I_1 is not chosen on the reverse path towards S, it will decrease its weighting as I_1.N_WGHT = 1 - 1 = 0. For the third round of route refreshing, I_2 will be directly chosen by S as the intermediate node for packet delivery since (I_2.N_WGHT = 3) > (I_1.N_WGHT = 0). Apparently, the value of I_2.N_WGHT will be counted up monotonously after the third round, which converges the original multicast structure $\mathcal{T}_o = \{S, I_1, I_2, R_1, R_2\}$ into the tree structure $\mathcal{T}_t = \{S, I_2, R_1, R_2\}$.

The mathematical analysis of the above process is shown as follows. It is assumed that R_1 selects its next hop node towards S as I_1 with probability p and I_2 with probability $1-p$ under the condition that I_1.N_WGHT = I_2.N_WGHT. It can be inferred that the process will be converged to the tree structure $\mathcal{T}_t$ in the first round with probability $(1-p)$; while converges to $\mathcal{T}_t$ in the second round with the probability $p \cdot (1-p)$. Therefore, the process is converged in the $(2k)^{th}$ round with the expected converge time equivalent to $2k \cdot p^k \cdot (1-p)$. It is noticed that the converge time is defined as the time period for the parameter I_1.N_WGHT to be reset to zero. As a result, the expected value of the required time T_1 for the process to converge is obtained as

$$E[T_1] = (1-p) + 2\sum_{k=1}^{\infty} kp^k(1-p) = \frac{1+p^2}{1-p} \tag{4.1}$$

Intuitively, it can be observed that the original multicast structure $\mathcal{T}_o$ will be converged to the tree structure $\mathcal{T}_t$ as long as $p < 1$, i.e., within finite value of $E[T_1]$. Moreover, another case is considered while the N_WGHT parameter is directly set to zero once the corresponding node is not selected as the next hop towards S. The expected value of the required time $E[T_2]$ can be solved by

$$E[T_2] = (1-p) + p(1 + E[T_2]) \tag{4.2}$$

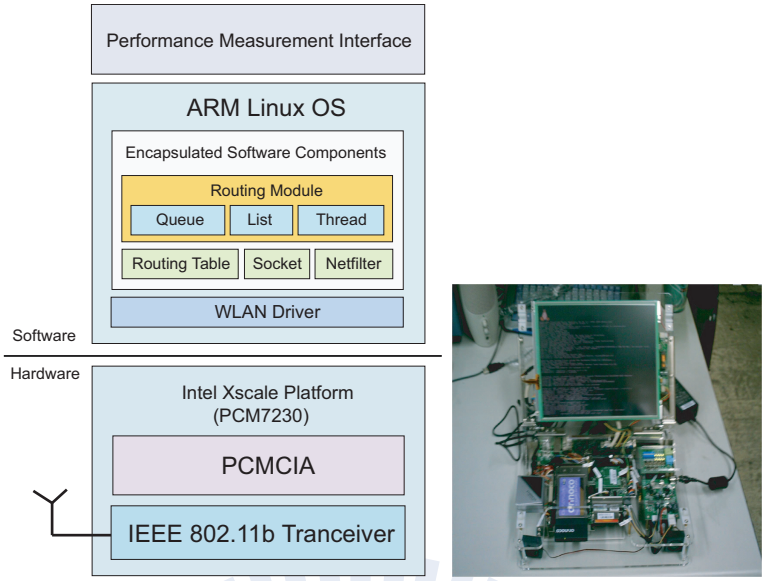

Figure 4.2: The software and hardware systems of the proposed CRP platform and the snapshot of the PCM-7230 embedded platform.

where the first term $(1-p)$ represents the expected converging time in the first round, and the second term $p(1+E[T_2])$ is the total expected converging time in the remaining rounds. Consequently, the expected value of the required converging time T_2 is acquired as

$$E[T_2] = \frac{1}{1-p} \tag{4.3}$$

Apparently, it can be observed from (4.1) and (4.3) that the expected converging time $E[T_2]$ is comparably faster than $E[T_1]$ under the condition with $p < 1$.

4.3 Proposed Component-based Routing Platform (CRP) with Encapsulated Software Design

4.3.1 Platform Overview

4.3.1.1 Software Platform

The software platform utilized for implementation is shown in the left schematic diagram of Fig. 4.2. On the top of the software system, the performance measurement interface (PMI)

is employed as the tool for collecting and recording the experimental results. The ARM Linux [56] with version 2.4.19 is adopted as the operating system, which handles the inserted software modules (i.e., the so-called kernel modules) with mutual interaction. Within the ARM Linux, all routing-related software components and kernel modules are wrapped as the ESCs for preventing the kernel panic (i.e., kernel fatal errors), leading to the convenience of protocol realization. At the bottom of the software system, the WLAN driver is served as the communication bridge for the software packet control and the physical hardware transmission. The WLAN driver for the AT&T/Lucent Wavelan adopted in the implementation is available under the GNU general public license (GPL).

4.3.1.2 Hardware Platform

Considering the hardware aspect, the PCM-7230 embedded platform [57] is shown in the right diagram of Fig. 4.2. It is an integrated embedded platform with an Intel XScale PXA-255 400MHz CPU, a PCMCIA interface, and other peripherals. It is noted that the PCM-7230 platform fulfills the essential hardware requirements for the design of the targeted routing protocol. Moreover, the Lucent Orinoco WLAN card, which supports the IEEE 802.11b via the PCMCIA interface, is utilized as the wireless interface for packet transmissions

4.3.2 Encapsulated Software Components (ESCs)

Due to the interrupts and procedure deadlocks, it is considered challenging to either modify or write the procedural calls within the kernel space of Linux systems. In order to prevent the occurrence of kernel panic, all kernel-supported software modules for implementing the routing mechanisms are wrapped as the ESCs within the proposed CRP platform. Contributing to the design of ESCs, the protocol implementation can therefore be focused on the realization of targeted routing algorithms, instead of dealing with abnormal kernel errors that frequently happen from the system modules. By adopting the ESCs, the efficiency of software design can be promoted with shortened coding and debugging time.

There are mainly seven ESCs that are incorporated into the ARM Linux in the proposed CRP platform, including the routing module, the packet queue, the list structure, the thread

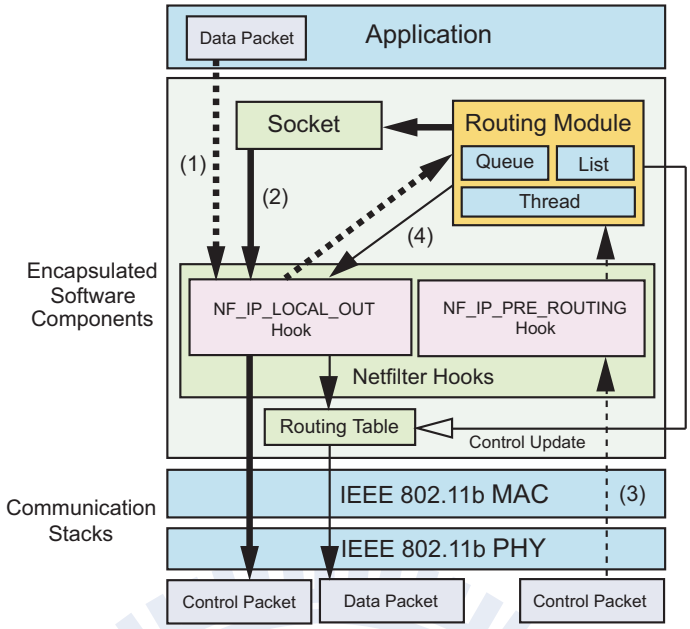

Figure 4.3: The schematic diagram of the packet flows for implementation.

element, the routing table, the Socket interface, and the Netfilter module [58]. The routing module implements all of the major routing mechanisms; while the packet queue is designed for the buffering of data packets. The list structure and the thread element are in general the two frequently-used components in the protocol implementation. The routing table handles the next-hop selection and mapping. The Socket interface provides a general operating interface of the transport layer, which supports both the TCP and the UDP packet transmissions. Moreover, the Netfilter module is adopted within the routing protocol for packet filtering.

4.3.3 ESC-based Packet Flow

Fig. 4.3 illustrates the schematic diagram of the packet flows for implementation; while the procedures for packet transmissions of a data source are explained. Initially, along the flow (1), the data packet is generated at the application layer and is sent to the ESCs. The data packet filtered by the NF_IP_LOCAL_OUT Netfilter hook is passed to the queue of the routing module in the case that the routing path has not been established. Next, along the flow (2), the routing module utilizes the Socket interface to create the control packet for constructing the routing paths. The control packet is passed via the Netfilter hooks down

Parameter Type	Parameter Value
JREQ Flood Timeout (FLDT)	6 sec
N_WGHT Count Down Timeout (CDT)	0.5 sec
CT_I	1.5 ms
CT_R	30 ms

Table 4.1: Parameter Values for the ECMR Protocol

to the communication stacks, and will consequently be transmitted to the neighbor nodes. After a period of time, the data source will receive incoming control packets generated by the neighbor nodes. These control packets, filtered by the NF_IP_PRE_ROUTING Netfilter hook along the flow (3), will both inform the routing module to update the routing table and flush the buffered data packets to the NF_IP_LOCAL_OUT Netfilter hook. In the end, along the flow (4), the data packets will be passed down to the communication stacks for transmission, forwarded by the neighbors of this data source, and arrived in the receiving node.

4.4 Performance Evaluation

Field experiments are conducted in order to evaluate the performance of the proposed ECMR protocol and validate the proposed CRP platform. The conventional ODMRP algorithm is also implemented for comparison purpose. Subsection 4.4.1 presents the parameters for protocol implementation; while the experimental results are shown in Subsection 4.4.2.

4.4.1 Parameters for Protocol Implementation

The implementation parameters of the proposed ECMR protocol are listed as in Table 4.1. The JREQ flood timeout (FLDT) is adopted as the time interval between two JREQ flooding processes initialized by the source node S. As the value of the FLDT is smaller, a multi-

Parameter Type	Parameter Value
JOIN QUERY Refresh Interval	6 sec
FG_FLAG Timeout	18 sec

Table 4.2: Parameter Values for the ODMRP Protocol

cast routing with comparably higher robust structure $\mathcal{T}$ can be achieved. However, increased control overhead which corresponds to higher power consumption will also be observed. The N_WGHT count down timeout (CDT) indicates the degree of the corresponding SN that participates in the multicast structure $\mathcal{T}$. The N_WGHT in the intermediate node will be decreased each time the CDT value is expired. As the N_WGHT is reduced to zero, the intermediate node will no longer be capable of forwarding the data packets for the multicast structure $\mathcal{T}$. Consequently, the larger value within CDT will result in more power consumption; while the robustness of the multicast structure can be enhanced. The values in the collection time for the intermediate node (CT_I) and the receiving node (CT_R) are denoted as the time intervals for the corresponding nodes to collect the JREQ packets. Based on the ECMR scheme, either a JREQ packet will be selected and rebroadcasted or a JREP packet will be generated.

The major parameters of the ODMRP protocol are listed in Table 4.2. The FG_FLAG parameter performs similarly to the N_WGHT parameter in the ECMR protocol except that it only possesses Boolean values, i.e., either *true* or $false$. The value within the FG_FLAG parameter will become $false$ either the FG_FLAG timeout expires or when the corresponding SN is not selected as the relay node. This indicates that the corresponding SN will not conduct further packet forwarding. The functionality of the JOIN QUERY refresh interval is considered similar to the FLDT as in the ECMR protocol. Both values are chosen to be the same (i.e., 6 sec) in order to provide fair comparison between these two algorithms. Moreover, the FG_FLAG timeout is selected as three times of the JOIN QUERY refresh interval, which was suggested by the original design of the ODMRP protocol [49].

4.4.2 Experiment Results

The network topology utilized in the experiments is illustrated as in Fig. 4.4. The source node S intends to deliver data packets to its corresponding receivers R_1, R_2, and R_3 via the intermediate nodes I_1 and I_2. Two metrics are employed for performance comparison: the energy consumption for relaying data packets and the packet delivery ratio.

Fig. 4.5 shows the performance comparison between the ECMR and the ODMRP algo-

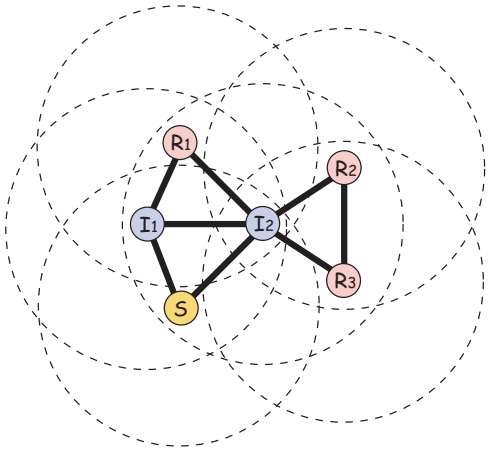

Figure 4.4: The network topology for field experiments.

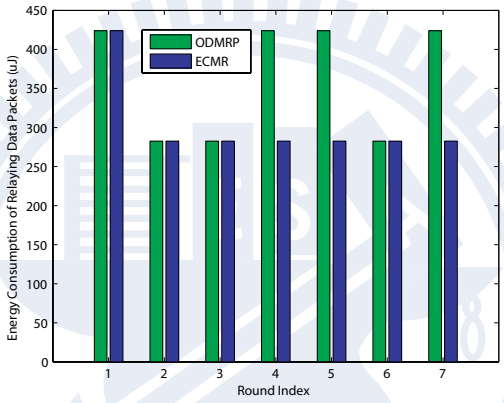

Figure 4.5: Energy consumption for relaying data packets versus round index.

rithms by observing the energy consumption versus the round index. It is noted that the round index considers the time interval defined by the FLDT parameter which conducts one set of JREQ/JREP process. The energy consumption for relaying data packets is calculated by multiplying the total data packets transmitted between every two rounds with the energy consumption for each packet transmission. It is noted that the transmitter bit rate is equal to 11 Mbps; while the transmitting power is 15 dBm. The data rate is fixed on 6 packets per round with each packet size of 1024 bytes.

Since the ODMRP protocol is designed based on the shortest path route construction, node R_1 will randomly select either I_1 or I_2 as its upstream node associated with the corresponding FG_FLAG set to be true. It is noted that the FG_FLAG parameter of I_2 is consistently set

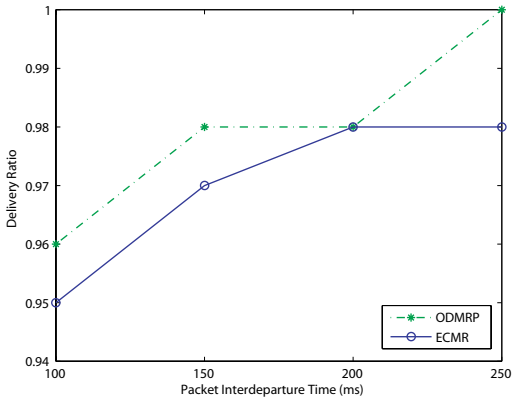

Figure 4.6: Packet delivery ratio versus packet interdeparture time.

to be true since it is the only node on the shortest path to both R_2 and R_3. Consequently, the number of required intermediate nodes by adopting the ODMRP algorithm will alternate between one and two, which results in the fluctuation on the energy consumption versus the round index, i.e., the green bars as shown in Fig. 4.5. On the other hand, the number of intermediate nodes will always be one after the second round by exploiting the proposed ECMR protocol. Considering the worst case, node R_1 will select I_1 as the upstream node to S in the first round. In the remaining rounds, node R_1 will always select I_2 as the upstream node to S since the P_WGHT value via node I_2 is greater than that via node I_1. It can be seen from the experiment results (in Fig. 4.5) that the energy consumption by using the ECMR protocol is comparably less than that from the ODMRP algorithm. It is also noted that as the available number of intermediate nodes is increased, the benefits of adopting the ECMR algorithm will become more observable.

Fig. 4.6 shows the performance comparison by exploiting the packet delivery ratio versus the interdeparture time with packet size of 1024 bytes. It is noted that the packet interdeparture time represents the time interval for delivering two consecutive data packets. It can be seen that both the ECMR and the ODMRP protocols can provide high packet delivery ratio (with almost 100%) under different packet interdeparture time. The slightly low delivery ratio resulting from the ECMR algorithm is attributed to its comparably less duplicated data packet transmissions.

4.5 Summary

An energy conserving multicast routing (ECMR) protocol and the component-oriented routing platform (CRP) with encapsulated design are proposed in this chapter. Thanks to the proposed encapsulated software components (ESCs) within the CRP testbed and the component-oriented nature, the engineers can simply focus on the realization of routing mechanisms without the strange errors from the underlying operating system. Moreover, the debugging process can also be simplified into the correctness checking of each component-related procedure, which accelerates the protocol implementation. Both the proposed ECMR protocol and the existing mesh-based ODMRP algorithm are implemented on the proposed CRP embedded platform for performance evaluation. The implementation methodology of the proposed ECMR algorithm and the corresponding software/hardware architectures are properly illustrated. The experiment results show that the ECMR protocol can provide high packet delivery ratio under different packet interdeparture time; while comparably less energy is consumed. Since the energy consumption can be effectively reduced, the proposed ECMR protocol associated with high packet delivery ratio can be adopted as a multicast routing protocol in the construction of the green wireless access networks.

Chapter 5

Greedy Fast-Shift Block Acknowledgement Mechanism

Chapter Overview

In the data link layer protocol design for achieving the green wireless access networks, the throughput enhancement can be considered a feasible way since less power will be consumed with regard to the same amount of data information. This chapter is with the main theme of the wireless local area network (WLAN) due to the popularity of the WiFi technologies. More people can benefit greatly from the proposed green protocol. The techniques of frame aggregation and block acknowledgement are utilized in the IEEE 802.11n standard for achieving high throughput performance from the medium access control perspective. The conventional greedy scheme for block acknowledgement adopts the transmitter-defined starting sequence number (SSN) to construct the acknowledgement window for recognizing the correctness of data packets. However, there exist correctly received packets that lie outside of the acknowledgement window which will unavoidably be retransmitted by adopting the conventional scheme. In this chapter, a greedy fast-shift (GFS) block acknowledgement mechanism is proposed to provide the receiver-defined SSN, which can both implicitly acknowledge the correctly received packets before the SSN and explicitly identify the correctness information for the packets after the SSN. In order to evaluate the effectiveness of the GFS scheme, the

analytical models for these two mechanisms are proposed based on the window utilization. Compared to the conventional greedy scheme, it is observed from the simulation results that the proposed GFS method can provide better performance owing to its fast-shift behavior on acknowledgement window. The proposed GFS scheme can therefore be utilized as the data link protocol in the construction of the green wireless access networks.

5.1 Introduction

A wireless network is a type of computer networks that utilizes wireless communication technologies to maintain connectivity and exchange messages between stations over wireless media, such as infrared, laser, ultrasound, and radio waves. Due to the wireless nature, wireless networks possess many advantages against its wired counterpart, e.g., support of device mobility, simple installation, and ease of deployment. Depending on the size of wireless coverage, wireless networks can in general be divided into five different categories, including wireless regional area networks (WRANs), wireless wide area networks (WWANs), wireless metropolitan area networks (WMANs), wireless local area networks (WLANs), and wireless personal area networks (WPANs). The IEEE standards association establishes five standard series of IEEE 802.22, 802.20, 802.16, 802.11, and 802.15 for the corresponding networks. Among these wireless standard series, the IEEE 802.11 standard is considered the well-adopted suite due to its remarkable success in both design and deployment.

Various amendments are contained in the IEEE 802.11 standard suite, mainly including IEEE 802.11a/b/g [59–61], IEEE 802.11e [62] for quality-of-service (QoS) support, and the newly-issued IEEE 802.11n [63] for high throughput performance. In order to fulfill the requirement for achieving enhanced throughput, the IEEE 802.11 Task Group N (TGn) enhances the physical layer (PHY) data rate by adopting advanced communication techniques, such as orthogonal frequency-division multiplexing (OFDM) [64] and multi-input multi-output (MIMO) [65] technologies. However, it has been investigated in [66] that simply improves the PHY data rate will not suffice for enhancing the system throughput from the medium access control (MAC) perspective. Accordingly, the IEEE 802.11 TGn further exploits packet

aggregation techniques to moderate the drawbacks that are originated form the MAC/PHY overheads.

There are research works proposed in [67–70] that focus on the schemes for data packet aggregation. Yang [67] has suggested to adopt packing, concatenation, and multiple frame transmission in order to reduce the MAC/PHY overheads. Lu et al. [68] recommended the MAC queue aggregation (MQA) scheme for the enhancement of VoIP traffic; while Wu [69] proposed the differentiated data aggregation (DDA) mechanism which exploited the multilevel modulation from the PHY layer for improving the data aggregation of the WLANs. Ghazisaidi et al. [70] further considers the joint aggregation effects with the Ethernet passive optical network (EPON) [71] system in the hybrid optical fiber-wireless (FiWi) broadband access networks [72]. It is also noted that two-level aggregation techniques, i.e., the aggregate MAC service data unit (A-MSDU) and the aggregate MAC protocol data unit (A-MPDU), are adopted within the IEEE 802.11n standard for performance enhancement of the network throughput. The performance of the A-MSDU and A-MPDU schemes has been analyzed in the research works [73–76], and the decision of the optimal frame size can be found in [77]. Finally, the implementation and experiments are conducted in [78] for validating the effectiveness of the frame aggregation schemes.

It has been studied that the large amount of small-sized control packets, i.e., the acknowledgement (ACK) packets, can significantly degrade the throughput performance [79]. The use of the stop-and-wait automatic repeat request (ARQ) [80] in the prior wireless LAN standard takes the major blame for the creation of these small ACK packets since each data packet should be acknowledged by an independent ACK packet. Due to the observed inefficiency, the block ACK mechanism has been proposed in both the IEEE 802.11e and IEEE 802.11n standards for the aggregation of ACK packets. It is noted that the block ACK scheme utilizes comparably longer payload to accommodate the information from numerous ACK packets, which can effectively reduce the total number of required ACK packets.

The representative block ACK scheme such as the extended block ACK (EBA) mechanism [81, 82] is denoted as the greedy scheme (GS) which can be utilized in the IEEE 802.11n standard. Initially, the transmitter assigns each packet with a specific sequence number.

Based on these sequence numbers, the receiver initiates the block ACK packet which contains the bitmap with its first bit beginning from a specific starting sequence number (SSN). The transmitter will be informed regarding the correctness of each numbered packet, i.e., the acknowledgement window ranging from the SSN to the end sequence number of the bitmap. Afterwards, the GS scheme will resend the unsuccessfully received packets together with the new-coming packets in order to both recover the packet errors and enhance the system throughput. However, the limited bitmap size may cause the problem that some correctly received data packets can not be properly acknowledged since these packets may lie outside of the acknowledgement window defined by the SSN value. In the conventional GS scheme, significant throughput degradation due to this problem can be frequently observed since the transmitter is in charge of determining the SSN value. It therefore lacks the flexibility of changing the SSN value since more information can be obtained from the receiver side. The details of the GS scheme and its underlying problem will further be described in the next section.

In this chapter, a greedy fast-shift (GFS) block acknowledgement mechanism is proposed from the receiver's point of view to reduce the occurrence of the aforementioned problem due to the insufficient bitmap size. Based on the proposed GFS scheme, the receiver will derive and provide the SSN value which carries additional information that the packet with sequence number (SN) smaller than the SSN are considered correctly received. It can both implicitly acknowledge the correctly received packets before the SSN and also explicitly provide the correctness information for the packets after the SSN. The SSN value can therefore be increased faster than the conventional GS scheme, which effectively mitigates the performance degradation resulting from the insufficient bitmap. Furthermore, analytical models for these two block acknowledgement mechanisms are proposed based on the Markov chain techniques [83] to evaluate the window utilization from the mathematical point of view. The correctness and effectiveness of the derived analytical models are validated via simulations. With respect to system throughput, end-to-end delay, and blocking overhead, it is observed from the simulation results that the proposed GFS scheme outperforms the conventional GS method under different packet error probabilities and window sizes.

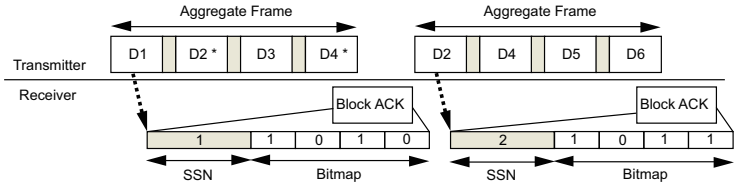

(a)

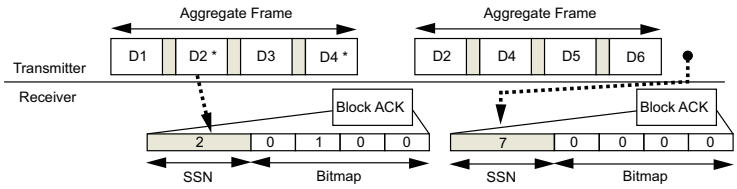

(b)

Figure 5.1: Examples for the two block ACK mechanisms under window size $W = 4$: (a) the conventional greedy scheme (GS), and (b) the proposed greedy fast-shift (GFS) scheme.

The rest of this chapter is organized as follows. Section 5.2 describes both the conventional GS scheme and the proposed GFS acknowledgement mechanism. The proposed analytical models for both schemes are further derived and explained in Section 5.3. Section 5.4 shows the performance validation and comparison of these two schemes via simulations. Section 5.5 summarizes the chapter.

5.2 Block Acknowledgement Mechanisms

In this section, the conventional GS scheme and its underlying problem will first be described. Furthermore, the proposed GFS mechanism for block acknowledgement will be further explained as follows.

5.2.1 Conventional Greedy Scheme

The conventional block acknowledgement mechanism denoted as the GS scheme is described in this subsection. For the generalization of data aggregation mechanisms, a system parameter called window size W is introduced to denote the maximum number of data packets that are contained within a single frame. The characteristics of the conventional GS scheme is explained with the example as shown in Fig. 5.1(a) under $W = 4$ as follows.

In the conventional GS scheme, the transmitter assigns each data packet with an SN for packet identification, e.g., SN = 1 for D1 and SN = 2 for D2. As illustrated in Fig. 5.1(a), the first aggregate frame consisting of W data packets from D1 to D4 is delivered by the transmitter; while both D2 and D4 packets denoted with the $*$ sign are considered corrupted. The block ACK packet consists of an additional SSN field in front of its bitmap array to record the sequence number of the starting packet within the aggregate frame, e.g., SSN = 1 denotes that D1 is the starting packet in the first frame; and SSN = 2 represents D2 as the starting packet for the second frame. Moreover, the bitmap array of size W within the block ACK packet indicates the packet correctness based on the consecutive SNs.

As shown in Fig. 5.1(a), the bitmap from the first block ACK packet $b = [1010]$ with SSN = 1 contains the correctness information of the aggregated data packets from SN = 1 to SN $= 1 + (W - 1) = 4$, i.e., for the consecutive D1 to D4 data packets. It is noticed that the one value within the bitmap denotes that the corresponding packet is correctly received; while the zero value implies that the correctness of the corresponding packet should be determined by the transmitter since the packet can be either corrupted or previously acknowledged. After the reception of the first block ACK packet, the transmitter redelivers the previously unacknowledged D2 and D4 packets together with the newly scheduled D5 and D6 packets in the second aggregate frame. Associated with SSN = 2 and bitmap $b = [1011]$ in the second block ACK packet, the receiver notifies the transmitter that D2, D4, and D5 packets are correctly received while the correctness of D3 packet is undetermined. Based on the previous reception within the transmitter, it can be observed that packet D3 was successfully received such that it is not required to be retransmitted. Furthermore, it is worthwhile to notice that the correctness of packet D6 becomes undetermined even though it is correctly received by the receiver. The performance degradation due to the insufficient bitmap for recording the correctness information can therefore be perceived.

5.2.2 Proposed Greedy Fast-Shift (GFS) Scheme

The greedy fast-shift (GFS) block acknowledgement mechanism is proposed in this subsection as an enhanced version of the conventional GS scheme. The main objective of the proposed

GFS scheme is to mitigate the performance degradation due to insufficient bitmap of the conventional GS scheme. The procedures of proposed GFS scheme with $W = 4$ is illustrated in the exemplified schematic diagram of Fig. 5.1(b). Inherited from the conventional GS scheme, the characteristics of both the SN and SSN fields in the transmitter side are still preserved. For efficiency consideration, the mechanism of retransmitting both the corrupted packets and the new-coming packets are also employed. The major differences between the proposed GFS mechanism and the conventional GS scheme are on the methodologies to determine the SSN value at the receiver side. In the GS scheme, the SSN of the feedback block ACK packet is determined by the SN of first packet in the aggregate frame. In other words, the receiver does not change the value of SSN, which is actually assigned by the transmitter. On the other hand, in the proposed GFS scheme, the SSN value is given by the receiver as the SN of the first unreceived data packet. Consequently, the SSN value of the block ACK packet may not necessarily be equal to the SN of first packet in the aggregate frame. It can be a larger value or even beyond the largest SN in the aggregate frame.

The bitmap array, i.e., the acknowledgement window, specified in the block ACK packet of the proposed GFS scheme still represents the packet correctness based on the consecutive SNs starting with the SSN value. Considering the same case as in Fig. 5.1(a), the packets D2 and D4 in the first aggregate frame of Fig. 5.1(b) are corrupted. Instead of receiving the block ACK with SSN = 1, the transmitter receives a block ACK packet with SSN = 2 in the proposed GFS scheme since the SSN is determined by the receiver as the SN of the first unreceived data packet, i.e., the packet D2. Likewise, after the reception of the first block ACK packet, the transmitter redelivers the previously unacknowledged D2 and D4 packets together with the newly scheduled D5 and D6 packets in the second aggregate frame. After receiving the second aggregate frame with correct D2, D4, D5, and D6 packets, the receiver knows that the data packets from D1 to D6 are correctly received. Therefore, the receiver assigns the SSN to be 7 which is the SN of the first unreceived packets. It can be observed that the SSN value will be larger than the SN's range of the aggregate frame. Afterwards, the receiver sends the block ACK packet with SSN = 7 and bitmap $b = [0000]$, which indicates that the receiver does not receive packets from D7 to D10 and all the packets before D7, i.e.,

D1 to D6, are correctly received.

Instead of providing explicit acknowledgement to each packet in the aggregate frame, the proposed GFS scheme adopts a hybrid method to both implicitly acknowledge the correctly received packets before the SSN and also explicitly provide the correctness information of those packets after the SSN. Contributing to this hybrid method, the SSN value will grow faster than that in the conventional GS scheme, resulting in the phenomenon of fast-shift acknowledgement window specified in the block ACK packet. The performance degradation due to the insufficient bitmap can therefore be mitigated. The detailed processes and the analytical model of the proposed GFS scheme are further explained in Subsection 5.3.2.

5.3 Proposed Markovian Chain-based Analytical Models for Block Acknowledgement Mechanisms

In this section, two proposed analytical models for the conventional GS scheme and the proposed GFS mechanism will be respectively formulated based on the Markov chain techniques. The main target of both analytical models is focused on the throughput performance based on the metrics of window utilization. The window utilization is defined as the average number of successfully acknowledged packets within an aggregate frame divided by the window size W. It is intuitive to directly relate the window utilization to the system throughput of the corresponding scheme. In order to simplify the derivations of the proposed analytical models, one transmitter/receiver pair for packet transmission is considered in the network. Moreover, it is assumed that all data packets possess the same packet error probability p_e; while the block ACK packets are considered correctly received. The explanation of the two proposed analytical models are stated as follows.

5.3.1 Analytical Model for Conventional Greedy Scheme

The analytical model for the conventional GS scheme is constructed by adopting the Markov chain techniques. Based on the Markovian approach, there exists a state transition diagram consisting of internal states and the respective state transition probability. In this subsection,

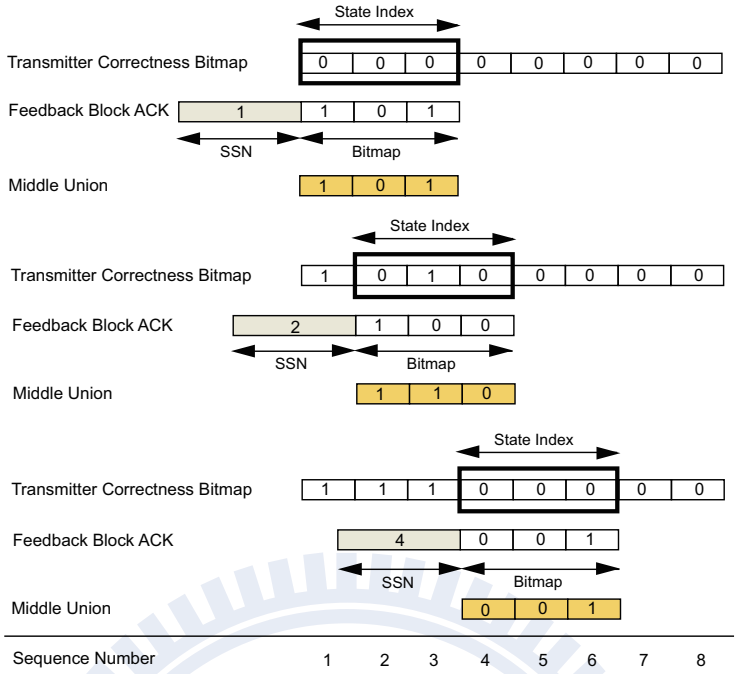

Figure 5.2: The three critical parameters for the internal state definition of the GS scheme: (a) the transmitter correctness bitmap, (b) the middle union, and (c) the state index.

the internal states for the analytical model of the GS scheme will first be defined. The underlying state transition diagram with the transition probability for the corresponding state transition is also properly formulated. Finally, the derivation of window utilization for the GS scheme concludes the analytical model. It is noted that all the context will be provided based on the generic analytical model with window size W. An illustrative example under $W = 3$ will be addressed for further explanation.

5.3.1.1 Internal States

In order to define the internal states of GS scheme, three parameters are first introduced, including the transmitter correctness bitmap, the middle union, and the state index. The transmitter correctness bitmap represents the Boolean correctness array for all numbered data packets from the transmitter's perspective. The state index is a set of W binary digits with its most significant bit located at the first zero of the transmitter correctness bitmap. The middle union is acquired by implementing the bitwise OR operation on the current state

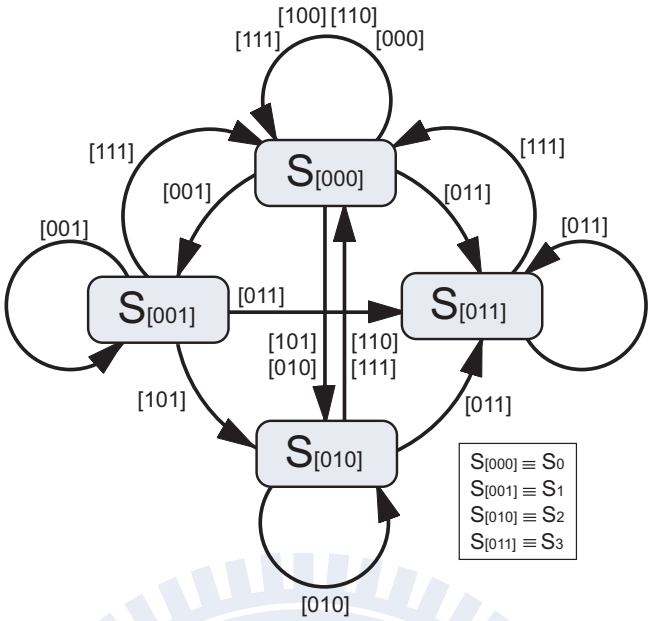

Figure 5.3: State transition diagram for the conventional GS scheme under the window size $W = 3$: each state transition is represented as a unidirectional link with the causal middle union of width W.

index and the feedback block ACK bitmap. It is also noted that the state index will be utilized to define its respective internal state.

The illustrative example for the three critical parameters under the window size $W = 3$ is shown in Fig. 5.2. Initially, the transmitter correctness bitmap is an all-zero array, which results in the state index $k = [000]$. The transmitter starts to deliver the numbered data packets D1, D2, and D3 to the receiver. It is assumed that a feedback block ACK packet with a bitmap of $b = [101]$ is consequently acquired by the transmitter. As a result, the middle union can be computed as $m = k \cup b = [000] \cup [101] = [101]$. As illustrated in Fig. 5.2, the transmitter correctness bitmap is also updated by recording the bit values in the middle union into its corresponding bits. As the transmitter correctness bitmap is changed, the state index is consequently shifted to become $k = [010]$ based on its definition. According to the conventional GS scheme, the transmitter redelivers the previously corrupted packet D2 together with the newly scheduled packets D4 and D5, and receives a feedback block ACK packet consisting of a bitmap $b = [100]$. As a consequence, the new state index will be calculated and obtained as $k = [000]$ as in Fig. 5.2.

Based on the definition, the state index must have the leading zero to represent either a previously corrupted or a newly scheduled packet. Therefore, the conventional GS scheme will possess a total of 2^{W-1} internal states that are denoted as S_k with the state index $k \in [0, 1, ..., (2^{W-1} - 1)]$. As shown in Fig. 5.3, four states S_0 to S_3 exist in the state transition diagram for the conventional GS scheme under the window size $W = 3$. In order to facilitate the explanation, each state can be represented by either the decimal or the binary subscript, i.e., $S_0 \equiv S_{[000]}$, $S_1 \equiv S_{[001]}$, $S_2 \equiv S_{[010]}$, and $S_3 \equiv S_{[011]}$.

5.3.1.2 State Transition Diagram

In the state transition diagram of window size W, there exist 2^{W-1} internal states and their corresponding state transitions. Each transition between two states is represented as a unidirectional link from the original state S_i to the resulting state S_k. Moreover, the potential middle unions that result in the state transition are also shown around the link. The representative state transition diagram under the window size $W = 3$ is illustrated in Fig. 5.3. Considering that the transition from $S_{[001]}$ to $S_{[010]}$ results from the middle union $m = [101]$, the middle union $m = [101]$ will consequently let the transmitter increase the SSN by one, causing the state index to become $k = [010]$, i.e., the state of $S_{[010]}$. It is noted that the mechanism for acquiring the resulting state can be generalized by the rule as to remove all the leading ones in the middle union and pad an equal number of zeros from the right side.

5.3.1.3 State Transition Probability

As shown in Fig. 5.3, the state transition probability from $S_{[001]}$ to $S_{[010]}$ can be computed from the bit values within the middle union $m = [101]$ as $G_{[001]\rightarrow[010]} = (1 - p_e) \cdot p_e$, where p_e denotes the packet error probability and $G_{[001]\rightarrow[010]}$ represents the transition gain from $S_{[001]}$ to $S_{[010]}$. It is noticed that the rightmost bit within the middle union is not considered in the computation of packet error probability since the data packet was correctly received in the previous transmission. The generic transition probability from S_i to S_k under the window size W is modeled as the transition gain $G_{i\rightarrow k}$ which can be computed via Algorithm 5.

As shown in the *for* loop of Algorithm 5, the transition gain $G_{i\rightarrow k}$ is acquired by adopting

Algorithm 5: *Transition Gain for Greedy Scheme*

```
Data: i, k, and r are unsigned binary integers of W digits
Result: G_{i→k}
begin
    G_{i→k} ⟵ 0
    for m ⟵ 0 to 2^W − 1 do
        if i = bitwise_and(i, m) then
            α ⟵ number_of_one(m) − number_of_one(i)
            β ⟵ number_of_zero(m)
            r = m
            while leftmost_bit(r) = 1 do
                shift r one bit left with zero padding
            end
            if r = k then
                G_{i→k} ⟵ G_{i→k} + (1 − p_e)^α p_e^β
            end
        end
    end
end
```

the exhaustive search method, i.e., to scan from every possible middle union m. Furthermore, the bitwise AND operation of the possible middle union and the state index k will consistently be equal to k since the bit values that denote correctly received packets in the transmitter correctness bitmap will always have the one value. For example, it can be observed that the bitwise AND operation on the middle union $m = [101]$ and the original state index $k = [001]$ is still equivalent to the original state index $k = [001]$.

As a result, the algorithm employs the function *bitwise_and*() and the state index i as a mask to filter out those unsuitable middle unions m recognized by the discriminant that the bitwise AND operation of i and m is not equal to i. Moreover, the number of newly correctly acknowledged packets is represented as the variable α. The variable β records the number of the remaining zeros, i.e., the number of those unacknowledged packets. The two variables α and β are utilized for the computation of packet error probability based on the corresponding middle union m. For the next step, the *while* loop generates the resulting state index r by the rule to suppress all leading one of the middle union m and to pad an equal number of zeros from the right-hand side. Consequently, the transition gain $G_{i\to k}$ can be computed via the sum of error probability from each suitable middle union m leading to the resulting state index $r = k$.

5.3.1.4 Window Utilization

The window utilization for the GS scheme can be derived from the saturated probability of internal states after the occurrence of an infinite number of state transitions. The saturated probability Θ_k for each internal state S_k under the window size W can be computed as the sum of all the possible 2^{W-1} state transitions as

$$\Theta_k = \sum_{i=0}^{2^{W-1}-1} G_{i \to k} \Theta_i, \tag{5.1}$$

for $\forall k \in [0, 1, ..., 2^{W-1} - 1]$. However, these state equations form an underdetermined linear system which has an infinite number of solutions for all the Θ_k. Therefore, for solving the saturated probability Θ_k, an additional constraint is imposed in order to make the underdetermined system possess a finite number of solutions, i.e.,

$$\sum_{k=0}^{2^{W-1}-1} \Theta_k = 1 \tag{5.2}$$

since the sum of all saturated state probability Θ_k in a Markov state transition diagram should be equal to one. After the derivation of saturated probability Θ_k from (5.1) and (5.2), the window utilization U_{GS}^{W} of the GS scheme under the window size W can be obtained as

$$U_{GS}^{W} = \frac{\sum_{k=0}^{2^{W-1}-1} (1 - p_e) Z_W(k) \Theta_k}{W}, \tag{5.3}$$

where the subscript GS is adopted to denote the conventional GS scheme. $Z_W(k)$ represents the number of zeros within the state index k of W digits, i.e., to indicate the number of unacknowledged data packets. It is noted that the product $(1 - p_e) \cdot Z_W(k)$ denotes the expected total number of properly acknowledged data packets that is forecasted in the next state transition of S_k.

An illustrative example under the window size $W = 3$ is provided as follows. Based on

(5.1), the four state equations under $W = 3$ are represented via the matrix form as follows:

$$\begin{bmatrix} \Theta_0 \\ \Theta_1 \\ \Theta_2 \\ \Theta_3 \end{bmatrix} = \begin{bmatrix} 1-2p_e+2p_e^2 & (p_e-1)^2 & 1-p_e & 1-p_e \\ (1-p_e)p_e^2 & p_e^2 & 0 & 0 \\ p_e(1-p_e) & p_e(1-p_e) & p_e^2 & 0 \\ p_e(p_e-1)^2 & (1-p_e)p_e & (1-p_e)p_e & p_e \end{bmatrix} \begin{bmatrix} \Theta_0 \\ \Theta_1 \\ \Theta_2 \\ \Theta_3 \end{bmatrix} \tag{5.4}$$

Associated with $\sum_{k=0}^{3} \Theta_k = 1$, the solution for each saturated probability Θ_k of S_k can be obtained as

$$\Theta_0 = \frac{1+p_e}{1+3p_e+2p_e^2+p_e^3} \tag{5.5}$$

$$\Theta_1 = \frac{p_e^2}{1+3p_e+2p_e^2+p_e^3} \tag{5.6}$$

$$\Theta_2 = \frac{p_e(1+p_e+p_e^2)}{1+4p_e+5p_e^2+3p_e^3+p_e^4} \tag{5.7}$$

$$\Theta_3 = \frac{p_e(1+2p_e+p_e^2+p_e^3)}{1+4p_e+5p_e^2+3p_e^3+p_e^4} \tag{5.8}$$

if $p_e \neq 1$. In the case of $p_e = 1$, it can be acquired that $\Theta_0 = 1$ and $\Theta_1 = \Theta_2 = \Theta_3 = 0$. As a result, the window utilization for the $W = 3$ case becomes

$$U_{GS}^3 = \frac{(1-p_e)(3\Theta_0+2\Theta_1+2\Theta_2+\Theta_3)}{3}, \tag{5.9}$$

which concludes the description and derivation of the analytical model for conventional GS scheme.

5.3.2 Analytical Model for Proposed Greedy Fast-Shift Scheme

The derivation of the analytical model for proposed GFS scheme is similar to that of the conventional GS scheme in the aspect of adopting the Markov chain techniques. Accordingly, the internal states, the state transition diagram, and the corresponding state transition probability will first be described and properly defined. With the help of these defined elements, the analytical model for the GFS scheme is concluded by the mathematical expression of window

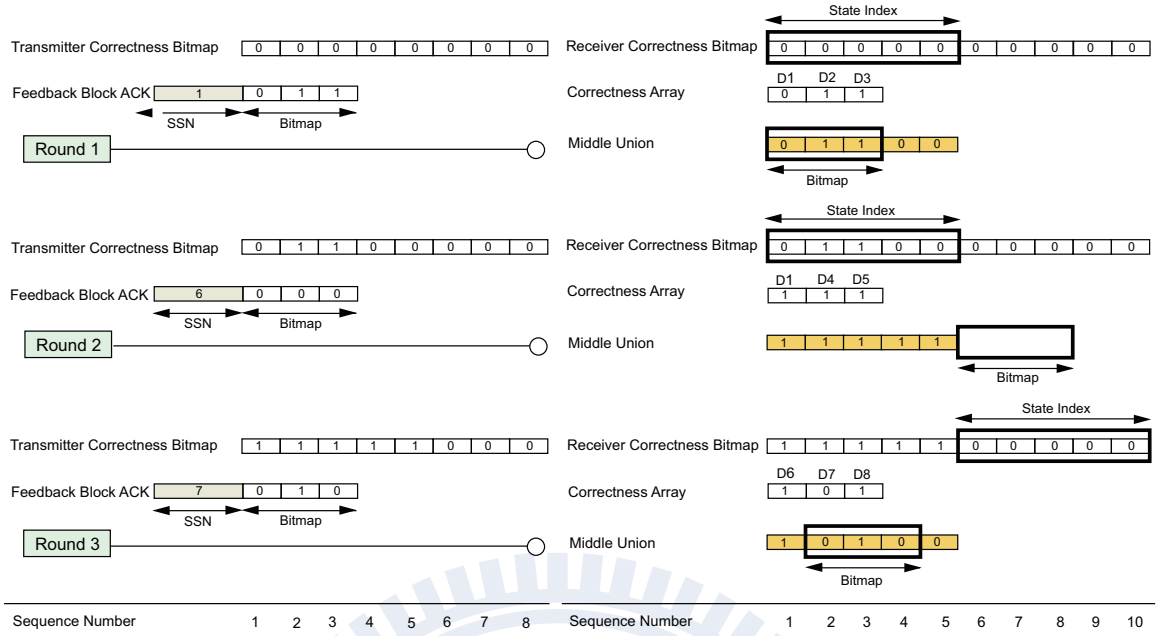

Figure 5.4: The five critical parameters for the internal state definition of the proposed GFS scheme: (a) the transmitter correctness bitmap, (b) the receiver correctness bitmap, (c) the state index, (d) the correctness array, and (e) the middle union.

utilization, and all the context will be provided by a generic analytical model for the window size W with an illustrative example under $W = 3$.

5.3.2.1 Internal States

In order to define the internal states of the proposed GFS scheme, five parameters should be introduced including (a) the transmitter correctness bitmap, (b) the receiver correctness bitmap, (c) the state index, (d) the correctness array, and (e) the middle union. The transmitter and receiver correctness bitmaps respectively represent the Boolean correctness array for all numbered data packets from the transmitter's and the receiver's perspectives. The state index is defined as a set of $2W - 1$ binary digits with its most significant bit at the first zero of the receiver correctness bitmap. It is noticed that the state index for the proposed GFS scheme is defined from the receiver's perspective instead of the transmitter's aspect as in the GS scheme. The correctness array represents the situations whether the individual data packet in the current aggregate frame is successfully received or not. In the end, the middle

union is defined as the combined result of the current state index and the correctness array. The combination is conducted by setting the corresponding bit in the current state index if the data packet is specified as correctly received by the correctness array. It is noted that the middle union also has the size of $2W - 1$ digits.

The illustrative example under the window size $W = 3$ is shown in Fig. 5.4. Initially, in the first round, both the transmitter and the receiver correctness bitmaps are all-zero arrays, which result in the state index $k = [00000]$. It is noted that the size of state index becomes $2W - 1 = 5$. The transmitter starts to deliver the numbered data packets from D1 to D3. Assuming the correctness array as $c = [011]$ which denotes that only the first packet D1 is corrupted, the middle union will become $m = [01100]$ since the corresponding fields for D2 and D3 in the state index are set to be 1. In the same time, based on the definition that the most significant bit of the state index must be the first zero of the receiver correctness bitmap, the new state index will therefore be $k = [01100]$ as shown in the second round of Fig. 5.4. According to the proposed GFS algorithm, the receiver will choose SSN to be the SN of the first unacknowledged packet, i.e., the packet D1. Consequently, the receiver will send the block ACK with SSN= 1 and the bitmap $b = [011]$ back to the transmitter.

After the reception of feedback block ACK packet, the transmitter correctness bitmap is updated as shown in the second round of Fig. 5.4. Therefore, the transmitter will send the previously corrupted packet D1 associated with new-coming packets D4 and D5 to the receiver. If the correctness array is $c = [111]$, i.e., all packets are correct, the middle union will become $m = [11111]$ since packets D1, D4 and D5 are correctly received. The new state index will therefore be right shifted five digits and become $k = [00000]$ as in the third round. Based on the GFS scheme, the SSN of the feedback block ACK packet in the second round will become 6 and the corresponding bitmap will be $b = [000]$. From the transmitter side, SSN= 6 indicates that all packets before D6 are successfully received. Therefore, the first five digits of the transmitter correctness bitmap are all 1 as in the third round of Fig. 5.4. The procedures will be repeatedly conducted if there is any data packet to be transmitted.

The reason for the state index to contain $2W - 1$ digits is stated as follows. Consider the worst case that the transmitter delivers an aggregate frame with W packets and only the

first packet is failed to be transmitted. The transmitter will retransmit the failed first packet together with the other $W-1$ new-coming packets. Therefore, from the receiver's perspective, the number of influenced digits in the receiver correctness bitmap will be $2W-1$, which also represents the total number of involved $W+(W-1)$ data packets during the transmissions.

Moreover, it is required to figure out the total number of state indexes and that for the corresponding internal states. The leftmost bit of the state index is always zero according to the definition of state index. It is also noted that the rightmost $W-1$ digits of the state index can be influenced by the remaining $W-1$ digits (i.e., from the second to the W-th digits) since these remaining $W-1$ digits actually control the number of new-coming packets in the next aggregate frame. Therefore, these $W-1$ digits are responsible for the calculation of total number of internal states. In the case that none of these $W-1$ digits is zero, the transmitter will transmit $W-1$ new-coming packets, which results in the total number of state indexes as $C_0^{W-1}2^{W-1}$, where C_a^b is denoted as the binomial coefficient. If one of these $W-1$ digits is zero, the transmitter will retransmit the failed packets with $W-2$ new-coming packets which will cause an additional number of $C_1^{W-1}2^{W-2}$ state indexes. As a result, the total number of state indexes or internal states can be obtained as

$$N_{GFS}^{W} = \sum_{i=0}^{W-1} C_i^{W-1} 2^{W-1-i}. \tag{5.10}$$

The proposed GFS scheme has N_{GFS}^{W} internal states that are denoted as V_k with the index $k \in \mathbb{I}$, where $\mathbb{I}$ is the set of all state indexes. As shown in Fig. 5.5, the nine internal states $V_{[00000]}$, $V_{[00100]}$, $V_{[01100]}$, $V_{[01000]}$, $V_{[00110]}$, $V_{[01110]}$, $V_{[01101]}$, $V_{[01111]}$, and $V_{[01010]}$ are depicted in the state transition diagram for the proposed GFS scheme under the window size $W=3$.

5.3.2.2 State Transition Diagram

The state transition diagram of GFS scheme under the window size W consists of N_{GFS}^{W} internal states and their possible state transitions. The exemplified state transition diagram under window size $W=3$ is illustrated in Fig. 5.5. Each transition between two states is represented as a unidirectional link from the original state V_i to the resulting state V_k.

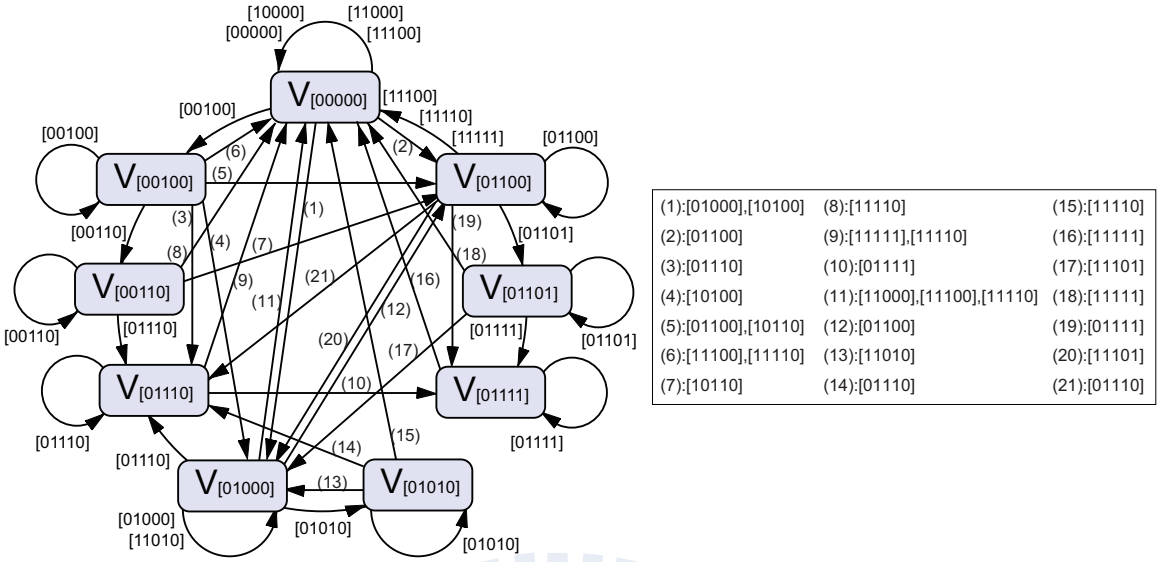

Figure 5.5: State transition diagram for the proposed GFS scheme under the window size $W = 3$: each state transition is represented as a unidirectional link with the causal middle union of width $2W - 1$.

Moreover, the middle unions that result in the state transitions are also shown around the link. For example, the state transition from $V_{[00100]}$ to $V_{[01000]}$ is obtained according to the middle union $m = [10100]$. This middle union $m = [10100]$ will consequently let the receiver increase the SSN by one, causing the state index to become $k = [01000]$, i.e., the state of $V_{[01000]}$. The state $V_{[01000]}$ can be obtained by suppressing all the leading ones within the middle union and padding an equal number of zeros from the right-hand side, which is considered the same technique as in the conventional GS scheme.

5.3.2.3 State Transition Probability

As shown in Fig. 5.5, the transition probability from the initial state $V_{[00100]}$ to the resulting state $V_{[01000]}$ can be computed from the bit values within the corresponding middle union $m = [10100]$. According to the initial state $V_{[00100]}$ and the window size $W = 3$, the transmitter will send an aggregate frame consisting of two previously corrupted packets and one new-coming packet. These packets are respectively represented by the first two bits and the fourth bit from the left-hand side since the third bit denotes the correctly received packet in the last aggregate frame. Accordingly, referring to the middle union $m = [10100]$, the

Algorithm 6: *Transition Gain for Proposed GFS Scheme*

Data: i, k, and r are unsigned binary integers of $2W-1$ digits
Result: $H_{i\to k}$

```
begin
    H_{i→k} ⟵ 0
    λ ← number_of_zero_in_the_leftmost_W_bits(i) − 1
    for s ⟵ 0 to 2^{2W−1−λ} − 1 do
        m ⟵ s_with_λ_zero_paddings_from_right
        if i = bitwise_and(i, m) then
            α ⟵ number_of_one(m) − number_of_one(i)
            β ⟵ number_of_zero(m) − λ
            r = m
            while leftmost_bit(r) = 1 do
                shift r one bit left with zero padding
            end
            if r = k then
                H_{i→k} ⟵ H_{i→k} + (1 − p_e)^α p_e^β
            end
        end
    end
end
```

casual correctness array can be obtained by its first two bits and the fourth bit as $c = [100]$. The transition gain from $V_{[00100]}$ to $V_{[01000]}$ is therefore computed by the probability of the correctness array $c = [100]$ and is denoted as $H_{[00100]\to[01000]} = (1-p_e)\cdot p_e^2$, where p_e is the packet error probability. The generic transition probability from V_i to V_k under the window size W is modeled as the transition gain $H_{i\to k}$ which can be computed via Algorithm 6.

The main idea of Algorithm 6 is to find the probability sum of all possible middle unions which can let the state V_i change to the state V_k. The algorithm first sets a parameter λ to record the number of zeros within W digits from the left-hand side of state index i, excluding the leftmost leading zero. The physical meaning of λ is to specify the number of zeros from the right-hand side of the state index since these zeros represent those packets that have not been transmitted. The remaining $2W-1-\lambda$ digits from the left-hand side of state index i is the only portion that can influence the state transition. Therefore, as shown in Algorithm 6, the variable s of the *for* loop represents all possible bit patterns within $2W-1-\lambda$ digits. All the possible middle union m can be obtained with λ zero paddings from the right-hand side. The bitwise AND operation of these middle unions with the state index i can filter out the

unsuitable middle unions m recognized by the discriminant that the bitwise AND operation of i and m is not equal to i. With regard to the state index i and the middle union m, the variable α represents the newly correctly received packets; while β indicates the number of unacknowledged packets. The value of β can be obtained by subtracting the total number of remaining zeros with the λ zeros from right-hand side. The probability for the middle union can therefore be formulated as $(1-p_e)^{\alpha} \cdot p_e^{\beta}$. Subsequently, the *while* loop generates the resulting state index by the rule of suppressing the leading one and padding an equal number of zeros. Finally, the transition gain $H_{i \to k}$ can be computed via the sum of probability from each suitable middle union m leading to the resulting state index $r = k$.

5.3.2.4 Window Utilization

The window utilization for proposed GFS scheme can be derived from the saturated probability of internal states after the occurrence of an infinite number of state transitions. The saturated probability Λ_k for each internal state V_k under the window size W can be computed as the sum of all the possible state transition as

$$\Lambda_k = \textstyle\sum_{i \in \mathbb{I}} H_{i \to k} \Lambda_i \tag{5.11}$$

for $\forall k \in \mathbb{I}$, where $\mathbb{I}$ is the set of all state indexes. Similarly, in order to solve the saturated probability Λ_k, an additional constraint is imposed to make the underdetermined system possess a finite number of solutions, i.e.,

$$\sum_{k \in \mathbb{I}} \Lambda_k = 1, \tag{5.12}$$

since the sum of all saturated state probability Λ_k in a Markov state transition diagram should be equal to one. Based on (5.11), the nine state equations derived from the exemplified state transition diagram under $W = 3$ are represented via the matrix form as

$$\mathbf{\Lambda} \;=\; [\mathbf{A}|\mathbf{B}]_{9 \times 9}\, \mathbf{\Lambda}, \tag{5.13}$$

where

$$\mathbf{\Lambda} = \begin{bmatrix} \Lambda_{[00000]} \\ \Lambda_{[00100]} \\ \Lambda_{[01100]} \\ \Lambda_{[01000]} \\ \Lambda_{[00110]} \\ \Lambda_{[01110]} \\ \Lambda_{[01101]} \\ \Lambda_{[01111]} \\ \Lambda_{[01010]} \end{bmatrix}, \tag{5.14}$$

$$\mathbf{A}_{9\times 4} = \begin{bmatrix} 2p_e^2-2p_e+1 & 1-2p_e+p_e^2 & 1-2p_e+2p_e^2-p_e^3 & 1-2p_e+2p_e^2-p_e^3 \\ p_e^2-p_e^3 & p_e^3 & 0 & 0 \\ p_e-2p_e^2+p_e^3 & p_e-p_e^2 & p_e^3 & p_e^2-p_e^3 \\ p_e-p_e^2 & p_e^2-p_e^3 & p_e-2p_e^2+p_e^3 & p_e-2p_e^2+2p_e^3 \\ 0 & p_e^2-p_e^3 & 0 & 0 \\ 0 & p_e-2p_e^2+p_e^3 & p_e^2-p_e^3 & p_e-2p_e^2+p_e^3 \\ 0 & 0 & p_e^2-p_e^3 & 0 \\ 0 & 0 & p_e-2p_e^2+p_e^3 & 0 \\ 0 & 0 & 0 & p_e^2-p_e^3 \end{bmatrix}, \tag{5.15}$$

and

$$\mathbf{B}_{9\times 5} = \begin{bmatrix} 1-2p_e+p_e^2 & 1-p_e & 1-2p_e+p_e^2 & 1-p_e & 1-2p_e+p_e^2 \\ 0 & 0 & 0 & 0 & 0 \\ p_e-p_e^2 & 0 & 0 & 0 & 0 \\ 0 & 0 & p_e-p_e^2 & 0 & p_e-p_e^2 \\ p_e^2 & 0 & 0 & 0 & 0 \\ p_e-p_e^2 & p_e^2 & 0 & 0 & p_e-p_e^2 \\ 0 & 0 & p_e^2 & 0 & 0 \\ 0 & p_e-p_e^2 & p_e-p_e^2 & p_e & 0 \\ 0 & 0 & 0 & 0 & p_e^2 \end{bmatrix}. \tag{5.16}$$

Associated with (5.12), if $p_e \neq 1$, the solution for each saturated probability Λ_k of V_k can be obtained as

$$\mathbf{\Lambda} = \begin{bmatrix} \frac{(p_e^3+2p_e^2+2p_e+1)(p_e^5+3p_e^4+3p_e^3+4p_e^2+2p_e+1)}{C_1(p_e)} \\ \frac{p_e^2(p_e+1)(p_e^5+3p_e^4+3p_e^3+4p_e^2+2p_e+1)}{C_1(p_e)} \\ \frac{p_e(p_e^7+3p_e^6+5p_e^5+7p_e^4+7p_e^3+5p_e^2+2p_e+1)}{C_1(p_e)} \\ \frac{p_e(p_e^7+4p_e^6+8p_e^5+11p_e^4+12p_e^3+9p_e^2+5p_e+1)}{C_1(p_e)} \\ \frac{p_e^4(p_e^5+3p_e^4+3p_e^3+4p_e^2+2p_e+1)}{C_1(p_e)} \\ \frac{C_2(p_e)(p_e^7+3p_e^6+6p_e^5+11p_e^4+11p_e^3+8p_e^2+6p_e+1)}{(p_e+1)C_3(p_e)} \\ \frac{p_e^3(p_e^7+3p_e^6+5p_e^5+7p_e^4+7p_e^3+5p_e^2+2p_e+1)}{(p_e+1)C_1(p_e)} \\ \frac{p_e^2(C_4(p_e)+39p_e^4+27p_e^3+14p_e^2+4p_e+1)}{(p_e+1)C_3(p_e)} \\ \frac{p_e^3(p_e^7+4p_e^6+8p_e^5+11p_e^4+12p_e^3+9p_e^2+5p_e+1)}{C_3(p_e)} \end{bmatrix}, \tag{5.17}$$

where

$$\begin{aligned} C_1(p_e) &= p_e^{10} + 6p_e^9 + 20p_e^8 + 42p_e^7 + 62p_e^6 \\ &\quad + 72p_e^5 + 63p_e^4 + 42p_e^3 + 20p_e^2 + 6p_e + 1 \\ C_2(p_e) &= p_e^4 + p_e^3 + p_e^2 \\ C_3(p_e) &= p_e^{11} + 7p_e^{10} + 26p_e^9 + 62p_e^8 + 104p_e^7 \\ &\quad + 134p_e^6 + 135p_e^5 + 105p_e^4 + 62p_e^3 \\ &\quad + 26p_e^2 + 7p_e + 1 \\ C_4(p_e) &= p_e^{10} + 4p_e^9 + 11p_e^8 + 24p_e^7 + 36p_e^6 + 42p_e^5. \end{aligned} \tag{5.18}$$

If p_e is equal to one, it is acquired that $\Lambda_{[00000]} = 1$ and the others are equal to 0.

After the derivation of saturated probability Λ_k from (5.11) and (5.12), the window utilization U_{GFS}^W of the proposed GFS scheme under the window size W can be obtained as

$$U_{GFS}^W = \sum_{k \in \mathbb{I}} \frac{E[N_{new}^k]\Lambda_k}{W}, \tag{5.19}$$

where $E[N_{new}^k]$ represents the expected total number of newly acknowledged data packets that

Parameter Type	Parameter Value
Network Area	Disk with a radius of 250 m
Simulation Time	40 sec
Transmission Range	250 m
Routing Protocol	DumbAgent
Traffic Type	Constant Bit Rate (CBR)
Data Packet Size	500 bytes
Number of Base Station	1
Number of Channel Contender	5, 10, 15
Queue Size	100 packets
PHY Data Rate	100 Mbps

Table 5.1: Simulation Parameters

is forecasted in the next state transition of V_k. It can be computed as

$$E[N_{new}^k] = \sum_{j \in \mathbb{M}_k} P_W^j(k) S_W^j(k), \tag{5.20}$$

where $\mathbb{M}_k$ is the set of all possible middle union outgoing from the state V_k. The parameter $P_W^j(k)$ denotes the probability of the corresponding outgoing middle union j; while $S_W^j(k)$ denotes the newly acknowledged data packets under the same middle union j. As shown in Fig. 5.5, for example, the middle union $j = [01110]$ is one of the outgoing middle unions from the state $V_{[00110]}$. Based on the state index, two corrupted packets and one new-coming packet will be delivered since the transmitter can only recognize the first $W = 3$ bits due to the window size constraint. Moreover, the fourth bit as 1 represents the data packet that is previously correctly received but not properly acknowledged. The last bit will remain 0 since the next aggregate frame transmission will not include the corresponding packet. Finally, according to the middle union $j = [01110]$, the correctness array becomes $c = [01X]$ where X is denoted as the don't-care bit. Therefore, $P_W^j(k)$ can be obtained as $p_e \cdot (1 - p_e)$; while $S_W^j(k)$ is computed as 1 since only one packet is newly acknowledged as correct. Considering another middle union $j = [11110]$ of the same state $V_{[00110]}$, the correctness array will be $c = [11X]$ associated with $P_W^j(k) = (1 - p_e)^2$ and $S_W^j(k) = 3$. The reason for $S_W^j(k) = 3$ is that the previously correctly received data packet denoted by the fourth bit in the state index

can be detected as correct in conjunction with the two correct packet receptions in the current aggregate frame. According to (5.19) and (5.20), the window utilization for the exemplified state transition diagram of $W = 3$ can be obtained as

$$U_{GFS}^{3} = \frac{C_5(p_e) - 151p_e^3 - 72p_e^2 - 21p_e - 3}{-3(p_e + 1)C_3(p_e)}, \tag{5.21}$$

where $C_3(p_e)$ is specified in (5.18) and

$$\begin{aligned} C_5(p_e) = {} & p_e^{13} + 11p_e^{12} + 47p_e^{11} + 117p_e^{10} \\ & + 186p_e^9 + 190p_e^8 + 105p_e^7 \\ & - 41p_e^6 - 168p_e^5 - 201p_e^4. \end{aligned} \tag{5.22}$$

It concludes the description and derivation of the analytical model for proposed GFS scheme.

5.4 Performance Evaluation

In this section, model validation of the proposed analytical models for both the conventional GS mechanism and the proposed GFS scheme is conducted via the simulations. Furthermore, the comparison between these two schemes is performed under different simulation scenarios. The network scenario includes one base station (BS) and multiple channel contenders, where the channel contenders are randomly placed within the transmission range of the BS. The simulations are conducted in the network simulator (NS-2, [36]) with wireless extension, using the IEEE 802.11n distributed coordination function (DCF) as the MAC protocol. The parameters utilized in the simulations are listed as shown in Table 5.1.

5.4.1 Model Validation

In order to illustrate the effectiveness of proposed analytical models, both block acknowledgement mechanisms are validated with simulation results. The window utilization which is defined as the average number of successfully acknowledged packets of an aggregate frame divided by the window size W is utilized as the validation index. Figs. 5.6 and 5.7 illustrate

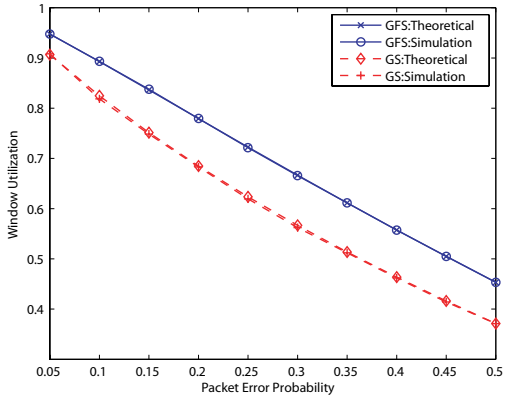

Figure 5.6: Model validation: window utilization versus packet error probability under window size $W = 3$.

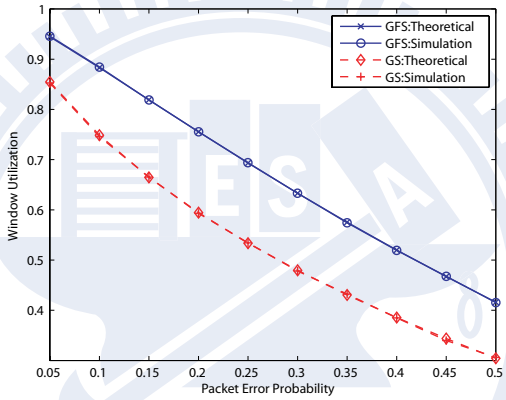

Figure 5.7: Model validation: window utilization versus packet error probability under window size $W = 6$.

the comparison for window utilization W with different packet error probabilities p_e under the window size $W = 3$ and 6, respectively. It can be observed that the proposed theoretical models can almost match and predict the performance of the two schemes via simulation results, which validates the correctness of proposed models. Furthermore, in the performance comparison between the two schemes based on the metric of window utilization, Figs. 5.6 and 5.7 show that the proposed GFS scheme outperforms the conventional GS mechanism under both window size $W = 3$ and $W = 6$.

The performance gaps between the proposed GFS scheme and the GS method can be attributed to the different acknowledgement feedback mechanisms. In addition to providing

explicit acknowledgement to each packet in the aggregate frame after the SSN, the proposed GFS scheme furthermore implicitly acknowledges the correctly received packets before the SSN. Contributing to this hybrid method, the SSN in the proposed GFS scheme will slide faster than that in the GS mechanism which results in higher window utilization. All the performance curves in Figs. 5.6 and 5.7 have the trend that the window utilization is degraded with the increase of packet error probability p_e. Intuitively, as p_e becomes larger, more packet errors will occur, which consequently decrease the window utilization.

5.4.2 Performance Comparison

For the purpose of comparing the performance between the GFS and the GS mechanisms, three performance metrics are utilized in the simulations as follows.

1. Blocking Overhead: The number of additional data packets per second which have been retransmitted due to the insufficient window size.

2. End-to-End Delay: The duration between the time when the packet arrives at the transmitter queue and the time when the packet is successfully acknowledged by the receiver.

3. Throughput: The total number of successfully received packets per second.

The comparisons between the proposed GFS scheme and the conventional GS mechanism under these three metrics will be performed under different window sizes W, packet error probabilities p_e, and the number of contending nodes N.

Figs. 5.8 to 5.10 show the performance comparison based on the three metrics versus packet error probability with window size $W = 64$ under the number of contending nodes $N =$ 5, 10, and 15. Fig. 5.8 illustrates the comparison of blocking overhead between the proposed GFS scheme and the GS method. The blocking overhead becomes smaller with the increased number of nodes, which can be contributed to the smaller system throughput caused by higher packet collisions from more contending nodes. With lowered throughput performance, the chance for the occurrence of additional retransmitted packets will consequently be reduced.

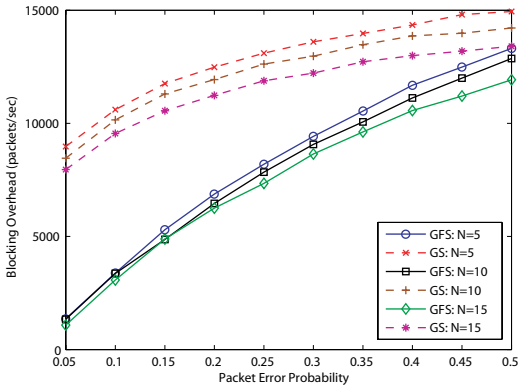

Figure 5.8: Performance comparison: blocking overhead versus packet error probability under the window size $W = 64$.

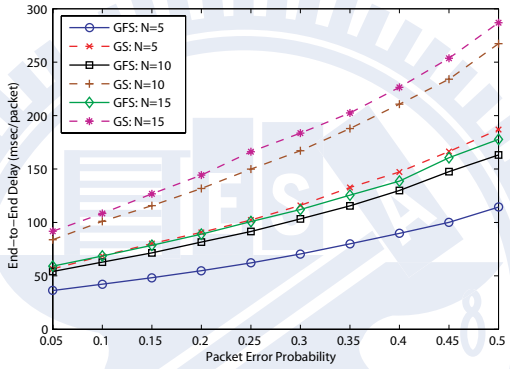

Figure 5.9: Performance comparison: end-to-end delay versus packet error probability under the window size $W = 64$.

It is also observed that the blocking overhead becomes larger with regard to the increase of packet error probability. As the packet error happens frequently, it becomes difficult to enlarge the SSN value in the block acknowledgement packet which causes more packets outside of the acknowledgement window, i.e., from SSN to SSN+$(W-1)$, to be retransmitted. Furthermore, as shown in Fig. 5.8, the proposed GFS scheme outperforms the GS method due to its fast-shift mechanism for packet acknowledgements, which consequently reduce the number of retransmitted blocked packets. In the proposed GFS scheme, the receiver can shift the SSN to the maximal value of $2W-1$; while the GS method can only increase the SSN value up to W. As a result, the proposed GFS scheme will cause less blocking overhead compared to the GS method.

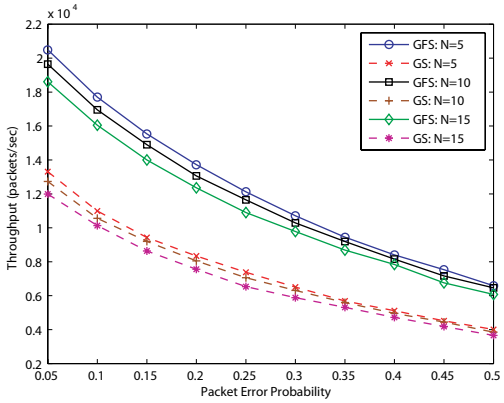

Figure 5.10: Performance comparison: throughput versus packet error probability under the window size $W = 64$.

The end-to-end delay under different packet error probabilities and the number of nodes is shown in Fig. 5.9. It is intuitively to notice that as the number of contending nodes is increased, more packet collisions and retransmissions will consequently occur, leading to the enlargement of packet delay. Based on the same reason, the delay will be prolonged with regard to the increase of packet error probability since more retransmissions will be required. As shown in Figs. 5.6 to 5.8, the proposed GFS scheme has higher window utilization and smaller blocking overhead compared to that from the conventional GS method. Therefore, more packets can be successfully transmitted in one aggregate frame by adopting the GFS scheme, which results in the shorter delay as shown in Fig. 5.9.

Fig. 5.10 illustrates the comparison of throughput performance between the proposed GFS scheme and the GS method. It is observed that the system throughput is decreased as the packet error probability is augmented since more transmission attempts will be required to recover the packet errors. Moreover, the throughput performance is decreased in both schemes with the increased number of nodes, which is contributed to the additional packet collisions if there exists more channel contenders. Based on (5.3) and (5.19) and Figs. 5.6 and 5.7, the window utilization of the proposed GFS scheme is larger than the conventional GS scheme. Therefore, as shown in Fig. 5.10, the system throughput of the proposed GFS scheme will be higher than that of the GS method since the window utilization is a positive-related metric with respect to the throughput performance. This result further validates the

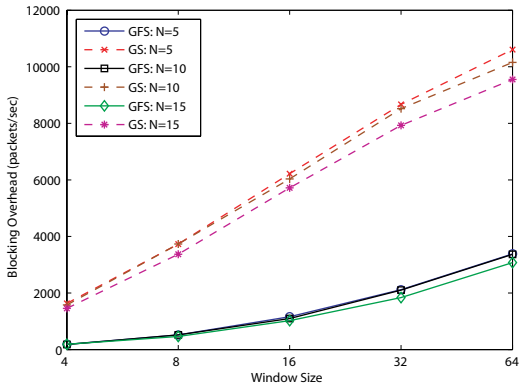

Figure 5.11: Performance comparison: blocking overhead versus window size under packet error probability $p_e = 0.1$.

effectiveness of our proposed analytical models and the analysis based on window utilization.

Figs. 5.11 to 5.13 depict the comparison with respect to the three metrics versus window size with packet error probability $p_e = 0.1$ under the number of contending nodes $N = 5$, 10, and 15. Fig. 5.11 shows the blocking overhead performance for the proposed GFS and the conventional GS schemes. It is observed that the blocking overhead becomes larger when the window size is extended, which can be explained as follows. From the transmitter side, considering that the SSN ξ_o of the block ACK packet is known, the packet with SN in the range from ξ_o to $\xi_o + (2W - 2)$ will possibly be included in the aggregate frame for the next transmission. After the receiver receives the aggregate frame, a new SSN ξ_n will be created. There is potential for the packets with SN in the range from $\xi_n + W$ to $\xi_o + (2W - 2)$ to induce the blocking overhead. As the window size increases, this range will be extended which consequently results in more blocking overhead. Nevertheless, the proposed GFS scheme causes significant less blocking overhead compared to the GS method owing to its efficient determination of the SSN value, which has been described as the explanation for Fig. 5.8.

The end-to-end delay performance under different window sizes and number of nodes is shown in Fig. 5.12. As the window size becomes larger, there are two situations to happen which are explained as follows: (a) Since each aggregate frame can accommodate more packets, the end-to-end delay is decreased for the reason that packets will spend less time in the transmitter's queue; (b) With increased blocking overhead as in Fig. 5.11, additional time is

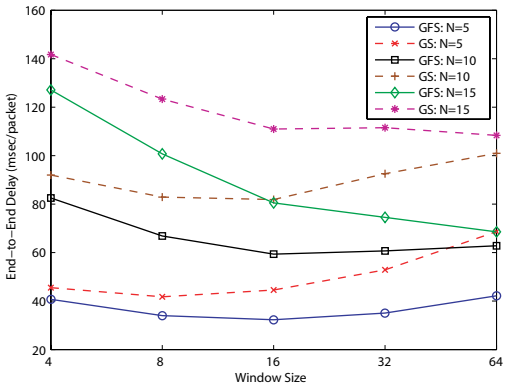

Figure 5.12: Performance comparison: end-to-end delay versus window size under packet error probability $p_e = 0.1$.

required for the packets to be successfully acknowledged which contributes to larger packet delay. Based on the joint effects from these two cases, the end-to-end delay will be observed to first decrease and then increase as the window size is enlarged. Moreover, owing to the smaller blocking overhead and larger window utilization, the proposed GFS scheme possesses smaller end-to-end delay compared to the GS method. From the delay performance of Fig. 5.12, the evaluation on the throughput metric of Fig. 5.13 can be predicted and explained in a similar manner. As the window size becomes larger, the throughput performance of both schemes will first be increased and then decreased afterwards. Similar to the reason as explained in Fig. 5.10, due to the less blocking overhead and higher window utilization, the proposed GFS scheme will have significant throughput gain in comparison with the conventional GS method. The effectiveness of the proposed mechanism and analytical models can therefore be perceived, which concludes the performance evaluation of this section.

5.5 Summary

In this chapter, a greedy fast-shift (GFS) block acknowledgement mechanism is proposed to alleviate the performance degradation due to insufficient bitmap within the acknowledgement window. Instead of adopting the transmitter-defined starting sequence number (SSN) in the conventional greedy block acknowledgement scheme, the design of receiver-defined SSN is

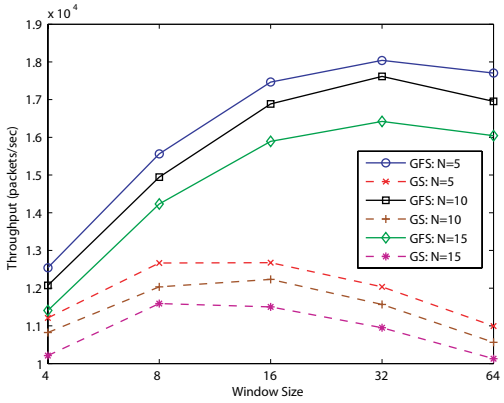

Figure 5.13: Performance comparison: throughput versus window size under packet error probability $p_e = 0.1$.

utilized in the proposed GFS scheme. The proposed mechanism can effectively reduce the occurrence of packet retransmissions for those correctly received packets but are outside of the acknowledgement window. Moreover, based on the Markovian techniques, the analytical models for both schemes are also constructed to measure the throughput-related performance metric, i.e., the window utilization. Simulations are performed to validate the proposed analytical models and to evaluate the performance for these two schemes. It can be observed from the performance comparison that the proposed GFS scheme can outperform the conventional greedy scheme on the throughput, delay, and blocking overhead under different window sizes and packet error probabilities. Based on the merits of high throughput performance and low blocking overhead, the proposed GFS scheme can therefore be adopted as the data link protocol in achieving the green wireless access networks.

Chapter 6

Frame Aggregation-based Power-Saving Scheduling Algorithm

Chapter Overview

In the data link layer protocol design for achieving the green wireless access networks, the proposals of power saving mechanisms are regarded as the direct methods to reach the goal of reducing the total energy consumption. Due to the urgent bandwidth demands of the future mobile applications, the main theme of the broadband wireless network (BWN) with the green concept is considered in this chapter. The limitation on the battery lifetime has been a critical issue for the advancement of mobile computing. Different types of power-saving techniques have been proposed in various fields. In order to provide feasible energy-conserving mechanisms for the mobile subscriber stations (MSSs), three power-saving types have been proposed for the IEEE 802.16e broadband wireless networks. However, these power-saving types are primarily targeting for the cases with a single connection between the base station (BS) and the MSS. With the existence of multiple connections, the power efficiency obtained by adopting the conventional scheduling algorithm can be severely degraded. In this chapter, with the consideration of the multiple connections and their quality-of-service (QoS) constraints, a frame aggregation-based power-saving scheduling (FAPS) algorithm is proposed to enhance the power efficiency by aggregating multiple under-utilized frames into

fully-utilized ones. The optimality on the minimum number of listen frames in the proposed FAPS algorithm is also provided under the stepwise grant space set and further verified via the correctness proof. The performance evaluation is conducted and compared via the simulations. Simulation results show that the sleep frame ratio (i.e., a power efficiency metric) of the proposed FAPS algorithm outperforms the baseline protocols with tolerable delay. Thanks to the high power efficiency, the proposed FAPS algorithm can therefore be regarded as the green data link protocol in the establishment of the green wireless access networks.

6.1 Introduction

The IEEE 802.16 and 802.16e standards for the broadband wireless networks (BWNs) are designed to fulfill various demands for higher capacity, higher data rate, and advanced multimedia services [84–88]. In order to prolong the battery lifetime of the mobile subscriber stations (MSSs), the design of a feasible power-saving mechanism is considered a major issue in the IEEE 802.16e standard [89–92]. Three different power-saving types are specified (i.e., type I, II, and III) in the IEEE 802.16e point-to-multipoint (PMP) mode so as to meet different demands of traffic between the base station (BS) and the MSSs. Two specific intervals are defined as 1) the sleep interval for saving energy and 2) the listen interval for listening to the direction from the BS and conducting the packet transmission. The power-saving class of type I defines the exponential-growing sleep intervals associated with fixed listen intervals. On the other hand, periodic occurrences of both the sleep and listen intervals are considered in type II. The power-saving class of type III consists of the pre-determined longer sleep interval without the existence of the listen period.

There are significant amounts of research work [93–95] focusing on the energy-saving issues for battery-powered mobile devices. Different types of energy efficient algorithms have been studied in [93] for generic central-controlled wireless data networks. Based on the IEEE 802.11 power-saving mechanism [63], several energy conservation schemes have been proposed in both centralized [94] and decentralized [95] manners. There are still some research works [96–99] targeted for the power-saving issues in IEEE 802.11 WLAN systems. However, these

existing techniques are not designed and intended to satisfy the requirements as defined in the IEEE 802.16e standard. In recent research studies, the performance analysis of the IEEE 802.16e power-saving types are investigated. Most of the work concentrate on constructing the analytical models for power-saving class of type I [100–104]; while the enhanced model as proposed in [105] switches the power-saving class between type I and II according to the network traffic. A longest virtual burst first (LVBF) scheduling algorithm has been proposed in [106], which considers both the energy conservation and resource allocation between the BS and multiple MSSs. Nevertheless, these analytical results and scheduling schemes only consider a single connection between the BS and each MSS, i.e., a single connection is assigned to each MSS.

In view of the multi-connection scenarios, some studies [107–110] on the connection-oriented methods are investigated. The maximum unavailability interval (MUI) scheme [107, 108] is dedicated to the connections of power-saving class of type II in the IEEE 802.16e standard. Based on the Chinese remainder theorem, the proper start frame will be identified for each type II connection in order to reduce the total energy consumption. Based on some extension, the extended maximizing unavailability interval (eMUI) [109] is further proposed for the mixture of the power-saving classes of type I and II. The periodic on-off scheme (PS) and the aperiodic on-off scheme (AS) [110] are another two connection-oriented schemes. The objective of the PS scheme is to provide a scheduling algorithm with periodic sleep and listen intervals, which can elongate the total sleep intervals. However, since connections may have aperiodic traffic pattern, the PS scheme with periodic pattern is not ideal to accommodate these traffics in terms of the power efficiency. For further enhancement, the AS scheme with aperiodic sleep and listen intervals is therefore suggested. According to the delay constraint of each connection, the connection-oriented AS scheme schedules each connection from the one with the smallest delay constraint (i.e., the connection with tight QoS delay first). For each packet in the connection, the AS scheme delay the packet as much as possible in order to acquire the chance of aggregating with other packets, which can improve the power efficiency.

Instead of the connection-oriented method, a packet-level frame aggregation-based power-saving scheduling (FAPS) algorithm is proposed in this chapter with the consideration of the

multiple connections and their QoS constraints. The FAPS scheme consists of two procedures, including the frame aggregation (FA) procedure and the backward adjustment (BA) procedure. The proposed FA procedure acts as the default routine of maximizing the number of sleep frames by aggregating multiple under-utilized frames into fully-utilized ones; while the proposed BA procedure is utilized when the FA procedure encounters procedure exceptions. The optimality on the minimum number of listen frames produced by the proposed FAPS algorithm for the stepwise grant space set can be obtained and verified via the proof of correctness. The performance evaluation is subsequently conducted and compared via the simulations under different cases. Simulation results show that the power efficiency of the proposed FAPS algorithm outperforms the baseline protocols with tolerable delay.

The rest of this chapter is organized as follows. The targeted problem and the corresponding system model are formulated in Section 6.2. Section 6.3 explains the proposed FAPS algorithm. The optimality of the proposed FAPS protocol for the stepwise grant space set is further described and verified in Section 6.4; while the performance evaluation of the proposed FAPS scheme is subsequently conducted in Section 6.5. Section 6.6 summarizes this chapter.

6.2 Problem Formulation

6.2.1 IEEE 802.16e Sleep Mode Operation

According to the IEEE 802.16e specification [85], the sleep mode is defined to reduce the power consumption of an MSS. As a connection is established between the BS and the MSS, the MSS can be switched to the sleep mode if there is no packet to be transmitted or received during a certain time period. The time duration within the sleep mode is divided into cycles, where each cycle can contain both the sleep and the listen intervals. In the listen interval, the MSS can either transmit/receive data or listen to the MAC messages acquired from the BS. During the sleep interval, on the other hand, the MSS may turn into its sleep power state or associate with other neighbor BSs for handover scanning purpose. It is noticed that the sleep mode can be initiated by either the MSS or the BS. For the MSS-initiated process, the

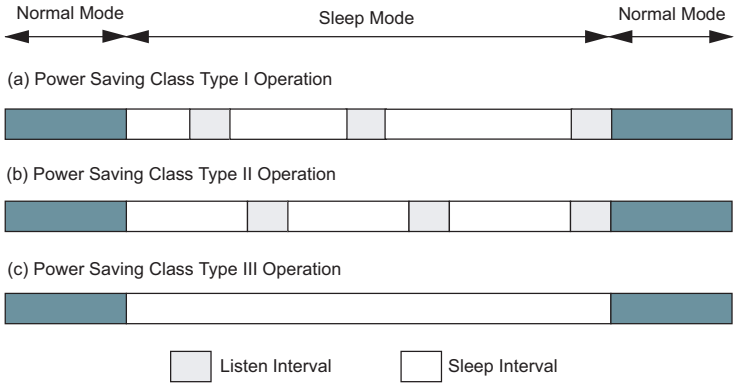

Figure 6.1: Power-saving classes defined in the IEEE 802.16e.

MSS sends a MOB_SLP-REQ massage to the BS for requesting the permission of entering the sleep mode. The BS will reply with a MOB_SLP-RES massage, which also includes the parameters of the connection type, the size of the sleep and listen intervals, and the starting time for the sleep mode.

As mentioned in Section 6.1, three power saving types are specified for the connections between the BS and the MSS in order to facilitate different characteristics of services. The sleep mode of the MSS with the power-saving class of type I consists of exponential-growing sleep intervals and fixed-length listen intervals. Within its listen intervals, the MSS will listen for the MOB_TRF-IND massage obtained from the BS in order to determine if it should return back to the normal mode. In the case that the MSS is determined not to switch back to the normal mode, the length of the next sleep interval will be doubled until the pre-defined maximum sleep window size has been reached. Based on the QoS requirements as defined in [84], this type is suitable for non-realtime traffic variable-rate (NRT-VR) connections and the best-effort (BE) services between the BS and the MSSs. The power-saving class of type II defines the repetitive occurrences of the sleep and listen intervals, where the sizes of both intervals are pre-determined fixed parameters. The MSS is allowed to transmit/receive data periodically within the listen intervals. It is noticed that this power-saving type is especially suitable for QoS-guaranteed services, e.g., the unsolicited grant service (UGS) and the realtime traffic variable-rate (RT-VR) connections. Furthermore, without the assignment of the listen interval, the power-saving class of type III pre-specifies a long sleep interval for the MSS

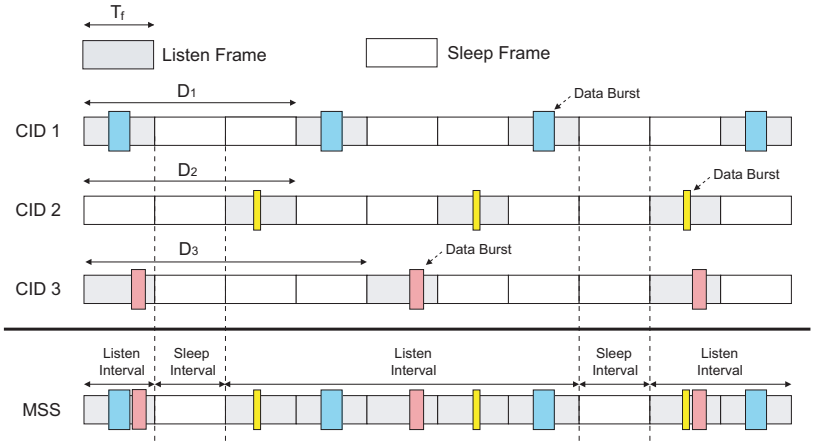

Figure 6.2: Schematic diagram of three connections with sleep mode operation between the BS and the MSS with the conventional IEEE 802.16e power-saving algorithm.

before it returns back to the normal mode. This type is suggested to be utilized for multicast connections and management operations. Fig. 6.1 summaries these three type power-saving modes.

6.2.2 Inefficiency of IEEE 802.16e Sleep Mode Operation

Since the power-saving types are defined based on a single connection between the BS and the MS, the degraded effect from the allowable multiple connections has not been considered in the specification. For example, three real-time UGS connections are considered in Fig. 6.2. The parameter D_i is denoted as the delay constraint for the i^{th} connection. It means the data burst in this connection should be transmitted in the defined D_i interval. The time interval t_f is defined as the duration of a frame as shown in Fig. 6.2. It is noted that the power-saving class of type II is considered for all the three connections (i.e., with CID 1, 2, and 3), which are characterized as follows: (i) CID 1 with traffic parameters: period $= 3 \cdot T_f$, sleep interval $= 2 \cdot T_f$, listen interval $= T_f$, and $D_1 = 3 \cdot T_f$; (ii) CID 2 with traffic parameters: period $= 3 \cdot T_f$, sleep interval $= 2 \cdot T_f$, listen interval $= T_f$, and $D_2 = 3 \cdot T_f$; (iii) CID 3 with traffic parameters: period $= 4 \cdot T_f$, sleep interval $= 3 \cdot T_f$, listen interval $= T_f$, and $D_3 = 4 \cdot T_f$.

It can be observed that only one sleep frame per four frames will be obtained by directly combining the sleep intervals from these three connections, i.e., with the adoption of the

conventional IEEE 802.16e scheme as shown in Fig. 6.2. It can easily be extended that the sleep interval may become zero frame in certain multi-connection scenarios, which can severely degrade the efficiency for power conservation. Therefore, it is necessary to provide a feasible scheduling algorithm in order to reschedule the sleep intervals based on the combined effects from the multiple connections.

6.2.3 Packet-based Power-Saving Scheduling (PPS) Problem

Based on the aforementioned inefficiency problem of the traditional IEEE 802.16e sleep mode operation, it is motivated that a feasible scheduling algorithm should be proposed to enhance the efficiency of the power scheduling under the scenarios of multiple connections. Before diving into the scheduling protocol design, the system model and our targeted problem should be delivered first. In order to model the combined effects of the multiple connections with QoS delay constraints, a packet-based modeling technique is suggested since all the connections can be divided into data packets respectively. The proposed grant space (GS) is employed as the QoS data packet model to represent each QoS data burst of connections, which is defined as in Definition 12.

Definition 12 (Grant Space). *Given a frame s_i with a pre-scheduled grant for a data burst, a grant space $G_i(s_i, g_i, t_i)$ is defined as the adjacent frames ranging from s_i to $t_i = s_i + D_i - 1$, where D_i is the maximum QoS delay constraint for this data burst. The frames s_i and t_i are respectively called the start and the termination for this grant space, and the grant frame g_i is the frame for containing the data burst.*

Fig. 6.3 illustrates the grant space $G_i(s_i, g_i, t_i)$ with the delay constraint D_i. The start and the termination of $G_i(s_i, g_i, t_i)$ are also indicated at the two terminals respectively. The data burst should be scheduled within the grant frame g_i, where $s_i \leq g_i \leq t_i$ (i.e., between the start and the termination frames). If the data burst is successfully scheduled within $G_i(s_i, g_i, t_i)$, it is considered that the QoS for this data burst is guaranteed. Thanks to the adoption of the grant spaces, the whole system can therefore be modeled by multiple grant spaces acquired from multiple connections. As shown in Fig. 6.4, there are nine connections

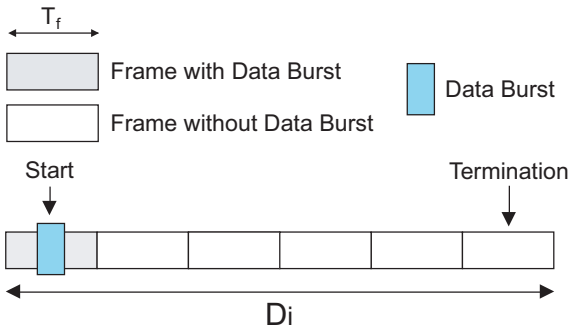

Figure 6.3: The grant space $G_i(s_i, g_i, t_i)$ with the delay constraint D_i and its start and termination frames.

(i.e., CID 1, 2, 3, 4, 5, 6, 7, 8 and 9) and each connection consists of multiple data bursts with their maximum QoS delay constraints. Based on Definition 12, each data burst with its delay constraint can be modeled as a grant space. For example, the first data burst u of CID 1 with delay constraint $5 \cdot T_f$ is modeled as a grant space with $D_u = 5 \cdot T_f$ and its start and termination are at frame $s_u = 3$ and frame $t_u = 7$ respectively; while the second data burst d of CID 8 with delay constraint $6 \cdot T_f$ is represented as a grant space with $D_d = 6 \cdot T_f$ and its start and termination are at frame $s_d = 10$ and frame $t_d = 15$ respectively. When completing the representation of data bursts, the MSS listen and sleep frames can be determined by the arrangement of each data burst. For example, the frame 1 of the MSS should be a listen frame since the first data packet a of CID 9 is scheduled within this frame; while the frame 6 is a sleep frame because of no scheduled data packet. Finally, all MSS listen frames are represented as the grey frames; while the sleep frames can be identified as the white ones in Fig. 6.4. It is noted that each MSS frame can only contain F_{max} data bursts at most since the accommodation of a frame is usually limited. After the description of the system model, our targeted packet-based power-saving scheduling (PSS) problem is formulated as follows:

Problem 6 (Packet-based Power-Saving Scheduling Problem). *Given a set* **G** *of multiple grant spaces and the maximum accommodation* F_{max} *of an MSS frame, how to arrange the data bursts within the grant spaces in order to maximize the power efficiency (i.e., the number of sleep frames) of the MSS?*

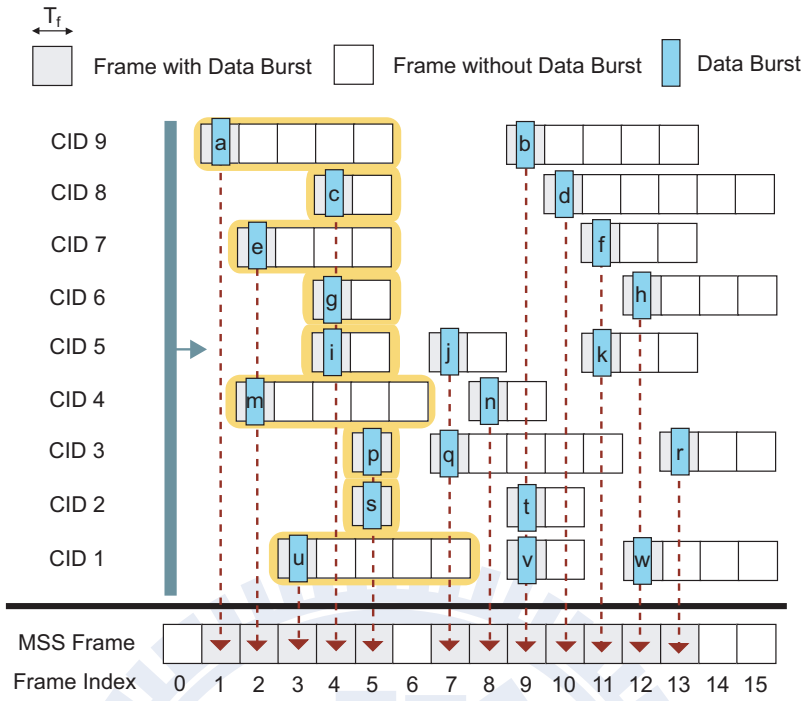

Figure 6.4: The whole system is modeled by multiple grant spaces acquired from multiple connections.

6.3 Proposed Frame Aggregation-based Power-Saving Scheduling (FAPS) Algorithm

As shown in Fig. 6.2, it can be observed that if without appropriate arrangement of data bursts, the QoS data bursts of multiple connections of an MSS can result in lowered power-saving efficiency. With the consideration of multiple connections, a packet-based power-saving scheduling (PPS) problem is formulated in Problem 6 as our targeted problem. As a remedy of the targeted PPS problem, a frame aggregation-based power-saving scheduling (FAPS) algorithm is proposed. With the proper arrangement of data bursts, the proposed FAPS algorithm can enhance the power efficiency under the constraint of the pre-specified QoS delay requirement. The proposed FAPS scheme consists of two procedures, including the frame aggregation (FA) procedure and the backward adjustment (BA) procedure. The FA procedure acts as the default routine of maximizing the number of sleep frames in the proposed FAPS scheme; while the proposed BA procedure is utilized when the FA procedure encounters

exceptions. The two procedures are described as in the following subsections. Subsection 6.3.1 describes the FA procedure; while the BA procedure is provided in Subsection 6.3.2.

6.3.1 Frame Aggregation (FA) Procedure

The objective of the proposed FA procedure is to acquire more sleep frames by aggregating some under-utilized listen frames into a fully-utilized one. For example, the maximum accommodation F_{max} of an MSS frame is assumed to be 3. As shown in Fig. 6.4, the two under-utilized listen frame (i.e., the frame 7 and the frame 8) can be aggregated into the frame 8 together since the three corresponding data bursts (i.e., the bursts j and q in the frame 7 and the burst n within the frame 8) can be scheduled at the frame 8 without breaking the QoS delay constraints specified in their grant spaces. The additional sleep frame at the frame 7 can therefore be acquired, which improves the power efficiency of the system. The proposed FA procedure is described as follows:

6.3.1.1 Forward Collection Mechanism

It is noted that if a data burst λ can be delayed, there is more chance to aggregate with other data burst, gaining more sleep frames. However, in order to meet the QoS delay constraint, the data burst λ must be scheduled before the termination t_λ specified within the grant space $G_\lambda(s_\lambda, g_\lambda, t_\lambda)$. Therefore, the first step of our procedure is to delay all data bursts from left to right before some data burst violates its delay constraint. For example, as shown in Fig. 6.4, the set of data bursts $\mathbf{D} = \{a, c, e, g, i, m, p, s, u\}$ (i.e., their grant spaces are with yellow background color) can be delayed to the frame 5. However, the data bursts p and s will violate their delay constraints if continuing to delay them to the frame 6. This action can be viewed as using a windscreen wiper, i.e., the solid bar at the frame 0 in Fig. 6.4. The windscreen wiper will be stuck at the frame $x_{\mathbf{G}} = 5$ since hazards are encountered, i.e., the data bursts p and u. Therefore, the corresponding unscheduled grant spaces stuck at the frame $x_{\mathbf{G}}$ (i.e., the grant spaces for the set $\mathbf{D}$) can be formally defined as the stuck group in the following definition:

Definition 13 (Stuck Group). *Given a set* $\mathbf{G}$ *of unscheduled grant spaces, the stuck group of* $\mathbf{G}$ *is defined as the set*

$$\mathbf{S_G} = \{\zeta \in \mathbf{G} \mid F_s(\zeta) \leq x_{\mathbf{G}}\}, \tag{6.1}$$

where $x_{\mathbf{G}} = \min F_t(\mathbf{G})$ *is called the stuck frame of* $\mathbf{G}$ *and the functions* $F_s(\cdot)$ *and* $F_t(\cdot)$ *are denoted as the start and the termination of a grant space.*

In a stuck group, there may exist some data bursts in the grant spaces, which still can be delayed. As shown in Fig. 6.4, the data bursts u and m with their grant spaces specified in the stuck group $\mathbf{S_G}$ can be delayed to the frame 6 and the frame 7 respectively. In order to distinguish these data bursts and their corresponding grant spaces, the stuck group $\mathbf{S_G}$ is divided into two sorted subgroups as follows:

Definition 14 (Strictly and Non-strictly Stuck Subgroups). *Let* $\mathbf{S_G}$ *be a stuck group which is sorted in ascending order by the termination of each grant space. If two grant spaces have the same termination, the parameter start of the grant spaces is utilized as the sorting order. The strictly and non-strictly stuck subgroup of* $\mathbf{S_G}$ *are respectively defined as the set*

$$\mathbf{S}_{\mathbf{G}}^{S} = \{\zeta \in \mathbf{S_G} \mid F_t(\zeta) = x_{\mathbf{G}}\}, \tag{6.2}$$

and the set

$$\mathbf{S}_{\mathbf{G}}^{\overline{S}} = \mathbf{S_G} - \mathbf{S}_{\mathbf{G}}^{S}, \tag{6.3}$$

where the function $F_t(\cdot)$ *represents the termination of a grant space and* $x_{\mathbf{G}}$ *is the stuck frame defined by the stuck group.*

6.3.1.2 Backward Push Mechanism

As shown in Fig. 6.5, the stuck group $\mathbf{S_G}$ obtained from the data burst set $\mathbf{D} = \{a, c, e, g, i, m, p, s, u\}$ in Fig. 6.4 is sorted and separated into the strictly stuck subgroup $\mathbf{S}_{\mathbf{G}}^{S}$

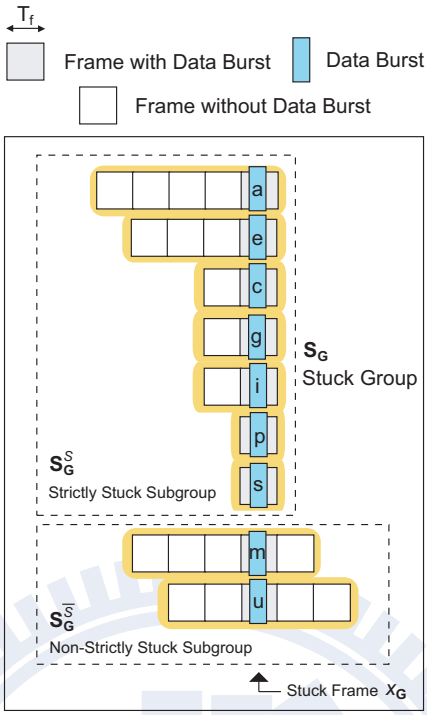

Figure 6.5: The strictly stuck subgroup $\mathbf{S}_{\mathbf{G}}^{S}$ and the non-strictly stuck subgroup $\mathbf{S}_{\mathbf{G}}^{\overline{S}}$.

and the non-strictly stuck subgroup $\mathbf{S}_{\mathbf{G}}^{\overline{S}}$. It can be observed that all data bursts in $\mathbf{D}$ will be stuck at the stuck frame $x_{\mathbf{G}}$. However, it is impossible to schedule all of them into the frame $x_{\mathbf{G}}$ if the maximum accommodation F_{max} of an MSS frame is less than the size of $\mathbf{S_G}$. Therefore, in the second step of our proposed frame aggregation procedure, the maximum frame accommodation of F_{max} should be considered. In addition, the scheduling of data bursts specified in the grant spaces of $\mathbf{S}_{\mathbf{G}}^{S}$ should be done prior to $\mathbf{S}_{\mathbf{G}}^{\overline{S}}$ since all data bursts in $\mathbf{S}_{\mathbf{G}}^{S}$ must be scheduled before the stuck frame $x_{\mathbf{G}}$. The arrangement of the data bursts specified in $\mathbf{S}_{\mathbf{G}}^{S}$ can be done as follows: Let N_s be the number of grant spaces in $\mathbf{S}_{\mathbf{G}}^{S}$ and $P_n = \lceil N_s/F_{max} \rceil$ be the number of partitions utilized to separate $\mathbf{S}_{\mathbf{G}}^{S}$ from the first grant space. It is noted that each partition of $\mathbf{S}_{\mathbf{G}}^{S}$ may have F_{max} data bursts at most so as to meet the requirement of the frame accommodation. Finally, referenced at the stuck frame $x_{\mathbf{G}}$, let the data bursts of each partition i move back $P_n - i$ frames gradually if possible. Otherwise, stop moving at the frame unable to proceed. If no exception occurs, it completes the arrangement of the data bursts specified in $\mathbf{S}_{\mathbf{G}}^{S}$. For example, as shown in Fig. 6.6, the

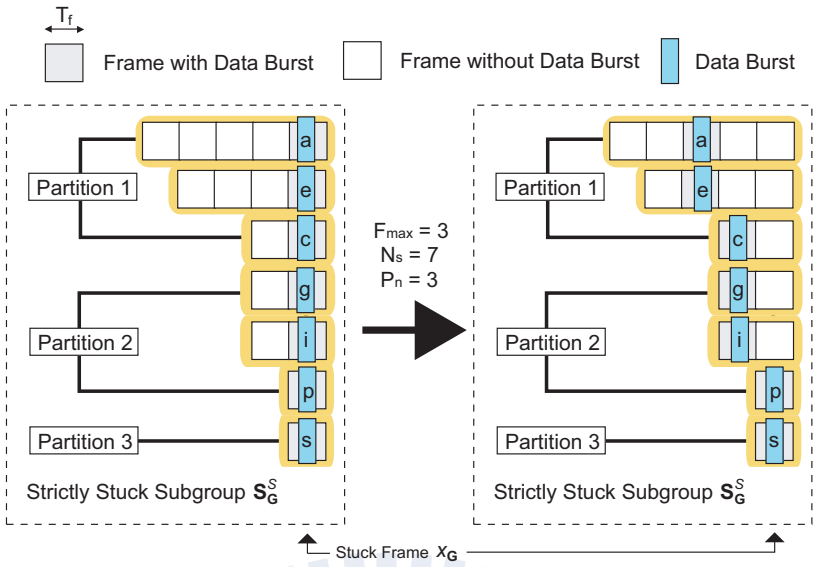

Figure 6.6: The arrangement of the strictly stuck subgroup $\mathbf{S}_{\mathbf{G}}^{S}$.

maximum frame accommodation is $F_{max} = 3$, the number of grant spaces in $\mathbf{S}_{\mathbf{G}}^{S}$ is $N_s = 7$, and the number of partitions is $P_n = \lceil N_s/F_{max} \rceil = 3$. The data bursts in the partition 1 should be moved back $P_n - 1 = 2$ frames. However, the data burst c will simply be proceeded back one frame since it is limited by the grant space $G_c(s_c, g_c, t_c)$. In the partition 2, the same situation can also be found at the data burst p which is constrained by the grant space $G_p(s_p, g_p, t_p)$. Finally, the data bursts a and e will be scheduled in the same frame. The bursts c, g, and i can also be aggregated; while the stuck frame can accommodate the remaining data bursts p and s. It can be observed that all data bursts in $\mathbf{S}_{\mathbf{G}}^{S}$ can be properly scheduled without breaking their QoS delay constraints and the accommodation limit of an MSS frame.

6.3.1.3 Packet Padding for Backward Push Mechanism

On the other hand, the scheduling of the non-strictly stuck subgroup $\mathbf{S}_{\mathbf{G}}^{\overline{S}}$ can be considered as a data burst stuff for some under-utilized listen frame to improve the power efficiency. Therefore, the data bursts specified in $\mathbf{S}_{\mathbf{G}}^{\overline{S}}$ can be scheduled with those in $\mathbf{S}_{\mathbf{G}}^{S}$ as follows: Starting from the left, for a under-utilized listen frame δ, find a proper number of grant spaces in $\mathbf{S}_{\mathbf{G}}^{\overline{S}}$ whose data burst can be scheduled in the frame δ. It is noted that the acquisition order of the grant spaces is the same as the order defined in Definition 14. As shown in Fig. 6.7, the first

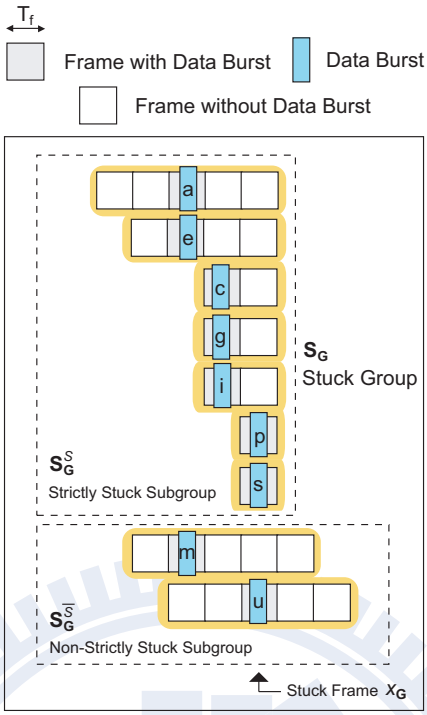

Figure 6.7: The complete arrangement of the strictly stuck subgroup $\mathbf{S}_\mathbf{G}^S$ and the non-strictly stuck subgroup $\mathbf{S}_\mathbf{G}^{\overline{S}}$.

under-utilized listen frame is the frame with data bursts a and e, and the second one is the frame with data bursts p and s. Based on the aforementioned technique, the data burst m will be arranged together with the data bursts a and e; while the burst u will be accommodated with the bursts p and s, leading to the fully-utilized listen frames. Finally, if there still remain some data bursts specified in the grant spaces of $\mathbf{S}_\mathbf{G}^{\overline{S}}$, these data bursts should be considered with the other unscheduled grant spaces as the new input grant spaces for the next round of the FA procedure. It can be perceived that the data burst set $\mathbf{D} = \{a, c, e, g, i, m, p, s, u\}$ as in Fig. 6.4 can be successfully scheduled within three listen frames, which is smaller than the original five listen frames. Furthermore, Fig. 6.8 shows the scheduling result of the complete power-saving system exemplified in Fig. 6.4 after five rounds of execution of the FA procedure. It can be observed that the required listen frames are decreased from the original 12 to the current 7 listen frames. The enhancement of power efficiency can be obtained in the proposed FA procedure.

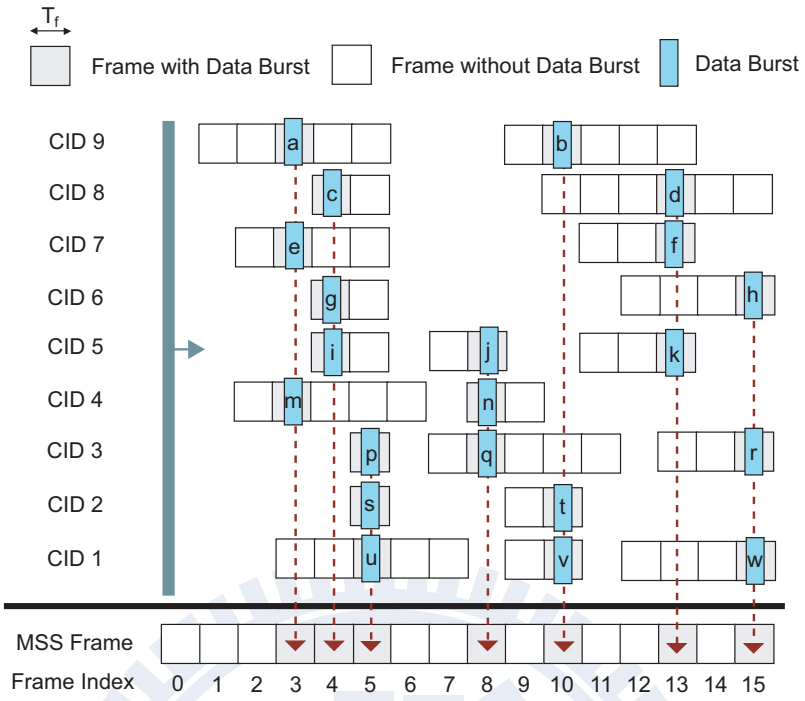

Figure 6.8: The scheduling result of the proposed frame aggregation procedure in the example system with multiple connections.

6.3.2 Backward Adjustment (BA) Procedure

As shown in Fig. 6.9, there are eight data bursts (i.e., a, b, c, d, e, f, g, and h) from the eight connections, and the maximum accommodation F_{max} of an MSS frame is assumed to be 2. In the first round of the execution of the FA procedure, the data bursts a and b is completely scheduled. Moreover, the data bursts c and d are also successfully aggregated in the second round without exceptions. In the third round of execution, there are four unscheduled grant spaces for the data bursts e, f, g, and h, which are separated into the strictly and non-strictly stuck subgroups $\mathbf{S}_{\mathbf{G}}^{S}$ and $\mathbf{S}_{\mathbf{G}}^{\overline{S}}$. Based on the FA procedure, the grant spaces of $\mathbf{S}_{\mathbf{G}}^{S}$ will be divided into multiple partitions. For example, as shown in Fig. 6.9, the partition 1 consisting of data bursts e and f and the partition 2 containing g will be constructed. In the partition 1, each data burst should be moved backward $P_n - 1 = \lceil N_s/F_{max} \rceil - 1 = 1$ frame. Nevertheless, it is unable to let them backward since the frame 5 is full of data bursts, i.e., the data bursts c and d. Fortunately, the data bursts e and f still can be placed at the frame 6. On the other hand, for the data burst g specified in the partition 2, they should

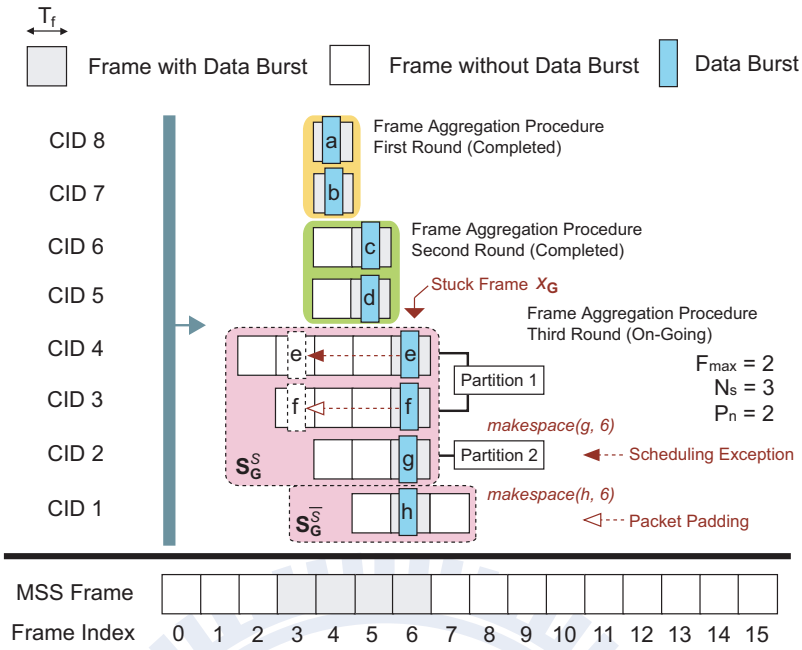

Figure 6.9: The proposed backward adjustment procedure for the scheduling exceptions of the frame aggregation procedure.

be scheduled at the frame 6. However, the exception of the proposed FA procedure occurs since the frame 6 has the maximum number $F_{max} = 2$ of data bursts e and f and the frame 6 is the only choice for the partition 2. It will violate the frame capacity constraint if no proper scheduling adjustment. The proposed BA procedure is therefore utilized to solve the scheduling exceptions encountered by the aforementioned FA procedure. The whole procedure can be described in the following two steps.

6.3.2.1 Recursive Backward Movement

The recursive backward movement of the proposed BA procedure can be found in Algorithm 7 and described as follows: Given a data burst λ and the targeted frame θ, a function $makespace(\lambda, \theta)$ is utilized to make a space for λ at the frame θ by the backward recursive data burst movement. If λ can be scheduled in θ, the function $makespace$ will return $true$. Consequently, the data burst λ will be scheduled in the targeted frame θ, solving the exception resulting from the proposed FA procedure. If λ can not be scheduled into the frame θ, let ξ be the data burst in θ whose grant space $G_\xi(s_\xi, g_\xi, t_\xi)$ has the smallest start frame. Subsequently,

based on the same function *makespace*, try to backward search the non-saturated frame π ranging from the frame $(\theta - 1)$ to the start frame s_ξ. If the frame π can be found, schedule the data burst ξ into this frame π. Finally, put the unscheduled data burst λ into the frame θ, completing the recursive backward movement of the proposed BA procedure for scheduling the data burst λ.

As shown in Fig. 6.9, in the third round of the proposed FA procedure, when starting to arrange the data burst g in the partition 2, the data burst g will encounter the exception of the FA procedure. Therefore, based on the recursive backward movement of the proposed BA procedure, the function $makespace(\lambda, \theta)$ will be invoked, where $\lambda = g$ and $\theta = 6$. For the data bursts e and f scheduled in the frame 6, the grant space $G_e(s_e, g_e, t_e)$ of the data burst e has the smallest start (i.e., $s_e = 2$). Consequently, the data burst e is selected as the burst which should be moved back.

Subsequently, the function $makespace(\lambda, \theta)$ will be re-conducted for the new input $\lambda = e$ and several new input θ of $\pi = \theta - 1, \ldots, s_i$ (i.e., π = 5, 4, 3, and 2 for each time). When the first function $makespace(e, 5)$ for scheduling the data burst e is invoked, the next selected data burst which may be moved back is the burst c in the frame 5 since it has the smallest start, i.e., the frame 4. Recursively, when $makespace(c, 4)$ for arranging the data burst c is invoked, the burst a is also chosen as the candidate to move back. However, a can not be moved back since it is at the start frame 4 of the grant space $G_a(s_a, g_a, t_a)$. Since the burst a can not be moved, the data burst c simply can be scheduled at the frame 5. Moreover, since c can not be moved back, the burst e should not be scheduled at the frame 5. Therefore, $makespace(e, 5)$ can not make a space for e at the frame 5.

The second function $makespace(e, 4)$ for scheduling the data burst e will continually be invoked to check if the burst e can be scheduled at the frame 4. For the same reason, the burst e also can not be arranged at the frame 4. Finally, the data burst e will be scheduled at the frame 3 since the third function $makespace(e, 3)$ for scheduling the burst e will return the value of *true*, representing the vacancy of the frame 3. When the burst e is placed into the frame 3, it leaves a vacancy in the frame 6 for the data burst g. Therefore, g can be scheduled at the frame 6, completing the scheduling of the burst g.

Algorithm 7: *Recursive Backward Movement: makespace(λ, θ)*

Input: λ: data burst, θ: targeted frame
Output: *true* or $false$: can λ be scheduled in θ ?

```
1  begin
2      if λ can be placed into the frame θ then
3          return true
4      else
5          let ξ be the data burst in the frame θ whose grant space G_ξ(s_ξ, g_ξ, t_ξ) has the smallest
           start frame
6          for π = θ − 1 to s_ξ do
7              if makespace(ξ, π) then
8                  put the data burst ξ into the frame π
9                  return true
10             end
11         end
12         return false
13     end
14 end
```

6.3.2.2 Packet Padding for Recursive Backward Movement

After the execution of the recursive backward movement, there may exist some under-utilized frames. For example, it can be observed that there is a under-utilized frame caused by the *makespace* function at the frame 3, i.e., only the data burst e in the frame 3. Therefore, in order to gain more power efficiency, the packet padding mechanism can be utilized by the *makespace* function with the stuck frame $x_{\mathbf{G}}$ and the data burst in the non-strictly stuck subgroup $\mathbf{S}_{\mathbf{G}}^{\overline{S}}$ as the function inputs. The packet padding is continuously conducted until the false return value is obtained or before the additional listen frame is introduced. In other words, this packet padding mechanism will not lead to any new listen frame. As shown in Fig. 6.9, based on the packet padding mechanism, the data burst h in $\mathbf{S}_{\mathbf{G}}^{\overline{S}}$ can be scheduled at the stuck frame $x_{\mathbf{G}} = 6$ by conducting the function *makespace*$(h, 6)$. The fully-utilized frame 3 can therefore be observed. Thanks to the recursive backward movement and the packet padding mechanism of the proposed BA procedure, the third round of the proposed FA procedure can therefore be completed associated with enhanced power efficiency.

6.4 Optimality of Proposed FAPS Algorithm

In this section, the optimality that the proposed FAPS algorithm produces the minimum number of listen frames are proven under the input scenario of the stepwise grant space set. The stepwise grant space set is described as follows:

Definition 15 (Stepwise Grant Space Set). *A grant space set* $\mathbf{G}$ *is called stepwise if the two properties can be achieved as follows:*

1. *The order for each grant space in* $\mathbf{G}$ *is identified in the ascending manner by the termination and further by the start if encountering the same termination.*

2. *For each pair of consecutive grant spaces* $G_i(s_i, g_i, t_i)$ *and* $G_j(s_j, g_j, t_j)$ *in* $\mathbf{G}$*, the start and the termination of the former are respectively less than or equal to those of the latter, i.e.,* $s_i \leq s_j$ *and* $t_i \leq t_j$.

As shown in Fig. 6.10, all grant spaces in the stepwise grant space set $\mathbf{G}$ are ordered based on Definition 15, and the order numbers are also specified at the left side. If the set $\mathbf{G}$ exists a feasible packet arrangement under the frame capacity constraint F_{max}, the proposed FAPS algorithm can produce the minimum number of listen frames. Based on the flow for the proposed FAPS algorithm in Fig. 6.11, the proof of correctness begins as follows:

In the first round, with regard to the given stepwise grant space set $\mathbf{G}$, the proposed FAPS algorithm will conduct the forward collection mechanism to construct the stuck group and further determine the strictly and non-strictly stuck subgroups. Subsequently, the backward push mechanism will be executed to properly rearrange the data bursts under the capacity constraint F_{max}. As shown in Fig. 6.10, the stepwise grant space set $\mathbf{G}$ consists of the grant spaces of data bursts $\{a, b, c, d, e, f, g, h, m, n, p, q\ r, u, \ldots\}$. Based on the backward push mechanism, the first partition $\{a, b, c\}$ should be scheduled at the frame $x_{\mathbf{G}} - 3$; while the second partition $\{d, e, f\}$ should be placed at the frame $x_{\mathbf{G}} - 2$. However, due to the grant space constraint on the start frame s_f, the data burst f will be scheduled at the frame $x_{\mathbf{G}} - 1$. The remaining data bursts in the strictly stuck subgroup $\mathbf{S}_{\mathbf{G}}^{S}$ are arranged as shown in Fig. 6.10. For facilitating the correctness proof, the no-follower frame is defined first.

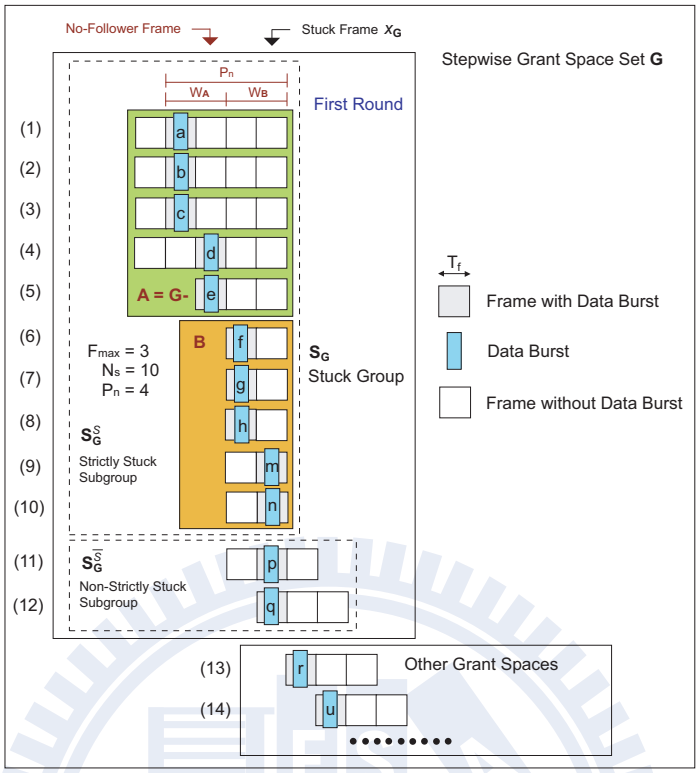

Figure 6.10: The exemplified packet arrangement in the first round of the proposed backward push mechanism.

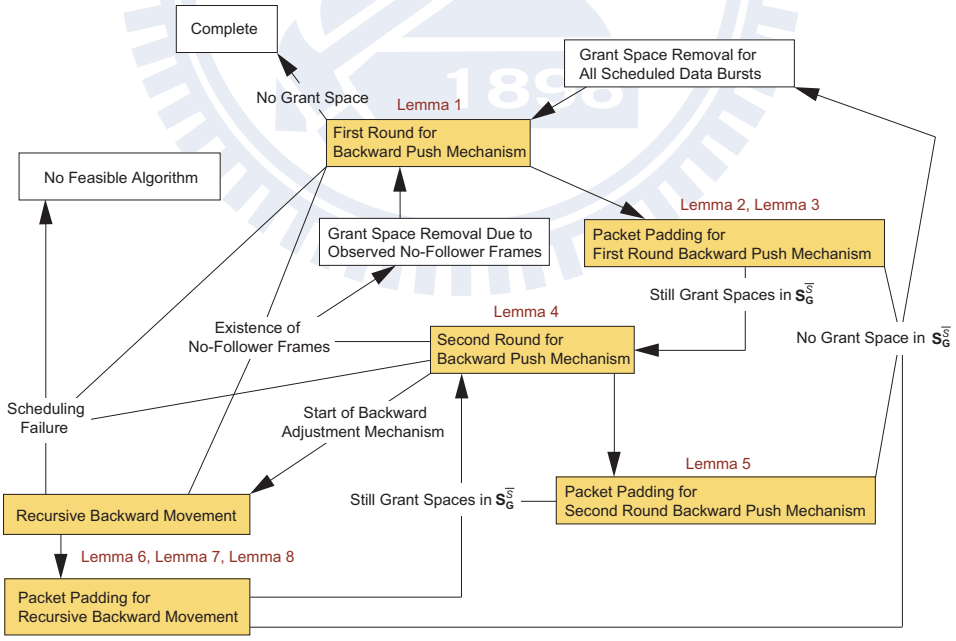

Figure 6.11: The flow of the correctness proof for the proposed FAPS algorithm.

Definition 16 (No-follower Frame). *The proposed FAPS algorithm is conducted on a stepwise grant space set* $\mathbf{G}$*. It is assumed that some grant spaces are scheduled together in a frame* θ_n *and the last grant space scheduled in* θ_n *is specified as* $G_\xi(s_\xi, g_\xi, t_\xi)$*. The frame* θ_n *is defined as a no-follower frame if there is no other data burst after the grant space* $G_\xi(s_\xi, g_\xi, t_\xi)$ *which has chance to be scheduled in this frame.*

As shown in Fig. 6.10, the frame $x_{\mathbf{G}} - 2$ is a no-follower frame since due to the properties of the stepwise grant space set in Definition 15, there is no other data burst after the grant space $G_e(s_e, g_e, t_e)$ which can be scheduled in this frame.

Fact 2. *Given the frame capacity* F_{max} *and a set of* $\mathbf{G}$ *with* $M_{\mathbf{G}}$ *grant spaces, all start and termination frames of the grant spaces in* $\mathbf{G}$ *are bounded in the frame range* $[\theta_s, \theta_t]$ *with width* $W = \theta_t - \theta_s + 1$*. If the number* $M_{\mathbf{G}}$ *can fit in with the following equation*

$$\lceil M_{\mathbf{G}}/F_{max} \rceil = W, \tag{6.4}$$

all frames ranging from θ_s *to* θ_t *must be necessary listen frames. On the other hand, if the following inequality can be unfortunately matched as*

$$\lceil M_{\mathbf{G}}/F_{max} \rceil > W, \tag{6.5}$$

there exists no scheduling algorithm which can arrange these data bursts based on the QoS constraints in the grant space set $\mathbf{G}$*.*

Fact 3. *The whole grant space set* $\mathbf{G}$ *consists of two disjoint sets* $\mathbf{G}_-$ *and* $\mathbf{G}_r$*, and it is assumed that at least* U_L *necessary listen frames exist before the end of a frame* θ_n*. The set* $\mathbf{G}_-$ *can be scheduled within the minimum number of listen frames and can be removed without interfering the scheduling of* $\mathbf{G}_r$ *if (i) the set* $\mathbf{G}_-$ *can have a feasible scheduling within* U_L *frames before the end of* θ_n*; and (ii) the data bursts in* $\mathbf{G}_r$ *are impossible to place in these* U_L *listen frames.*

Lemma 4. *In the first round of the backward push mechanism, given the first observed no-follower frame θ_n, the set $\mathbf{G}_-$ consisting of all grant spaces in $\mathbf{G}$ whose data bursts are scheduled before the end of θ_n can be removed without interfering the scheduling of the remaining grant spaces. The set $\mathbf{G}_-$ is considered completely scheduled within the minimum number of listen frames.*

Proof: The strictly stuck subgroup is denoted as $\mathbf{S}_{\mathbf{G}}^{S}$ with N_s grant spaces after the first round of the backward push mechanism. Based on the backward push mechanism, the number of partitions is obtained as

$$P_n = \lceil N_s / F_{max} \rceil. \tag{6.6}$$

For example, as shown in Fig. 6.10, the values can be obtained as $N_s = 10$, $P_n = 4$, and $F_{max} = 3$. The listen frames for accommodating all the data bursts specified in the grant spaces of $\mathbf{S}_{\mathbf{G}}^{S}$ will be within the range $[x_{\mathbf{G}} - P_n + 1, x_{\mathbf{G}}]$ since the maximum backward movement in the proposed backward push mechanism is $P_n - 1$ frames. Moreover, since the first no-follower frame θ_n can be observed during the first round of the backward push mechanism, the frame θ_n must be within the same listen frame range, i.e., $\theta_n \in [x_{\mathbf{G}} - P_n + 1, x_{\mathbf{G}}]$.

Based on the last grant space $G_\xi(s_\xi, g_\xi, t_\xi)$ scheduled in the no-follower frame θ_n, $\mathbf{S}_{\mathbf{G}}^{S}$ can be further divided into (i) the set $\mathbf{A}$ consisting of the grant space $G_\xi(s_\xi, g_\xi, t_\xi)$ and before and (ii) the other set $\mathbf{B}$ containing the remaining part. As shown in Fig. 6.10, for example, the last grant space in the no-follower frame θ_n is $G_e(s_e, g_e, t_e)$. The data bursts of the set $\mathbf{A}$ will be $\{a, b, c, d, e\}$; while those of the set $\mathbf{B}$ will be $\{f, g, h, m, n\}$. Given the size M_A of the set $\mathbf{A}$ and based on the backward push mechanism, the set $\mathbf{A}$ must be accommodated in the range $[x_{\mathbf{G}} - P_n + 1, \theta_n]$ with width $W_{\mathbf{A}}$, which can be determined as

$$W_{\mathbf{A}} = \lceil M_{\mathbf{A}} / F_{max} \rceil. \tag{6.7}$$

The grant spaces in the set $\mathbf{B}$ are constrained in the range $[\theta_n + 1, x_{\mathbf{G}}]$ due to the stuck frame and the no-follower frame definitions in Definitions 13 and 16. The width of the range

$[\theta_n + 1, x_{\mathbf{G}}]$ can be denoted and determined as

$$W_{\mathbf{B}} = P_n - W_{\mathbf{A}}. \tag{6.8}$$

Furthermore, the size $M_{\mathbf{B}}$ of the set $\mathbf{B}$ can be obtained as

$$M_{\mathbf{B}} = N_s - M_{\mathbf{A}}. \tag{6.9}$$

Therefore, based on (6.6) (6.7) (6.8) (6.9), the relation between $M_{\mathbf{B}}$ and $W_{\mathbf{B}}$ can be derived as the inequality

$$\lceil M_{\mathbf{B}}/F_{max} \rceil = \lceil (N_s - M_{\mathbf{A}})/F_{max} \rceil \geq \lceil N_s/F_{max} \rceil - \lceil M_{\mathbf{A}}/F_{max} \rceil = P_n - W_{\mathbf{A}} = W_{\mathbf{B}}. \tag{6.10}$$

Based on (6.10) and Fact 2, since the set $\mathbf{B}$ is bounded in the range $[\theta_n + 1, x_{\mathbf{G}}]$ with width $W_{\mathbf{B}}$, the frames in the range $[\theta_n+1, x_{\mathbf{G}}]$ must be necessary listen frames if a feasible scheduling method exists, i.e., $W_{\mathbf{B}} = \lceil M_{\mathbf{B}}/F_{max} \rceil$. Furthermore, it can also be observed that before the end of the stuck frame $x_{\mathbf{G}}$, there are at least $P_n = \lceil N_s/F_{max} \rceil$ listen frames required by all N_s data bursts in $\mathbf{S}^S_{\mathbf{G}}$. Therefore, there must be at least $U_L = P_n - W_{\mathbf{B}} = W_{\mathbf{A}}$ listen frames before the end of the no-follower frame θ_n since those $W_{\mathbf{B}}$ frames in the range $[\theta_n + 1, x_{\mathbf{G}}]$ have been proven as necessary.

The set $\mathbf{A}$ can fit in with the requirement of the set $\mathbf{G}_-$ since all data bursts of $\mathbf{A}$ are scheduled before the end of θ_n and no more grant space can be arranged within that range due to Definition 16. Furthermore, all data bursts in $\mathbf{A} = \mathbf{G}_-$ can be scheduled before the end of θ_n with $W_A = U_L$ frames. Therefore, based on Fact 3, the set $\mathbf{G}_-$ can be removed without interfering the scheduling of the remaining grant spaces. The scheduling of the set $\mathbf{G}_-$ is completed with the minimum number of listen frames. It completes the proof. □

Based on each observed no-follower frame, the corresponding grant space set $\mathbf{G}_-$ can be repeatedly removed from the stepwise grant space set $\mathbf{G}$ due to Lemma 4. All data bursts in the removed grant spaces are properly scheduled within the minimum number of listen frames.

Lemma 5. *After completing the possible grant space removal in* $\mathbf{S}_{\mathbf{G}}^{S}$ *based on Lemma 4, the remaining frames with data bursts are all fully-utilized except for the stuck frame which may be under-utilized.*

Proof: Based on the backward push mechanism, all grant spaces will be partitioned by the frame capacity F_{max}. All partitions are full of F_{max} grant spaces except for the last partition. Only the last partition can have the number of grant spaces which is less than F_{max}. Furthermore, all data bursts in the same partition will have the same pre-determined target frame, i.e., the i^{th} partition will be moved back $P_n - i$ frames from the stuck frame $x_{\mathbf{G}}$. If all data bursts in the same partition can reach the target frame, this target frame must be fully-utilized. On the other hand, if the data burst ξ can not be scheduled in its target frame θ_{ξ}^{t}, there will be two possible reasons as follows: The first one is that the frame θ_{ξ}^{t} must have no additional vacancy. It can be emphasized that the frame θ_{ξ}^{t} is fully-utilized. The other one can be that the data burst ξ in the grant space $G_{\xi}(s_{\xi}, g_{\xi}, t_{\xi})$ is constrained by the start frame index $s_{\xi} > \theta_{\xi}^{t}$. For example, as shown in Fig. 6.10, the first partition $\{a, b, c\}$ will be scheduled in the frame $x_{\mathbf{G}} - 3$ and occupy the whole frame. The second partition $\{d, e, f\}$ should be all scheduled in the frame $x_{\mathbf{G}} - 2$. However, due to the start frame constraint of the grant space, the data burst f can not reach the frame $x_{\mathbf{G}} - 2$.

In the above second reason, the target frame θ_{ξ}^{t} may be under-utilized. However, it must be a no-follower frame defined in Definition 16 since there is no other data burst after the grant space $G_{\xi}(s_{\xi}, g_{\xi}, t_{\xi})$ which has chance to be scheduled in the frame θ_{ξ}^{t}. For example, as shown in Fig. 6.10, the target frame θ_{ξ}^{t} of the data burst $\xi = f$ is the frame $x_{\mathbf{G}} - 2$, and there is no data burst after f which can be placed at this frame $x_{\mathbf{G}} - 2$. Based on Lemma 4, all grant spaces with the grant frame $g_i \leq \theta_{\xi}^{t}$ can be removed. Therefore, after completing all possible grant space removal, all the remaining frames with data bursts are fully-utilized except for the possible under-utilized stuck frame. It completes the proof. □

After the execution of the backward push mechanism, the packet padding in the proposed FA mechanism will be conducted. The data bursts specified in the non-strictly stuck subgroup $\mathbf{S}_{\mathbf{G}}^{\overline{S}}$ will be placed in the vacancy of the under-utilized frame. As shown in Fig. 6.10, the data

burst p will be scheduled with the data bursts $\{m, n\}$.

Lemma 6. *If all data bursts specified in the non-strictly stuck subgroup* $\mathbf{S}_{\mathbf{G}}^{\overline{S}}$ *are scheduled within the under-utilized frames of the first round backward push mechanism, the stuck group* $\mathbf{S_G}$ *can be removed without interfering the scheduling of the remaining grant spaces. All the removed grant spaces are considered completely scheduled within the minimum number of listen frames.*

Proof: Based on Lemma 4, all the grant spaces in $\mathbf{G}$ whose data bursts are scheduled before the end of the no-follower frame can be removed without interfering the scheduling of the remaining grant spaces. It leads to the reduction of the strictly stuck subgroup $\mathbf{S}_{\mathbf{G}}^{S}$. Based on Lemma 5, the remaining frames with data bursts will be all fully-utilized except for the stuck frame $x_{\mathbf{G}}$. In other words, the stuck frame $x_{\mathbf{G}}$ is the only frame which can accommodate the data bursts specified in the non-strictly stuck subgroup $\mathbf{S}_{\mathbf{G}}^{\overline{S}}$. If all data bursts specified in $\mathbf{S}_{\mathbf{G}}^{\overline{S}}$ are scheduled within the stuck frame $x_{\mathbf{G}}$, the number M_n of the grant spaces in the stuck group $\mathbf{S_G}$ and the number of listen frames L_n will have the relation as

$$L_n = \lceil M_n / F_{max} \rceil, \tag{6.11}$$

where F_{max} is the frame capacity. It is noted that L_n is also the minimum number of required frames before the end of the stuck frame $x_{\mathbf{G}}$. Moreover, due to the stuck group definition in Definition 13, there is no other grant space in ($\mathbf{G}$ - $\mathbf{S_G}$) which can be scheduled at the frame $\theta_\xi \leq x_{\mathbf{G}}$. The listen frames for accommodating the stuck group $\mathbf{S_G}$ will not be further updated or influenced by the scheduling of ($\mathbf{G}$ - $\mathbf{S_G}$). Therefore, based on Fact 3, the stuck group $\mathbf{S_G} = \mathbf{G}_{-}$ can be removed without interfering the scheduling of the remaining grant spaces. All the removed grant spaces are considered completely scheduled with the minimum number of listen frames. It completes the proof. □

If the stuck group $\mathbf{S_G}$ can be removed based on Lemma 6, the proposed FA mechanism can be re-conducted as the first round with the new stepwise grant space set ($\mathbf{G}$ - $\mathbf{S_G}$). On the other hand, if after the execution of the packet padding mechanism, some grant spaces

still exist in $\mathbf{S}_{\mathbf{G}}^{\overline{S}}$, the second round of the backward push mechanism will be conducted. The new stuck frame $x_{\mathbf{G}}$ will be therefore updated.

Lemma 7. *In the second round of the backward push mechanism, given the first observed no-follower frame θ_n, the set $\mathbf{G}_-$ consisting of all the grant spaces in $\mathbf{G}$ whose data bursts are scheduled before the end of θ_n can be removed without interfering the scheduling of the remaining grant spaces. The set $\mathbf{G}_-$ is considered completely scheduled within the minimum number of listen frames.*

Proof: In the second round of the backward push mechanism, based on the last grant space $G_\xi(s_\xi, g_\xi, t_\xi)$ scheduled in θ_n, the current strictly stuck subgroup can be divided into the grant space sets $\mathbf{A}$ and $\mathbf{B}$. The set $\mathbf{A}$ contains the grant space $G_\xi(s_\xi, g_\xi, t_\xi)$ and those before; while the remaining grant spaces are in the set $\mathbf{B}$. Moreover, the grant space set $\mathbf{C}$ is also introduced to include the previously scheduled and not-yet removed grant spaces. It is noted that the set $\mathbf{C}$ is perfectly scheduled within $L_{\mathbf{C}}$ full-utilized frames, i.e., the following relation will be hold as

$$M_{\mathbf{C}} = L_{\mathbf{C}} \cdot F_{max}, \tag{6.12}$$

where $M_{\mathbf{C}}$ is the number of the grant spaces in the set $\mathbf{C}$. The listen frames for containing the set $\mathbf{C}$, i.e., the previous scheduling results, may or may not influence the second round of the backward push mechanism. Therefore, the integer variable δ representing the number of the frames blocked by the set $\mathbf{C}$ is introduced. The equation in (6.8) will therefore be updated as

$$P_n = \delta + W_{\mathbf{A}} + W_{\mathbf{B}}. \tag{6.13}$$

With the new P_n in (6.13), the inequality specified in (6.10) can still be hold since $W_{\mathbf{B}} + \delta \geq W_{\mathbf{B}}$. Based on (6.10) and Fact 2, since the set $\mathbf{B}$ is bounded in the range $[\theta_n + 1, x_{\mathbf{G}}]$ with width $W_{\mathbf{B}}$, the frames in the range $[\theta_n+1, x_{\mathbf{G}}]$ must be necessary listen frames if the scheduling method exists, i.e., $W_{\mathbf{B}} = \lceil M_{\mathbf{B}}/F_{max} \rceil$. In other words, the variable δ must be zero in order to have a feasible solution.

It is noted that there are at least $V = \lceil (M_{\mathbf{C}} + M_{\mathbf{A}} + M_{\mathbf{B}})/F_{max} \rceil$ listen frames before

the end of the stuck frame $x_{\mathbf{G}}$ for containing the sets $\mathbf{A}$, $\mathbf{B}$ and $\mathbf{C}$. Moreover, since the $W_{\mathbf{B}}$ frames in the range $[\theta_n + 1, x_{\mathbf{G}}]$ have been proven as necessary ones, there must be at least $U_L = V - W_{\mathbf{B}} = L_{\mathbf{C}} + P_n - W_{\mathbf{B}} = L_{\mathbf{C}} + W_{\mathbf{A}}$ listen frames before the end of the no-follower frame θ_n. It can be observed that all data bursts in the sets $\mathbf{A}$ and $\mathbf{C}$ can be scheduled before the end of the no-follower frame θ_n with $U_L = L_{\mathbf{C}} + W_{\mathbf{A}}$ listen frames. Furthermore, based on Definition 16, there will be no other grant space after the last grant space $G_\xi(s_\xi, g_\xi, t_\xi)$ scheduled in θ_n which can affect the scheduling of the sets $\mathbf{A}$ and $\mathbf{C}$. Therefore, based on Fact 3, the set $\mathbf{G}_- = \mathbf{A} + \mathbf{C}$ can be removed without interfering the scheduling of the remaining grant spaces. The scheduling of $\mathbf{G}_-$ is completed with the minimum number of listen frames. It completes the proof. □

If there exists a no-follower frame in the second round of the backward push mechanism, the corresponding grant space set $\mathbf{G}_-$ can be removed from the stepwise grant space set $\mathbf{G}$ based on Lemma 7. All data bursts in the removed grant spaces are properly scheduled in the minimum number of listen frames. The remaining grant spaces lead to a new stepwise grant space set for the execution of the backward push mechanism as the first round again. If none of no-follower frames is encountered, only packet padding for the proposed FA mechanism or simply the proposed BA mechanism will be executed. The first case when the packet padding is conducted is considered as follows:

Lemma 8. *If all data bursts specified in the non-strictly stuck subgroup $\mathbf{S}_{\mathbf{G}}^{\overline{S}}$ are scheduled within the under-utilized frames of the second round backward push mechanism, the stuck group $\mathbf{S}_{\mathbf{G}}$ and all previously scheduled grant spaces can be removed without interfering the scheduling of the remaining grant spaces. All the removed grant spaces are considered completely scheduled within the minimum number of listen frames.*

Proof: It can be observed that all listen frames occupied by the data bursts of $\mathbf{S}_{\mathbf{G}}$ and all previously scheduled grant spaces are fully-utilized except for the possible under-utilized stuck frame. Moreover, since all data bursts of $\mathbf{S}_{\mathbf{G}}^{\overline{S}}$ can be placed within the stuck frame. Therefore, the stuck group $\mathbf{S}_{\mathbf{G}}$ and all previously scheduled grant spaces are properly scheduled within the minimum number of listen frames. Moreover, based on Definition 13, the remaining grant

spaces have no chance to place in the stuck frame and before. Finally, based on Fact 3, the stuck group $\mathbf{S_G}$ and all previously scheduled grant spaces can be removed without interfering the scheduling of the remaining grant spaces. All the removed grant spaces are considered completely scheduled with the minimum number of listen frames. It completes the proof. □

If the grant space removal can be done based on Lemma 8, the remaining unscheduled grant spaces can form the new stepwise grant space set as the input of the first round of the backward push mechanism. The second case when the proposed BA mechanism is executed is considered as follows:

Lemma 9. *If the recursive backward movement of the proposed BA mechanism can not properly schedule the data bursts, there exists no feasible scheduling algorithm.*

Proof: When the recursive backward movement of the proposed BA mechanism is employed, the stuck frame $x_{\mathbf{G}}$ must be full of data bursts and there is still at least one data burst which should be scheduled in the stuck frame or before. Based on the recursive backward movement, the grant space scheduled in $x_{\mathbf{G}}$ which has the smallest start will be moved back one frame in order to check whether there is any vacancy in the frame $x_{\mathbf{G}} - 1$ next to the current frame $\theta_c^1 = x_{\mathbf{G}}$. If the frame $x_{\mathbf{G}} - 1$ is also fully-utilized, the same process will be repeatedly conducted. The frame $x_{\mathbf{G}} - 2$ next to the current frame $\theta_c^2 = x_{\mathbf{G}} - 1$ will be checked. The only case that the recursive backward movement can not complete the scheduling is when all start frames of the grant spaces arranged in the current frame θ_c^i are the same as θ_c^i and θ_c^i is full of data bursts. It can be noted that there will be at least $(x_{\mathbf{G}} - \theta_c^i + 1) \cdot F_{max} + 1$ grant spaces bounded in the range $[\theta_c^i, x_{\mathbf{G}}]$. Therefore, based on Fact 2, there exists no feasible scheduling algorithm. It completes the proof. □

Lemma 10. *If there is a no-follower frame θ_n observed during the execution of the proposed BA mechanism, the set $\mathbf{G}_-$ consisting of all grant spaces whose data bursts scheduled in θ_n and before can be removed without interfering the scheduling of the remaining grant spaces. All the removed grant spaces are considered completely scheduled with the minimum number of listen frames.*

Proof: It is assumed that the no-follower frame θ_n is obtained during the scheduling the grant space $G_\xi(s_\xi, g_\xi, t_\xi)$. Based on Lemma 9, the data burst ξ in $G_\xi(s_\xi, g_\xi, t_\xi)$ will be properly scheduled if a feasible scheduling algorithm exists. In order to provide a vacancy for ξ, one data burst will be moved to the first observed under-utilized frame θ_u in the reverse direction. All previously scheduled and not-yet removed grant spaces can be divided into three sets. The set $\mathbf{A}$ contains all grant spaces whose data bursts are arranged in the range $[\theta_n + 1, x_{\mathbf{G}}]$. The set $\mathbf{B}$ includes those in the range $[\theta_u, \theta_n]$; while the remaining grant spaces are in the set $\mathbf{C}$. M_ξ and L_ξ are respectively denoted as the number of data bursts and listen frames in the set $\xi \in \{\mathbf{A}, \mathbf{B}, \mathbf{C}\}$. It can be observed that the listen frames for the set $\mathbf{A}$ and $\mathbf{C}$ are fully-utilized, i.e.,

$$M_{\mathbf{A}} = L_{\mathbf{A}} \cdot F_{max} \tag{6.14}$$

and

$$M_{\mathbf{C}} = L_{\mathbf{C}} \cdot F_{max}. \tag{6.15}$$

Furthermore, the listen frames for the set $\mathbf{B}$ have the relation as

$$L_{\mathbf{B}} = \lceil M_{\mathbf{B}}/F_{max} \rceil. \tag{6.16}$$

Based on Definitions 13 and 16, the grant spaces in $\mathbf{A}$ are bounded in the range $[\theta_n + 1, x_{\mathbf{G}}]$. Due to Fact 2, all $L_{\mathbf{A}}$ listen frames are necessary. Thanks to these necessary $L_{\mathbf{A}}$ frames, there must be at least

$$U_L = \lceil (M_{\mathbf{A}} + M_{\mathbf{B}} + M_{\mathbf{C}})/F_{max} \rceil - L_{\mathbf{A}} = L_{\mathbf{B}} + L_{\mathbf{C}} \tag{6.17}$$

listen frames before the end of θ_n. Based on Fact 3, the set $\mathbf{G}_- = \mathbf{B} + \mathbf{C}$ can be scheduled in these U_L listen frames and no other grant space can affect the scheduling of $\mathbf{G}_-$. Therefore, the set $\mathbf{G}_-$ can be removed without interfering the scheduling of the remaining grant spaces. All the removed grant spaces are considered completely scheduled within the minimum number of listen frames. It completes the proof. □

Lemma 11. *In the packet padding of the proposed BA mechanism, if no more grant space in*

the non-strictly stuck subgroup can be used, all scheduled grant spaces can be removed without interfering the scheduling of the remaining grant spaces. All the removed grant spaces are considered completely scheduled within the minimum number of listen frames.

Proof: The packet padding mechanism will occur if there exists an under-utilized frame θ_u after the execution of the recursive backward movement. This frame θ_u is also the only under-utilized frame in the current scheduled frames since the recursive backward movement will skip all fully-utilized frames from the stuck frame and find the first under-utilized frame to schedule the data burst. The packet padding mechanism will at most lead the frame θ_u to the fully-utilized frame. Therefore, if all grant spaces in the non-strictly stuck subgroup are used in the padding, the grant spaces scheduled before the end of stuck frame can be arranged in the minimum required number of listen frames. Moreover, since no more grant space in the non-strictly stuck subgroup can be used, there is no other grant space which can be scheduled in the stuck frame and before. Therefore, based on Fact 3, all scheduled grant spaces can be removed without interfering the scheduling of the remaining grant spaces. All the removed grant spaces are considered completely scheduled within the minimum number of listen frames. It completes the proof. □

If the removal is conducted, the new stepwise grant space set consisting of the remaining grant spaces can be constructed and the first round of the backward push mechanism can start again on the new set. On the other hand, if there are still grant spaces in the non-strictly stuck subgroup, the second round of the backward push mechanism will be conducted repeatedly with all frames fully-utilized. In the end, based on the above proofs of correctness for the flow of the proposed FAPS algorithm in Fig. 6.11, if the given stepwise grant space set $\mathbf{G}$ exists a feasible packet arrangement under the frame capacity constraint F_{max}, the proposed FAPS algorithm can produce the minimum number of listen frames. The optimality of the proposed FAPS algorithm can therefore be obtained.

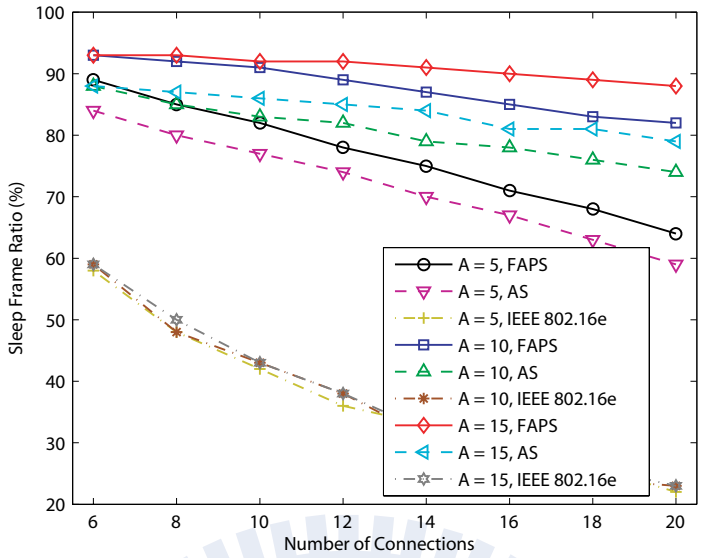

Figure 6.12: The performance comparison of sleep frame ratio versus number of connections under different maximum frame accommodation $A = F_{max} = 5$, 10, 15.

6.5 Performance Evaluation

In this section, simulations are conducted to evaluate the performance of the proposed FAPS scheduling algorithms in comparison with the AS scheme and the original power-saving mechanism in the IEEE 802.16e specification. A single BS/MSS pair with multiple connections are considered as the simulation scenario. 100 frames with each frame duration of 5 ms are utilized in the simulation. The default settings of each connection are listed as follows: The maximum frame accommodation F_{max} is 5. The connection period (i.e., the number of frames between each two consecutive packets) is 10; while the delay constraint is ranging from 50 ms to 75 ms. Two performance metrics are adopted for performance comparison: 1) the sleep frame ratio: the number of sleep frames divided by the total frames, 2) the grant delay: the average value of (g_i - s_i) for each grant space $G_i(s_i, g_i, t_i)$.

The performance curves of the sleep frame ratio under different maximum frame accommodations are shown in Fig. 6.12. The curves of IEEE 802.16e are almost the same under F_{max} of 5, 10, and 15 since the IEEE 802.16e does not rearrange the data packets and just schedules the packets at the original start frames specified in their grant spaces. On the other

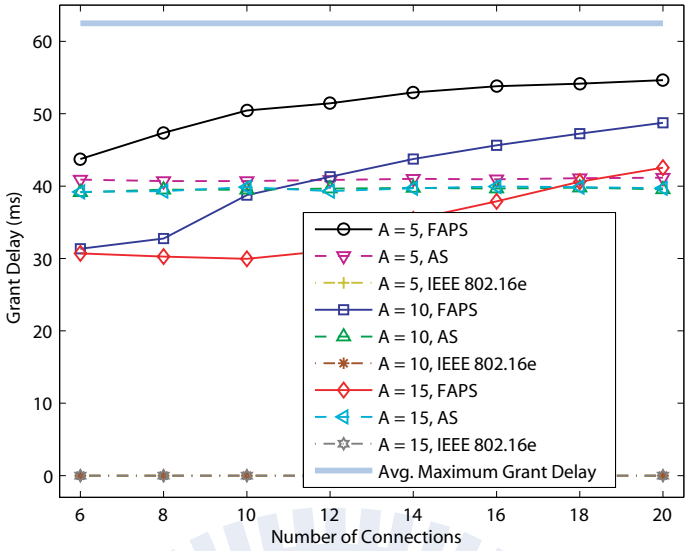

Figure 6.13: The performance comparison of grant delay versus number of connections under different maximum frame accommodation $A = F_{max} = 5$, 10, 15.

hand, the performance of the sleep frame ratio of the proposed FAPS protocol outperforms the other connection-oriented schemes under each F_{max} since the proposed FAPS protocol can effectively rearrange the data packets in the packet level. It is noted that when the number of connections is increased, the sleep frame ratio is decreased since more frames should be awake to serve the increased number of packets. It is also noted that when the maximum frame accommodation becomes larger, the sleep frame ratio is increased since less frames should be consumed to contain the packets.

Fig. 6.13 shows the performance curves of the grant delay under different maximum frame accommodations. The grant delay performance of the IEEE 802.16e should be zero since it does not delay its packets. In the curves of the proposed FAPS and the AS schemes, when the maximum frame accommodation becomes smaller, the more grant delay should be generated since more packets should be delayed to seek the proper position to accommodate themselves. The curves of the AS scheme maintain almost a constant trend since the AS scheme is a connection-oriented scheme for conducting scheduling from the connection with the smallest delay constraint, which dominates the performance curves. In general, the grant

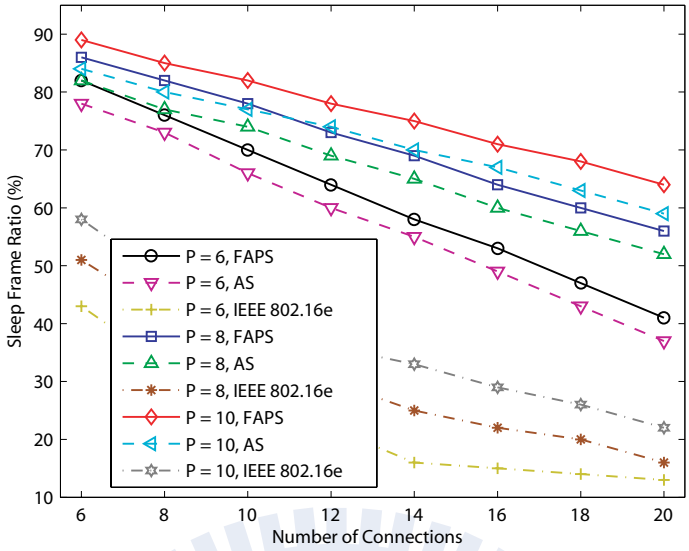

Figure 6.14: The performance comparison of sleep frame ratio versus number of connections under different connection period $P = 6, 8, 10$.

delay of the proposed FAPS scheme should be larger than that of the AS algorithm since the proposed FAPS scheme has higher performance in the sleep frame ratio. However, in some cases, the curves of the proposed FAPS scheme will violate this general thought because the connection-oriented AS scheme is dominated by the connection with the smallest delay, while the proposed FAPS algorithm is a fully packet-level method. The proposed FAPS can even find a better way with smaller delay to aggregate packets. In the end, it can be observed that all curves are below the average maximum grant delay, which maintains the QoS delay constraint requirements.

The performance curves of the sleep frame ratio under different connection periods are shown in Fig. 6.14. All these three protocols show the decreasing trend with regard to the number of connections since more frames are required to accommodate the packets provided by the connections. Since shorter connection period generates more packets, these protocols also have the increasing trend versus the connection period. The performance of the sleep frame ratio of the proposed FAPS protocol outperforms the other connection-oriented schemes under each connection period since the design of the proposed FAPS protocol considers the

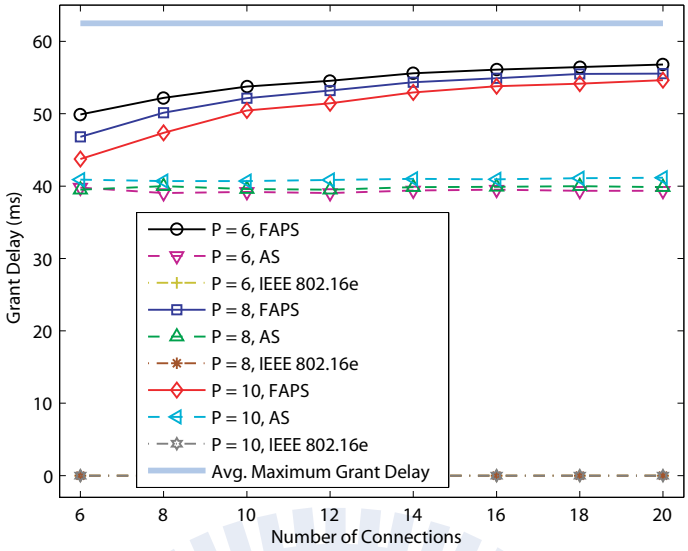

Figure 6.15: The performance comparison of grant delay versus number of connections under different connection period $P = 6, 8, 10$.

packet as the unit of scheduling instead of the connection, which will have more chance to leave the sleep interval.

Fig. 6.15 shows the performance curves of the grant delay under different connection periods. Due to the absence of the packet arrangement, the grant delay performance of the IEEE 802.16e is zero. In the curves of the proposed FAPS scheme, when the connection period becomes smaller, more grant delay should be generated to find the proper position to accommodate additional packets. On the contrary, the curves of the AS scheme will have higher grant delay when the connection period becomes larger. This phenomenon comes from the design of the AS scheme which arranges packets from their terminations; therefore, in the case of the large connection period, a large portion of packets are placed around the termination, leading to the higher grant delay. The grant delay of the proposed FAPS scheme is larger than that of the AS algorithm since the proposed FAPS protocol has higher performance in the sleep frame ratio. It is noted that the QoS delay constraint requirements are guaranteed since all curves are below the average maximum grant delay. The merits of the proposed FAPS scheme are fully supported via simulations with the tolerable delay.

6.6 Summary

In this chapter, with the consideration of the multiple connections and their QoS constraints, a packet-level frame aggregation-based power-saving scheduling (FAPS) algorithm is proposed to maximize the number of total sleep frames by frame aggregation techniques. Based on the stepwise grant space set, the optimality on the minimum number of listen frames in the proposed FAPS algorithm is also provided and further verified via the proof of correctness. Simulation studies show that the power efficiency of the proposed FAPS algorithm outperforms the other baseline protocols with tolerable delay. As a result of the high performance on the power efficiency, the proposed FAPS algorithm can therefore be utilized as a feasible green data link protocol design for achieving the green wireless access networks.

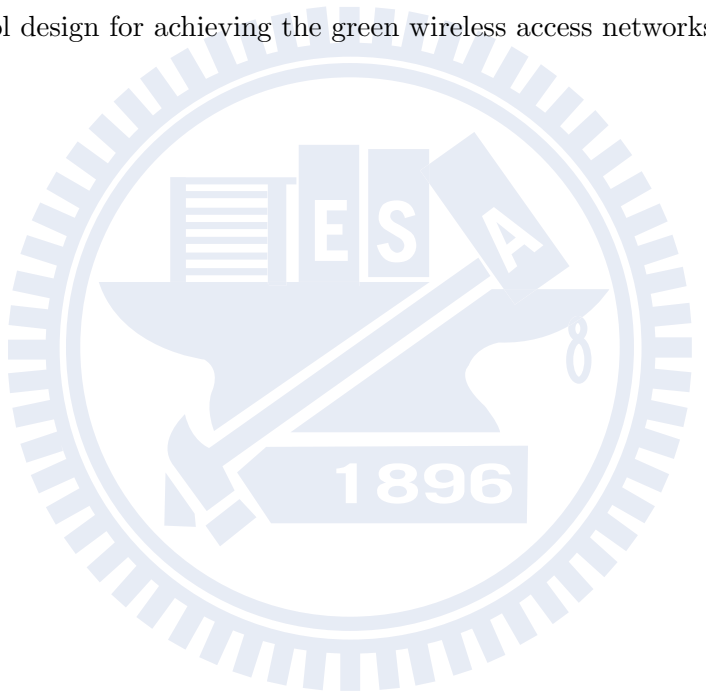

Chapter 7

Conclusion

In this dissertation, the development of the green wireless access networks is conducted by the protocol design and implementation within the network layer and the data link layer. In the network layer, two main categories of routing protocols are considered, including the unicast routing and the multicast routing protocols. In the unicast protocol design for achieving the green concept, a greedy anti-void routing (GAR) protocol is proposed for the two-dimensional network based on the well-known low-overhead greedy forwarding (GF) technique. In the unit disk graph (UDG) settings, the unreachability problem, i.e., the void problem, due to the GF scheme can be completely resolved by the proposed GAR protocol. It is attributed to the solving of the boundary finding problem by the proposed rolling-ball UDG boundary traversal (RUT) scheme. The proposed RUT scheme within the GAR protocol can find a rescue path to escape from the region where the void problem exists. The packet delivery can therefore be guaranteed. In the protocol realization, the boundary map (BM) and the indirect map searching (IMS) algorithm for the BM construction are proposed as feasible procedures to reduce the impractically high algorithm complexity required by the traditional method.

Moreover, several schemes are also provided for performance enhancement as the hop count reduction (HCR), the intersection navigation (IN), and the partial UDG construction (PUC) schemes. On the other hand, in the three dimensional space, a three-dimensional greedy anti-void routing (3D-GAR) protocol is proposed to solve the void problem under the unit ball graph (UBG) settings. The associated boundary finding problem in the 3D

space is also resolved by the proposed three-dimensional rolling-ball UBG boundary traversal (3D-RUT) scheme. The packet delivery can still be guaranteed in the 3D environment. The correctness proofs and the extensive simulations are provided for validating the merits of guaranteed delivery and evaluating the performance of the proposed schemes. The evaluation results show that the proposed schemes can have high routing efficiency with guaranteed packet delivery. The unicast routing protocols for achieving the green wireless access network can therefore be constructed.

In the aspect of the multicast protocol design for achieving the green wireless access networks, an energy conserving multicast routing (ECMR) protocol is proposed to reduce the unnecessary communication overheads by removing the unessential intermediate forwarding nodes in the construction of the multicast tree. The merits of the low overhead and high packet delivery ratio can be perceived in the performance evaluation. As a low-overhead multicast routing protocol, the proposed ECMR scheme can therefore be utilized in the construction of the green wireless access networks. Furthermore, in order to implement the routing protocols for field experiments, a component-based routing platform (CRP) is proposed as a generic implementation testbed based on the Linux embedded systems. The kernel software modules are properly designed for protocol developers to conduct the field experiments more easily. The proposed ECMR protocol and several existing schemes are realized on the proposed CRP system for performance comparison. The experimental results show that the proposed ECMR protocol can have low routing overhead and high packet delivery ratio. At the same time, the effectiveness of the proposed CRP implementation platform can also be observed by these field experiments.

In the data link layer protocol design for achieving the green wireless access networks, two main techniques are considered, including the system throughput enhancement and the design of the power-saving scheduling algorithm. In terms of the system throughput enhancement, a greedy fast-shift (GFS) block acknowledgement mechanism is proposed to provide the receiver-defined starting sequence number (SSN). The proposed GFS scheme can both implicitly acknowledge the correctly received packets before the SSN and explicitly provide the correctness information for the packets after the SSN. Focused on the throughput-related

performance metric of the window utilization, the analytical models for both the proposed GFS scheme and the conventional greedy scheme are also formulated for the correctness of performance evaluation. Based on the evaluation results, the proposed GFS method can outperform the conventional greedy scheme on the throughput performance and effectively reduce the inefficiency observed in the conventional block acknowledgement scheme. Thanks to the high throughput performance, the proposed GFS scheme can be considered a superior data link protocol for achieving the green wireless access network.

On the other hand, in the design of the power-saving scheduling algorithm, a frame aggregation-based power-saving scheduling (FAPS) algorithm is proposed as a data link protocol for constructing the green wireless access network. With the consideration of the multiple connection scenarios, the proposed FAPS scheme aggregates multiple under-utilized frames into fully-utilized ones in order to maximize the number of sleep frames for reducing the energy consumption. The quality-of-service (QoS) constraint of each connection can still be preserved in the proposed FAPS scheme. The optimality on the minimum number of listen frames in the proposed FAPS algorithm is also provided under the stepwise grant space set and further verified via the correctness proof. The evaluation results indicate that the proposed FAPS algorithm can outperform the conventional schemes on the power efficiency metric of sleep frame ratio. In the end, with the assistance of these proposed energy efficient software protocol designs in both the network layer and the data link layer, the green wireless access network can eventually be constructed for protecting our natural environments with reasonable system performance.

Bibliography

[1] C.S.R. Murthy and B.S. Manoj, *Ad Hoc Wireless Networks: Architectures and Protocols*, 1st ed. Pearson Education, Inc., 2004.

[2] PC Magazine, *PC Magazine Encyclopedia: Definition of Green.* Ziff Davis Publishing Holdings, Inc.

[3] S. Vadgama, "Trends in Green Wireless Access," *Fujitsu Sci. Tech. J.*, vol. 45, no. 4, pp. 404–408, Oct. 2009.

[4] G.G. Finn, "Routing and Addressing Problems in Large Metropolitan-Scale Internetworks," Info. Sci. Inst. (ISI), Tech. Rep. ISI/RR-87-180, Mar. 1987.

[5] B. Karp and H.T. Kung, "GPSR: Greedy Perimeter Stateless Routing for Wireless Networks," in *Proc. ACM/IEEE Int. Conf. Mobile Computing and Networking (MobiCom'00)*, Aug. 2000, pp. 243–254.

[6] F.K. Hwang, D.S. Richards, and P. Winter, *The Steiner Tree Problem.* Elsevier, North-Holland, 1992.

[7] D. Estrin, R. Govindan, J. Heidemann, and S. Kumar, "Next Century Challenges: Scalable Coordination in Sensor Networks," in *Proc. ACM/IEEE Int. Conf. Mobile Computing and Networking (MobiCom'99)*, Aug. 1999, pp. 263–270.

[8] I. Stojmenović and X. Lin, "Loop-Free Hybrid Single-Path/Flooding Routing Algorithms with Guaranteed Delivery for Wireless Networks," *IEEE Trans. Parallel Distrib. Syst.*, vol. 12, no. 10, pp. 1023–1032, Oct. 2001.

[9] R. Jain, A. Puri, and R. Sengupta, "Geographical Routing Using Partial Information for Wireless Ad Hoc Networks," *IEEE Pers. Commun. Mag.*, vol. 8, no. 1, pp. 48–57, Feb. 2001.

[10] D. Chen and P.K. Varshney, "On-demand Geographic Forwarding for Data Delivery in Wireless Sensor Networks," *Elsevier Computer Communications*, vol. 30, no. 14-15, pp. 2954–2967, Oct. 2007.

[11] I. Stojmenović, M. Russell, and B. Vukojevic, "Depth First Search and Location Based Localized Routing and QoS Routing in Wireless Networks," in *Proc. IEEE Int. Conf. Parallel Processing (ICPP'00)*, Aug. 2000, pp. 173–180.

[12] T. He, J.A. Stankovic, C. Lu, and T. Abdelzaher, "SPEED: A Stateless Protocol for Real-Time Communication in Sensor Networks," in *Proc. Int. Conf. Distributed Computing Systems (ICDCS'03)*, May 2003, pp. 46–55.

[13] V.C. Giruka and M. Singhal, "Angular Routing Protocol for Mobile Ad Hoc Networks," in *Proc. IEEE Int. Conf. Distributed Computing Systems Workshops (ICDCSW'05)*, Jun. 2005, pp. 551–557.

[14] W.J. Liu and K.T. Feng, "Largest Forwarding Region Routing Protocol for Mobile Ad Hoc Networks," in *Proc. IEEE Global Communications Conference (GLOBECOM'06)*, Nov. 2006, pp. 1–5.

[15] L. Zou, M. Lu, and Z. Xiong, "A Distributed Algorithm for the Dead End Problem of Location Based Routing in Sensor Networks," *IEEE Trans. Veh. Technol.*, vol. 54, no. 4, pp. 1509–1522, Jul. 2005.

[16] N. Arad and Y. Shavitt, "Minimizing Recovery State in Geographic Ad-Hoc Routing," in *Proc. ACM Int. Symp. Mobile Ad Hoc Networking and Computing (MobiHoc'06)*, May 2006, pp. 13–24.

[17] S. Chen, G. FAN, and J.H. Cui, "Avoid 'Void' in Geographic Routing for Data Aggregation in Sensor Networks," *Int. Journal of Ad Hoc and Ubiquitous Computing (IJAHUC)*, vol. 1, no. 4, pp. 169–178, 2006.

[18] D.D. Couto and R. Morris, "Location Proxies and Intermediate Node Forwarding for Practical Geographic Forwarding," MIT Laboratory for Computer Science, Tech. Rep. MIT-LCS-TR-824, Jun. 2001.

[19] J. Na, D. Soroker, and C.K. Kim, "Greedy Geographic Routing Using Dynamic Potential Field for Wireless Ad Hoc Networks," *IEEE Commun. Lett.*, vol. 11, no. 3, pp. 243–245, Mar. 2007.

[20] H. Frey and I. Stojmenović, "On Delivery Guarantees of Face and Combined Greedy Face Routing in Ad Hoc and Sensor Networks," in *Proc. ACM/IEEE Int. Conf. Mobile Computing and Networking (MobiCom'06)*, Sept. 2006, pp. 390–401.

[21] P. Bose, P. Morin, I. Stojmenović, and J. Urrutia, "Routing with Guaranteed Delivery in Ad Hoc Wireless Networks," *ACM/Kluwer Wireless Networks*, vol. 7, no. 6, pp. 609–616, Nov. 2001.

[22] E. Kranakis, H. Singh, and J. Urrutia, "Compass Routing on Geometric Networks," in *Proc. Canadian Conf. Computational Geometry (CCCG'99)*, Aug. 1999, pp. 51–54.

[23] F. Kuhn, R. Wattenhofer, and A. Zollinger, "Asymptotically Optimal Geometric Mobile Ad-Hoc Routing," in *Proc. Int. Workshop on Discrete Algorithms and Methods for Mobile Computing and Communications (Dial-M'02)*, Sept. 2002, pp. 24–33.

[24] F. Kuhn, R. Wattenhofer, and A. Zollinger, "Worst-case Optimal and Average-case Efficient Geometric Ad-hoc Routing," in *Proc. ACM Int. Symp. Mobile Computing and Networking (MobiHoc'03)*, Jun. 2003, pp. 267–278.

[25] F. Kuhn, R. Wattenhofer, Y. Zhang, and A. Zollinger, "Geometric Ad-hoc Routing: Of Theory and Practice," in *Proc. ACM Symp. Principles of Distributed Computing (PODC)*, Jul. 2003, pp. 63–72.

[26] B. Leong, S. Mitra, and B. Liskov, "Path Vector Face Routing: Geographic Routing with Local Face Information," in *Proc. IEEE Int. Conf. Network Protocols (ICNP'05)*, Nov. 2005, pp. 147–158.

[27] Q. Fang, J. Gao, and L. Guibas, "Locating and Bypassing Routing Holes in Sensor Networks," in *Proc. IEEE Int. Conf. Computer Communications (INFOCOM'04)*, Mar. 2004, pp. 2458–2468.

[28] D.B. West, *Introduction to Graph Theory*, 2nd ed. Prentice Hall, 2000.

[29] K.R. Gabriel and R.R. Sokal, "A New Statistical Approach to Geographic Variation Analysis," *Systematic Zoology*, vol. 18, no. 3, pp. 259–278, Sept. 1969.

[30] G.T. Toussaint, "The Relative Neighborhood Graph of a Finite Planar Set," *Pattern Recognition*, vol. 12, no. 4, pp. 261–268, 1980.

[31] Y.J. Kim, R. Govindan, B. Karp, and S. Shenker, "On the Pitfalls of Geographic Face Routing," in *Proc. ACM/SIGMOBILE Joint Workshop Foundations of Mobile Computing (DIALM-POMC'05)*, Sept. 2005, pp. 34–43.

[32] S. Datta, I. Stojmenović, and J. Wu, "Internal Node and Shortcut Based Routing with Guaranteed Delivery in Wireless Networks," *Kluwer Cluster Computing*, vol. 5, no. 2, pp. 169–178, 2002.

[33] V.C. Giruka and M. Singhal, "Hello Protocols for Ad-Hoc Networks: Overhead and Accuracy Tradeoffs," in *Proc. IEEE Int. Symp. World of Wireless, Mobile and Multimedia Networks (WoWMoM'05)*, Jun. 2005, pp. 354–361.

[34] E. Horowitz, S. Sahni, and D. Mehta, *Fundamentals of Data Structures in C++*, 2nd ed. Silicon Press, 2006.

[35] T.H. Cormen, C.E. Leiserson, R.L. Rivest, and C. Stein, *Introduction to Algorithms*, 2nd ed. The MIT Press, 2001.

[36] J. Heidemann, N. Bulusu, J. Elson, C. Intanagonwiwak, K. Lan, Y. Xu, W. Ye, D. Estrin, and R. Govindan, "Effects of Detail in Wireless Network Simulation," in *Proc. SCS Multiconference on Distributed Simulation*, Jan. 2001, pp. 3–11.

[37] M.C. Domingo and R. Prior, "Energy Analysis of Routing Protocols for Underwater Wireless Sensor Networks," *Computer Communications*, vol. 31, no. 6, pp. 1227–1238, Apr. 2008.

[38] A.E. Abdallah, T. Fevens, and J. Opatrny, "Hybrid Position-Based 3D Routing Algorithms with Partial Flooding," in *Proc. Canadian Conf. Electrical and Computer Engineering*, May 2006, pp. 227–230.

[39] G. Kao, T. Fevens, and J. Opatrny, "3-D Localized Position-Based Routing with Nearly Certain Delivery in Mobile Ad Hoc Networks," in *Proc. Int. Symp. Wireless Pervasive Computing*, Feb. 2007, pp. 344–349.

[40] D. Culler, D. Estrin, and M. Srivastava, "Overview of Sensor Networks," *IEEE Computer*, vol. 37, pp. 41–49, Aug. 2004.

[41] J. Hill, M. Horton, R. Kling, and L. Krishnamurthy, "Wireless Sensor Networks: The Platforms Enabling Wireless Sensor Networks," *Communication of ACM*, vol. 47, pp. 41–46, Jun. 2004.

[42] S. Park, J.W. Kim, K. Lee, K.Y. Shin, and D. Kim, "Embedded Sensor Networked Operating System," in *Proc. of IEEE Object and Component-Oriented Real-Time Distributed Computing (ISORC)*, Apr. 2006, pp. 24–26.

[43] R.S. Chang and C.J. Kuo, "An Energy Efficient Routing Mechanism for Wireless Sensor Networks," in *Proc. of IEEE Advanced Information Networking and Applications*, Apr. 2006.

[44] J.N. Al-Karaki and A.E. Kamal, "Routing Techniques in Wireless Sensor Networks: A Survey," *IEEE Wireless Commun. Mag.*, vol. 11, Dec. 2004.

[45] E.M. Royer and C.E. Perkins, "Multicast Operation of the Ad-Hoc On-Demand Distance Vector Routing Protocol," in *Proc. of the Fifth Annual ACM/IEEE International Conference on Mobile Computing and Networking*, Aug. 1999, pp. 207–218.

[46] C.W. Wu and Y.C. Tay, "AMRIS: A Multicast Protocol for Ad Hoc Wireless Networks," in *Proc. of IEEE Military Communications Conference*, Oct. 1999, pp. 25–29.

[47] J. Xie, R.R. Talpade, A. Mcauley, and M. Liu, "AMRoute: Ad Hoc Multicast Routing Protocol," *ACM/Kluwer Journal of Mobile Networks and Applications*, vol. 7, pp. 429–439, Dec. 2002.

[48] S.K.S. Gupta and P.K. Srimani, "An Adaptive Protocol for Reliable Multicast in Mobile Multi-Hop Radio Networks," in *Proc. of the Second IEEE Workshop on Mobile Computing Systems and Applications*, Feb. 1999, pp. 111–122.

[49] S.J. Lee, M. Gerla, and C.C. Chiang, "On-Demand Multicast Routing Protocol," in *Proc. IEEE Wireless Communications and Networking Conference (WCNC)*, Sept. 1999, pp. 1298–1302.

[50] J.J. Garcia-Luna-Aceves and E.L. Madruga, "The Core-Assisted Mesh Protocol," *IEEE J. Sel. Areas Commun.*, vol. 17, pp. 1380–1394, Aug. 1999.

[51] P. Sinha, R. Sivakumar, and V. Bharghavan, "MCEDAR: Multicast Core-Extraction Distributed Ad Hoc Routing," in *Proc. of IEEE Wireless Communications and Networking Conference (WCNC)*, Sept. 1999, pp. 1313–1317.

[52] L. Klein-Berndt, "Kernel AODV," National Institute of Standards and Technology (NIST), Tech. Rep., 2001.

[53] I.D. Chakeres and E.M. Belding-Royer, "AODV Routing Protocol Implementation Design," in *Proc. Int. Workshop on Wireless Ad Hoc Networking (WWAN)*, Mar. 2004.

[54] H. Lundgren, D. Lundberg, J. Nielsen, E. Nordstrom, and C. Tschudin, "A Large-scale Testbed for Reproducible Ad hoc Protocol Evaluations," in *Proc. IEEE Wireless Communications and Networking Conference (WCNC)*, Mar. 2002.

[55] P.M. Ruiz and A.F. Gomez-Skarmeta, "Approximating Optimal Multicast Trees in Wireless Multihop Networks," in *Proc. of IEEE Computers and Communications (ISCC)*, Jun. 2005, pp. 686–691.

[56] Wookey and Tak-Shing, "Porting the Linux Kernel to a New ARM Platform," *Wireless Solutions Journal*, vol. 4, pp. 52–59, 2002.

[57] Advantech Team, "PCM-7230 User's Manual," Advantech Co., Ltd., Tech. Rep., 2003.

[58] K. Wehrle, F. Pahlke, H. Ritter, D. Muller, and M. Bechler, *The Linux Networking Architecture: Design and Implementation of Network Protocols in the Linux Kernel.* Prentice Hall, Aug. 2004.

[59] IEEE 802.11 WG, *IEEE Std 802.11a-1999(R2003): Part 11: Wireless LAN Medium Access Control (MAC) and Physical Layer (PHY) Specifications: High-speed Physical Layer in the 5 GHz Band*, IEEE Standards Association Std., 2003.

[60] IEEE 802.11 WG, *IEEE Std 802.11b-1999(R2003): Part 11: Wireless LAN Medium Access Control (MAC) and Physical Layer (PHY) Specifications: Higher-Speed Physical Layer Extension in the 2.4 GHz Band*, IEEE Standards Association Std., 2003.

[61] IEEE 802.11 WG, *IEEE Std 802.11g-2003: Part 11: Wireless LAN Medium Access Control (MAC) and Physical Layer (PHY) Specifications: Amendment 4: Further Higher Data Rate Extension in the 2.4 GHz Band*, IEEE Standards Association Std., 2003.

[62] IEEE 802.11 WG, *IEEE Std 802.11e-2005: Part 11: Wireless LAN Medium Access Control (MAC) and Physical Layer (PHY) Specifications: Amendment 8: Medium Access Control (MAC) Quality of Service Enhancements*, IEEE Standards Association Std., 2005.

[63] IEEE 802.11 WG, *IEEE 802.11n-2009: Part 11: Wireless LAN Medium Access Control (MAC) and Physical Layer (PHY) Specifications: Amendment 5: Enhancements for Higher Throughput*, IEEE Standards Association Std., Oct. 2009.

[64] J. Heiskala and J. Terry, *OFDM Wireless LANs: A Theoretical and Practical Guide.* Sams, 2001.

[65] D. Tse and P. Viswanath, *Fundamentals of Wireless Communication.* Cambridge University Press, 2005.

[66] Y. Xiao and J. Rosdahl, "Throughput and Delay Limits of IEEE 802.11," *IEEE Commun. Lett.*, vol. 6, no. 8, pp. 355–357, Aug. 2002.

[67] X. Yang, "Packing Mechanisms for the IEEE 802.11n Wireless LANs," in *Proc. IEEE Global Telecommunications Conference (GLOBECOM)*, Nov. 2004, pp. 3275–3279.

[68] Y. Lu, C. Zhang, J. Lu, and X. Lin, "A MAC Queue Aggregation Scheme for VoIP Transmission in WLAN," in *Proc. IEEE Wireless Communications and Networking Conference (WCNC)*, Mar. 2007, pp. 2121–2125.

[69] Y. Wu, "Multilevel Modulation Based Differentiated Data Aggregation for Wireless LANs," in *Proc. IEEE Region 10 Conference (TENCON)*, Nov. 2006, pp. 1–4.

[70] N. Ghazisaidi and M. Maier, "Advanced Aggregation Techniques for Integrated Next-Generation WLAN and EPON Networks," in *Proc. IEEE Consumer Communications and Networking Conference (CCNC)*, Jan. 2010, pp. 1–5.

[71] G. Kramer, *Ethernet Passive Optical Networks.* McGraw-Hill, 2005.

[72] N. Ghazisaidi, M. Maier, and C.M. Assi, "Fiber-Wireless (FiWi) Access Networks: A Survey," *IEEE Commun. Mag.*, vol. 47, no. 2, pp. 160–167, Feb. 2009.

[73] B. Ginzburg and A. Kesselman, "Performance Analysis of A-MPDU and A-MSDU Aggregation in IEEE 802.11n," in *Proc. IEEE Sarnoff Symposium*, Apr. 2007, pp. 1–5.

[74] D. Skordoulis, Q. Ni, H.H. Chen, A.P. Stephens, C. Liu, and A. Jamalipour, "IEEE 802.11n MAC Frame Aggregation Mechanisms for Next-generation High-throughput WLANs," *IEEE Wireless Commun. Mag.*, vol. 15, no. 1, pp. 40–47, Feb. 2008.

[75] Y.W. Kuo, "Throughput Analysis for Wireless LAN with Frame Aggregation under Mixed Traffic," in *Proc. IEEE Region 10 Conference (TENCON)*, Oct. 2007, pp. 1–4.

[76] B.S. Kim, H.Y. Hwang, and D.K. Sung, "Effect of Frame Aggregation on the Throughput Performance of IEEE 802.11n," in *Proc. IEEE Wireless Communications and Networking Conference (WCNC)*, Mar. 2008, pp. 1740–1744.

[77] Y. Lin and V.W.S. Wong, "Frame Aggregation and Optimal Frame Size Adaptation for IEEE 802.11n WLANs," in *Proc. IEEE Global Telecommunications Conference (GLOBECOM)*, Nov. 2006, pp. 1–6.

[78] Y. Nagai, A. Fujimura, Y. Shirokura, Y. Isota, F. Ishizu, H. Nakase, S. Kameda, H. Oguma, and K. Tsubouchi, "324Mbps WLAN Equipment with MAC Frame Aggregation," in *Proc. IEEE Int. Symp. Personal, Indoor and Mobile Radio Communications (PIMRC)*, Sep. 2006, pp. 1–5.

[79] Y. Kim, S. Choi, K. Jang, and H. Hwang, "Throughput Enhancement of IEEE 802.11 WLAN via Frame Aggregation," in *Proc. IEEE Vehicular Technology Conference (VTC)*, Sept. 2004, pp. 3030–3034.

[80] B.A. Forouzan, *Data Communications and Networking.* McGraw-Hill, 2006.

[81] T. Nakajima, T. Nabetani, Y. Utsunomiya, T. Adachi, and M. Takagi, "A Simple and Efficient Selective Repeat Scheme for High Throughput WLAN, IEEE802.11n," in *Proc. IEEE Vehicular Technology Conference (VTC)*, Apr. 2007, pp. 1302–1306.

[82] T. Nakajima, Y. Utsunomiya, Y. Nishibayashi, T. Tandai, T. Adachi, and M. Takagi, "Compressed Block Ack, an Efficient Selective Repeat Mechanism for IEEE802.11n," in *Proc. IEEE Int. Symp. Personal, Indoor and Mobile Radio Communications (PIMRC)*, Sept. 2005, pp. 1479–1483.

[83] A. Papoulis and S.U. Pillai, *Probability, Random Variables, and Stochastic Processes*, 4th ed. McGraw-Hill, 2002.

[84] IEEE 802.16 WG, *IEEE Standard for Local and Metropolitan Area Networks - Part 16: Air Interference for Fixed Broadband Wireless Access Systems*, IEEE Standards Association Std., 2004.

[85] IEEE 802.16 WG, *IEEE Standard 802.16e-2005: Part 16: Air Interference for Fixed Broadband Wireless Access Systems, Amendment 2: Physical and Medium Access Control Layers for Combined Fixed and Mobile Operation in Licensed Bands and Corrigendum 1*, IEEE Standards Association Std., 2006.

[86] I. Koffman and V. Roman, "Broadband Wireless Access Solutions based on OFDM Access in IEEE 802.16," *IEEE Commun. Mag.*, vol. 40, pp. 96 – 103, Apr. 2004.

[87] C. Cicconetti, L. Lenzini, E. Mingozzi, and C. Eklund, "Quality-of-service Support in IEEE 802.16 Networks," *IEEE Network*, vol. 20, pp. 50 – 55, Mar. 2006.

[88] A. Ghosh, D. R. Wolter, J. G. Andrews, and R. Chen, "Broadband Wireless Access with WiMAX/802.16: Current Performance Benchmarks and Future Potential," *IEEE Commun. Mag.*, vol. 43, pp. 129 – 136, Feb. 2005.

[89] Y. Zhang, Y. Xiao, and V.C.M. Leung, "Energy Management Analysis and Enhancement in IEEE 802.16e WirelessMAN," *IEEE Trans. Veh. Technol.*, vol. 58, pp. 3738 – 3752, Sept. 2009.

[90] C. Cicconetti, L. Lenzini, E. Mingozzi, and C. Vallati, "Reducing Power Consumption with QoS Constraints in IEEE 802.16e Wireless Networks," vol. 9, pp. 1008 – 1021, Jul. 2010.

[91] L. Kong, G.K.W. Wong, and D.H.K. Tsang, "Performance Study and System Optimization on Sleep Mode Operation in IEEE 802.16e," *IEEE Trans. Wireless Commun.*, vol. 8, pp. 4518 – 4528, Sept. 2009.

[92] M.G. Kim, J. Choi, and M. Kang, "Enhanced Power-Saving Mechanism to Maximize Operational Efficiency in IEEE 802.16e Systems," *IEEE Trans. Wireless Commun.*, vol. 8, pp. 4710 – 4719, Sept. 2009.

[93] J.A. Stine and G. Veciana, "Improving Energy Efficiency of Centrally Controlled Wireless Data Networks," *ACM/Baltzer Wireless Networks*, vol. 8, pp. 681–700, 2002.

[94] R. Krashinsky and H. Balakrishnan, "Minimizing Energy for Wireless Web Access with Bounded Slowdown," in *Proc. ACM/IEEE International Conference on Mobile Computing and Networking (MobiCom)*, Sept. 2002, pp. 119–130.

[95] K.T. Feng and K.H. Chou, "Intelligent Router-Assisted Power Saving Medium Access Control for Mobile Ad Hoc Networks," in *Proc. IEEE Vehicular Technology Conference (VTC-2006 Spring)*, Melbourne, Australia, May 2006, pp. 304–308.

[96] D. Qiao, S. Choi, A. Soomro, and K.G. Shin, "Energy-Efficient PCF Operation of IEEE 802.11a Wireless LAN," in *Proc. IEEE Int. Conf. on Computer Communications (INFOCOM)*, Jun. 2002, pp. 580 – 589.

[97] G. Anastasi, M. Conti, E. Gregori, and A. Passarella, "A Performance Study of Power-Saving Polices for Wi-Fi Hotspots," *Computer Networks*, vol. 45, pp. 295 – 318, Jun. 2004.

[98] F. Zhang, T.D. Todd, D. Zhao, and V. Kezys, "Power Saving Access Points for IEEE 802.11 Wireless Network Infrastructure," vol. 5, pp. 144 – 156, Feb. 2006.

[99] J.C. Chen and K.W. Cheng, "EDCA/CA: Enhancement of IEEE 802.11e EDCA by Contention Adaption for Energy Efficiency," *IEEE Trans. Wireless Commun.*, vol. 7, pp. 2866 – 2870, Aug. 2008.

[100] Y. Xiao, "Energy Saving Mechanism in the IEEE 802.16e Wireless MAN," *IEEE Commun. Lett.*, vol. 9, pp. 595 – 597, Jul. 2005.

[101] K. Han and S. Choi, "Performance Analysis of Sleep Mode Operation in IEEE 802.16e Mobile Broadband Wireless Access Systems," in *Proc. IEEE Vehicular Technology Conference (VTC-2006 Spring)*, 2006, pp. 1141 – 1145.

[102] Y. Park and G.U. Hwang, "Performance Modelling and Analysis of the Sleep-Mode in IEEE802.16e WMAN," in *Proc. IEEE Vehicular Technology Conference (VTC-2007 Spring)*, Apr. 2007, pp. 2801 – 2806.

[103] Y. Zhang, "Performance Modeling of Energy Management Mechanism in IEEE 802.16e Mobile WiMAX," in *Proc. IEEE Wireless Communications and Networking Conference (WCNC)*, Mar. 2007, pp. 3205 – 3209.

[104] Y. Xiao, "Performance Analysis of an Energy Saving Mechanism in the IEEE 802.16e Wireless MAN," in *Proc. Consumer Communications and Networking Conference (CCNC)*, Jan. 2006, pp. 406 – 410.

[105] L. Kong and D.H.K. Tsang, "Optimal Selection of Power Saving Classes in IEEE 802.16e," in *Proc. IEEE Wireless Communications and Networking Conference (WCNC)*, Mar. 2007, pp. 1836–1841.

[106] J. Shi, G. Fang, Y. Sun, J. Zhou, Z. Li, and E. Dutkiewicz, "Improving Mobile Station Energy Efficiency in IEEE 802.16e WMAN by Burst Scheduling," in *Proc. IEEE Global Communications Conference (GLOBECOM)*, Nov. 2006, pp. 1–5.

[107] T.C. Chen, Y.Y. Chen, and J.C. Chen, "An Efficient Energy Saving Mechanism for IEEE 802.16e Wireless MANs," *IEEE Trans. Wireless Commun.*, vol. 7, pp. 3708 – 3712, Oct. 2008.

[108] T.C. Chen, J.C. Chen, and Y.Y. Chen, "Maximizing Unavailability Interval for Energy Saving in IEEE 802.16e Wireless MANs," vol. 8, pp. 475 – 487, Apr. 2009.

[109] T.C. Chen and J.C. Chen, "Extended Maximizing Unavailability Interval (eMUI): Maximizing Energy Saving in IEEE 802.16e for Mixing Type I and Type II PSCs," *IEEE Commun. Lett.*, vol. 13, pp. 151–153, Feb. 2009.

[110] Y.L. Chen and S.L. Tsao, "Energy-efficient Sleep-mode Operations for Broadband Wireless Access Systems," in *Proc. IEEE Vehicular Technology Conference (VTC-2006 Fall)*, Sept. 2006, pp. 1 – 5.